UV-Induced Intrinsic Fabry-Perot Interferometric Fiber Sensors and Their Multiplexing for Quasi-Distributed Temperature and Strain Sensing

Fabin Shen

Dissertation submitted to the Faculty of the
Virginia Polytechnic Institute and State University
in partial fulfillment of the requirements for the degree of

Doctor of Philosophy
in
Electrical Engineering

Dr. Anbo Wang, Chair
Dr. Ahmad Safaai-Jazi
Dr. Ira Jacobs
Dr. Yilu Liu
Dr. Guy Indebetouw

June 1, 2006
Blacksburg, Virginia

Keywords: Fiber Optic Sensors, Intrinsic Fabry-Perot Interferometers, UV-induced, Multiplexing, FDM, Temperature, Strain, and Distributed Sensing

UV-Induced Intrinsic Fabry-Perot Interferometric Fiber Sensors and Their Multiplexing for Quasi-Distributed Temperature and Strain Sensing

Fabin Shen

(ABSTRACT)

Distributed temperature and strain sensing is demanded for a wide range of applications including real-time monitoring of industrial processes, health monitoring of civil infrastructures, etc. Optical fiber distributed sensors have attracted tremendous research interests in the past decade to meet the requirements of such applications.

This research presents a multiplexed sensor array for distributed temperature and strain sensing that can multiplex a large number of UV-induced sensors along a single fiber. The objective of this research is to develop a quasi-distributed sensing technology that will greatly increase the multiplexing capacity of a sensor network and can measure temperature and strain with a high accuracy and high resolution.

UV-induced intrinsic Fabry-Perot interferometric (IFPI) optical fiber sensors, which have low reflectance and low power loss, are good candidates for multiplexed sensors networks. Partial reflectors are constructed by irradiating photosensitive fiber with a UV laser beam. A pair of reflectors will form a Fabry-Perot interferometer that can be used for temperature and strain sensing. A sensor fabrication system based on a pulsed excimer laser and a shadow mask is developed.

A spectrum-based measurement system is presented to measure the interference fringes of IFPI sensors. A swept coherent light source is used as the light source. The spectral responses of the IFPI sensors at different wavelengths are measured. A frequency division multiplexing (FDM) scheme is proposed. Multiple sensors with different optical path differences (OPD) have different sub-carrier frequencies in the measured spectrum of the IFPI sensors. The

multiplexing capacity of the sensor system and the crosstalk between sensors are analyzed.

Frequency estimation based digital signal processing algorithms are developed to determine the absolute OPDs of the IFPI sensors. Digital filters are used to select individual frequency components and filter out the noise. The frequency and phase of the filtered signal are estimated by means of peak finding and phase linear regression methods. The performance of the signal processing algorithms is analyzed.

Experimental results for temperature and strain measurement are demonstrated. The discrimination of the temperature and strain cross sensitivity is investigated. Experimental results show that UV-induced IFPI sensors in a FDM scheme have good measurement accuracy for temperature and strain sensing and potentially have a large multiplexing capacity.

This work was supported in part by the U.S. Department of Energy and the National Science Foundation.

Dedication

To my wife, Jie, who has dedicated tremendous patience, encouragement and support to my doctoral study, and my son, Jiayi, who has given me so much happiness in my daily life.

Acknowledgments

At first, I would like to express my deepest gratitude to my advisor, Dr. Anbo Wang, for his continuous advice, guidance, support, supervision, and encouragement throughout my doctoral study and research at Virginia Tech. I thank him for offering me financial supports, for being both an academic and a life advisor, for providing so many research opportunities for me to work on, for constantly giving encouragements when I encounter difficulties in my research, for being a friend, and for the leisure time we have spent for fishing.

I would also like to thank my committee members, Dr. Ahmad Safaai-Jazi, Dr. Ira Jacobs, Dr. Guy Indebetouw, and Dr. Yilu Liu for their suggestions throughout my doctoral research.

Many thanks go to Dr. Gary Pickrell, Dr. Kristie Cooper, Mrs. Debbie Collins, and Mr. Bill Cockey for the suggestions, encouragements, supports, and cooperations during my stay at the Center for Photonics Technology (CPT).

I would like to thank current and past group members that I have worked with during my research in CPT. Special thanks to Yizheng Zhu, Dr. Zhengyu Huang, and Zhuang Wang for the numerous time we have spent together in idea discussion, sensor preparation, and field test applications. Many thanks to Dr. Wei Peng, Dr. Bing Yu, and Dr. Ming Han for their helps in laboratory research and for being my neighbors. Thanks also go to Xaiopei Chen, Dr. Juncheng Xu, Dr. Yan Zhang, Dr. Jiangdong Deng, Dr. Po Zhang, Daewoong Kim, Yongxin Wang, Bo Dong, and Xingwei Wang, for the contributions to the projects we

have worked together. I would like to extend my thanks to all of my friends who have been always ready to help and have made my life in Virginia Tech and Blacksburg, VA a great pleasure.

Finally, I would like to thank my family members. I am deeply grateful to my wife, Jie, for her great patience and dedication, to my parents, Chengru and Jiuying, for their encouragement and support, and to my son, Jiayi, for his love and smile.

Contents

List of Acronyms

AM	Amplitude Modulated
CDM	Code Division Multiplexing
CM	Coherence Multiplexing
EFPI	Extrinsic Fabry-Perot Interferometer
FBG	Fiber Bragg Grating
FDM	Frequency Division Multiplexing
FFT	Fast Fourier Transform
FIR	Finite Impulse Response
FMCW	Frequency Modulated Continuous Wave
FP	Fabry-Perot
HR-SLI	High Resolution Swept Laser Interrogator
IFPI	Intrinsic Fabry-Perot Interferometer
OFDR	Optical Frequency Domain Reflectmetry
OPD	Optical Path Difference
OTDR	Optical Time Domain Reflectmetry
SDM	Spatial Division Multiplexing
SNR	Signal to Noise Ratio
TDM	Time Division Multiplexing
UV	Ultraviolet
WDM	Wavelength Division Multiplexing

List of Figures

List of Tables

Chapter 1

Introduction

1.1 Motivation

Distributed temperature and strain sensing is demanded for a wide range of applications, which include real-time monitoring of industrial processes, health monitoring of industrial and civil infrastructures, etc. Such industrial and civil infrastructures range from oil/gas production to delivery pipelines, from electric power generation to transmission and distribution networks, and from large bridges, dams to even commercial and residential buildings. The monitoring of these structures usually requires the sensors and measurement devices to have such features as large area coverage, unattendance with minimum maintenance, low cost per measurement point, and capability of operation in harsh environments.

Many different kinds of electrical and optical sensors have been investigated to meet the requirement of such applications. Optical fiber sensors, which have characteristic advantages including intrinsic immunity to electromagnetic interference, high sensitivity, high accuracy, small size, capability of remote operation and survivability in harsh environment,[1] have attracted tremendous research interests for infrastructure monitoring.

Optical fiber sensors have been demonstrated for the detection of a large variety of physi-

cal, chemical and biomedical parameters.[1][2] Most physical properties, including displacement, rotation, temperature, strain, pressure, flow, electrical field, magnetic field etc, can be sensed with optical fibers. Temperature and strain are among the parameters mostly desired in quasi-distributed and fully distributed sensing applications such as industrial process monitoring and civil structure health monitoring.

Optical fiber sensors can be configured as a fully distributed sensing mode for temperature and strain measurement, where the measurands can be accessed at any location along a single fiber with a certain spatial resolution.[3]–[5] This is a unique and powerful characteristic of optical fiber sensors. Common distributed sensing technologies use Rayleigh, Raman, or Brillouin scattering to determine the parameters of interest by measuring the intensity or the frequency of the scattered light. In such applications, the location of the measurands is usually determined by the flight time of light pulses and the spatial resolution is determined by the width of light pulses. The signal to noise ratio (SNR) of these measurement systems is usually limited because of the weak power of the scattered light and the narrow width of light pulses. Therefore, the integration of the scattered signal over a relatively long fiber segment and a relative long time period is necessary to obtain a reasonable measurement accuracy.

For many applications, optical fiber sensors can be configured to be a point measurement mode in which the parameter of interest is measured at a specific location. This is the general working mode of conventional electrical sensors such as a pressure probe, a thermometer and a strain gage. Optical fiber sensors can work as well as conventional sensors and provide better performance in most cases. However, fiber sensor technology is more costly as a whole due to the complexity of the measurement system and the small markets of productions. The deployment of fiber sensors is thus usually restricted to the applications with special needs, such as a non-electrical sensor head, a remote sensor location and the need for a lightweight sensor probe.

The ability to efficiently multiplex fiber sensors gives an advantage to fiber sensor technology

over other technologies and can potentially reduce the average cost of the measurement system. Thus researchers have been trying to multiplex as many sensors as possible in a system so the cost per measurement point can be significantly lowered. Such a multiplexed sensor system is usually called a quasi-distributed sensing system in which one use a common interrogation system to simultaneously monitor the measurands at different locations. Many kinds of fiber sensor multiplexing technologies, including time division multiplexing (TDM), frequency division multiplexing (FDM), wavelength division multiplexing (WDM), coherence multiplexing (CM), code division multiplexing (CDM), spatial division multiplexing (SDM) etc, have been proposed and demonstrated.[5]–[7]

Theoretically, almost all kinds of sensors, whether they are intensity-modulated, phase-modulated or wavelength-modulated, can be multiplexed in one of the multiplexing schemes mentioned above. However, for a quasi-distributed temperature and strain sensing system in which multiple sensors are arranged along a single fiber, only the in-line sensor types with low insertion and return losses are preferred. Such sensors include in-line Fabry-Perot (FP) interferometric sensors and fiber Bragg grating (FBG) sensors.

There are several kinds of in-line FP interferometric fiber sensors reported, which are constructed by building partial mirrors into a fiber. These partial mirrors can be dielectric thin films,[8]–[10] air-glass interfaces,[11]–[14] or reflectors induced by ultraviolet (UV) irradiation.[15]–[17] FP sensors with thin film mirrors and air-glass mirrors usually have either high return loss or high insertion loss and their multiplexing capacity are usually limited to a small number. FP sensors with UV-induced internal mirrors may have low reflectance and low power loss and have the potential to be densely multiplexed. However, because of the low reflectance of UV-induced mirrors, the optical detection and signal processing have been challenging tasks for the multiplexing of UV-induced FP sensors.

FBG sensors, which are constructed by generating periodic refractive index change inside a photosensitive fiber with UV irradiation, are narrow band reflectors with low insertion loss and have the potential to be densely multiplexed.[18]–[20] A straightforward multiplexing

scheme for FBG sensors is WDM based interrogation in which FBG sensors have different Bragg wavelengths. However, the multiplexing number of FBG sensors is limited due to the limited bandwidth of the light source. FBG sensors with different Bragg wavelengths also require extra complexity and cost for sensor fabrications. Some researchers proposed a FDM method to multiplex low-reflectance FBG sensors with nominally equal Bragg wavelengths, thus to increase the multiplexing capacity and ease the fabrication complexity.[21] However, the signal-processing task is challenging and the measurement accuracy is restricted.

In this research, we focus on the fabrication and interrogation system for UV-induced intrinsic Fabry Perot interferometric (IFPI) sensors and their multiplexing for quasi-distributed temperature and strain sensing. The objective of this research is to develop UV-induced IFPI optical fiber sensor networks and optical measurement systems that can multiplex a large number of sensors for temperature and strain measurement with high accuracy.

1.2 Scope of the research

The main achievements of this research include

- Design of IFPI sensors.

  When a short section of photosensitive fiber is exposed to UV laser, the refractive index of the fiber core will be changed. The refractive index mismatch will reflect part of the light guided in the fiber. A pair of these UV-inscribed partial reflectors will form a FP interferometer that can be used for temperature and strain sensing. The UV-induced refractive index profile along the fiber is investigated. The interferometric signal of the sensor is analyzed.[17]

- Development of sensor fabrication systems.

  A fabrication system for UV-induced IFPI sensors, which contained a $248nm$ pulsed excimer UV laser, UV-grade mirrors and lens, a metallic shadow mask, and translation

stages, is developed. A point-by-point laser writing procedure is developed.[17]

- Development of measurement systems.

  The absolute optical path difference (OPD) between the two reflectors in an IFPI sensor is determined by measuring the interference spectrum of the two reflected beams in a certain wavelength range. A high resolution swept laser interrogator is used to measure the interference spectrum of the sensor. The wavelength of the laser is swept in $1520 - 1570nm$ range. The reflectivity of the sensor at each wavelength step is measured.[17]

- Design and implementation of multiplexing schemes.

  A FDM scheme based on a frequency modulated continuous wave (FMCW) technique is developed to multiplex IFPI sensors along a single fiber. When sensors have different OPDs from one another, their interference spectra will have different sub-carrier frequencies. Therefore, the measured signal from an array of multiplexed sensors will have multiple frequency components corresponding to the different OPDs.[22][23]

- Development of signal processing algorithms.

  The OPDs of sensors are determined by estimating the frequencies and the phases of the sinusoidal components in the signal of the sensor array. Finite impulse response (FIR) digital filters are used to select each frequency component and filter out the noise. Two kinds of frequency estimation methods, namely the peak finding method and the phase regression method, are developed to determine the frequency and the phase of the sinusoidal signal and thus the OPD of each sensor.[24]

- Performance analysis of multiplexing system.

  The performances of multiplexed sensor system, including the accuracy of the frequency estimation, the accuracy of the OPD determination, the noise source, the multiplexing capacity, and the crosstalk of the sensor array, are investigated and analyzed.

- Software programming for the measurement systems.

  Matlab routines are programmed to evaluate the performance of signal processing algorithms. A Win32 multithreaded program is developed to retrieve the interference spectrum from the instrument and demodulate the sensor signal with a high speed.

- Demonstration of temperature and strain sensing applications.

  The experimental results of multiplexed IFPI sensors shows a 0.1^oC and $0.5\mu\epsilon$ resolution for temperature and strain measurement. The results of a multiplexed sensor array, as well as the discrimination of the temperature and strain measurement, are demonstrated.

The contents of this dissertation are arranged as follows. After an introduction of the research in Chapter 1, a review of the optical fiber distributed sensing and multiplexing technology is given in Chapter 2. In Chapter 3, the principle of operation of the UV-induced Fabry-Perot (FP) interferometer and the sensor fabrication system are discussed. In Chapter 4, the measurement system for IFPI sensors and the FDM scheme based on the FMCW technique are discussed. The multiplexing capacity of the sensor system and the crosstalk between sensors are analyzed. In Chapter 5, frequency-estimation-based signal processing algorithms for the FDM scheme are discussed. In Chapter 6, experimental results of IFPI sensors for temperature and strain sensing are demonstrated. A brief summary and a recommendation of future work are given in Chapter 7, followed by the list of references.

1.3 Summary

This chapter discusses the motivation, the objective, the achievements of this doctoral research as well as the content structure of this dissertation.

Chapter 2

Research Background

2.1 Distributed Sensing

There are two main categories of optical sensing systems that measure space-mapped parameters such as temperature and strain. One category is intrinsic distributed sensing in which optical fibers are used for both sensing and light guiding.[3][4][5] Intrinsic distributed sensing technologies usually use Rayleigh, Raman, and Brillouin scattering phenomena in optical fiber to determine the parameters of interest along the fiber. The measurands can be determined at any location with a certain spatial resolution. The other category is quasi-distributed sensing in which multiple point sensors are multiplexed in various topology and multiplexing schemes.[5]–[7] The measurands can be only measured at the point where sensing element is located. The main role of optical fibers in a quasi-distributed sensing system is to deliver light to and collect light from the multiplexed sensors. Some sensors in a quasi-distributed system, like the IFPI sensors in this research, use optical fibers both as the light waveguides and the sensing elements.

2.1.1 Intrinsic Distributed Sensing

An intrinsic distributed sensing system allows the environmental parameters to be measured at any point along the length of the fiber with a certain spatial resolution. It is also called a fully distributed sensing system. Usually, communication grade fiber, which has no discontinuous points, can be used to measure the field over kilometers with a resolution interval from centimeters to meters. Common measurands include distributed temperature and strain along the fiber.

Many fully distributed sensing systems use time domain techniques, in which the position of the measurement point is located by the time of flight of a back-scattered or forward-scattered light pulse. A well-known optical time domain reflectometry (OTDR) technique is often used to measure the back scattering of the light pulse, which is modulated by the environmental parameter along the fiber. In these systems, a short pulse of light is launched into the fiber and a small portion of light is back scattered and detected. The spatial resolution depends on the width of the light pulse. The measurand can be determined by measuring the intensity or wavelength of the reflected light pulse.[25]–[27]

An alternative approach is the optical frequency domain reflectometry (OFDR) technique. It is essentially derived from the frequency modulated continuous wave (FMCW) technique used in radar systems.[28]–[29] In an OFDR system, a continuous wave (CW) light source is frequency-modulated and launched into a fiber. The frequency modulation can be done either by varying the optical carrier itself or its modulation envelope, and thus OFDR technique can be classified as coherent FMCW and incoherent FMCW.[30] In coherent FMCW, the reflected light from different locations will have different optical frequencies and beat with the reflection from a reference point. The position information can be retrieved from the frequencies of the beating signal. The measurands can be determined by the magnitude of the beating signal.[31] Incoherent OFDR technique actually measures the transfer function of the segment of the optical fiber. Its Fourier transform (FT) will give the time-domain response of the system under test.[32]

Based on the types of the scattered light, fully distributed can be classified into three main sub-classes, namely Rayleigh scattering, Raman scattering and Brillouin scattering. Usually, backscattering are detected in most OTDR and OFDR based measurement systems. Forward-scattering can also be used as in stimulated Raman scattering and Brillouin scattering based systems. Some other optical effect, such as evanescent wave and Kerr effect etc can also be used for distributed sensing.[33]

Traditional OTDRs and OFDRs usually detect the Rayleigh back scattered light of the fiber. Variations of OTDR and OFDR for Raman scattering and Brillouin scattering, known as RODTR, ROFDR and BOTDR, BOFDR have been developed. In some Brillouin scattering based system, configurations named Brillouin optical time domain analysis (BOTDA) and Brillouin optical frequency domain analysis (BOFDA) were used to measure distributed temperatures and strains.[34][35]

Rayleigh Scattering

Rayleigh backscattering has been widely used in an OTDR or OFDR based system for fault location, loss measurement and distributed sensing. Rayleigh scattering is an elastic scattering process in which the scattered light has the same wavelength as the incident light. In a distributed sensing system, the intensity or the state of polarization of the back-scattered light is modulated by environmental parameters such as temperature and strain. Hartog introduced a distributed temperature measurement system based on the temperature-dependent absorption of a liquid-core fiber.[25] Rogers suggested polarization optical time reflectometry (POTDR) technique for distributed measurement of magnetic field, electric field, temperature and pressure by detecting the polarization state change during the round trip propagation of a light pulse.[37] Froggatt *et al.* introduced a distributed strain measurement system using a FMCW-based system.[36]

Rayleigh backscattering systems usually measure the intensity of the backscattered light. However, the intensity of the light is also influenced by the fluctuation of light source, the

optical connections between optical components, and the fiber bending in the optical path. Thus Rayleigh scattering based systems usually have limited accuracy and their practical applications in distributed sensing are limited.

Raman Scattering

Raman scattering is a non-linear process in an optical fiber. Raman scattering generates two side lobes centered at the spectrum of incident light, known as Stokes and anti-Stokes scattered light. These two Raman side lobes can be used to detect temperature profiles along a communication-grade optical fiber. The ratio of Stokes and anti-Stokes Raman scattered light can provide an absolute indication of temperature around the fiber which are not related to the incident light intensity, the power attenuation and the material composition of fiber. One can use optical filters to select the Raman scattered light and eliminate the Rayleigh scattering and Brilluoin scattering. Both OTDR and OFDR based Raman scattering distributed temperature measurement systems have been reported.[38]–[40] Commercial Raman scattering based distributed temperature sensors (York Sensors, DTS) are available. To the author's knowledge, no Raman scattering based strain sensing has been reported.

Compared with the Rayleigh back scattering in a fiber, the intensity of the Raman back scattering is low and thus causes a low signal to noise ratio (SNR) in a Raman scattering based system especially when a narrow pulse width is used for higher spatial resolution. The low SNR limits the measurement accuracy of the distributed temperature sensing. Therefore, a large number of average (up to hundreds of samples) or a long time integration (up to tens of minutes) is usually needed in a Raman distributed temperature sensing system.

Brillouin Scattering

Distributed temperature and strain sensing based on Brillouin scattering in an optical fiber is a relatively new technique and has attracted considerable research interests in the past

few years. Brillouin scattering is a non-linear scattering process caused by the refractive index variation arising from acoustic waves. The wavelength shift in Brillouin scattered light, which is characteristic of the acoustic velocity in silica fiber, is a function of both temperature and strain around the fiber,[41]–[44] and thus can be used for both temperature and strain sensing.

Compared with the wavelength shift of Raman scattered light, which can be tens of nanometers, frequency shift of Brillouin scattered light is very small (11GHz). One can use an optical filter to select the Brillouin scattered light out[43][44] or can use a heterodyne scheme to detect the beating frequency between the Brillouin scattering and the incident light.[45][46] Both spontaneous[45][46] and stimulated Brillouin scatterings[42] have been used for distributed temperature and strain sensing along a communication-grade fiber. One advantage of Brillouin scattering based system is that distributed temperature and strain profiles can be monitored simultaneously.[42]–[45]

Spontaneous Brillouin scattering based systems usually use the BOTDR technique in which a light pulse was injected to the fiber and back scatter Brillouin light pulse was measured.[45][46] Some stimulated Brillouin scattering based systems use Brillouin optical time domain analysis (BOTDA)[42][47][48] and Brillouin optical frequency domain analysis (BOFDA) [49] techniques in which Brillouin interaction between a pumping optical pulse and a counter-propagating continuous wave is used to generate stimulated Brillouin scattering. Commercial Brillouin scattering based distributed temperature and strain sensing systems (Neubrex NBX-6000) are available.

2.1.2 Quasi-Distributed Sensing With Point Sensors

A quasi-distributed sensing system is actually a sensor multiplexing system in which multiple sensors are arranged at pre-defined locations and integrated into a single measurement system to measure the desired environment parameters such as temperature and strain. A quasi-distributed optical fiber sensor system usually contains a multiplexed point sensor network,

a common light source and a common signal-conditioning unit.

Various kinds of optical fiber sensors, light from which can be modulated in intensity, wavelength, phase and polarization state, can be integrated into a sensor network with different structures and multiplexing technologies for a wide variety of applications. We will discuss sensor structures in Section 2.2 and discuss the multiplexing technology in Section 2.3.

2.2 Optical Fiber Sensors

The electric field of the light from a sensor can be expressed as

$$\overrightarrow{E} = \overrightarrow{e} A exp(j\omega t + \phi) \tag{2.1}$$

where A is the amplitude, ω is the angular frequency, ϕ is the phase, and $\overrightarrow{e}$ is a unit vector that represents the state of polarization. The intensity of the light is proportional to $|A|^2$. The wavelength of the light is $\lambda = 2\pi c/\omega$ where c is the speed of light in vacuum. Intensity, wavelength, phase and state of polarization are the four fundamental elements of the light field.

A perturbation of the measurand will change either one or multiple fundamental elements above. Correspondingly, optical fiber sensors can be classified to four main categories: intensity modulated, phase modulated, wavelength modulated and polarization modulated. Some literature[1] includes polarization-modulated sensors into the category of phase-modulated sensors owing to the fact that many systems use an interferometric technique to detect the change of polarization state.

2.2.1 Intensity-Modulated Sensors

Intensity-modulated sensors are the sensors that detect the variation of light intensity associated with the perturbing environment. The perturbation of the environment parameters

causes a change of the light intensity transmitted by or reflected from the sensor. The measurand can be determined by the received light intensity.

There are many kinds of intensity-modulated sensors reported.[1][2] One of them is the microbending fiber sensor.[50]–[52] Figure 2.1 shows a typical microbend pressure sensor. When external pressure is applied, the fiber is bent, and thus the transmitted light intensity is reduced due to the bending loss caused by the leakage of light out of the fiber. The intensity of the received light is related to the perturbation of displacement caused by external force or pressure.

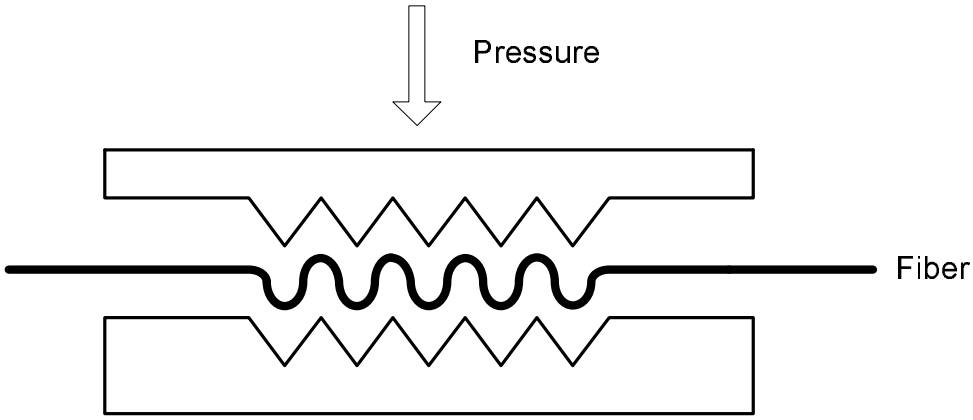

Figure 2.1: Sturcture of a microbend pressure sensor.

Microbend fiber sensors have been reported for distributed sensing applications of strain, pressure etc.[52][53] The principle of operation and structure of a microbend sensor are simple and the multiplexing of microbend sensors is straightforward. However, the performance of intensity based sensors is limited by the intensity variation of the light source, the bending loss of the fiber, and power loss at optical connectors. The long time stability of microbend sensors is poor. The practical applications of micro-bending sensors are limited.

2.2.2 Phase-Modulated Sensors

Phase-modulated optical fiber sensors are usually associated with interferometers because the optical phase of light wave or the phase difference between two light waves is usually detected by mean of interferometric technique. They usually employ coherent light sources and can precisely detect the phase shift caused by the environment parameters of interests. There are mainly four configurations of interferometric optical fiber sensors: the Michelson, the Mach-Zehnder, the Fabry-Perot, and the Sagnac.[1]

Mach-Zehnder

A Mach-Zehnder interferometer is a two-beam interferometer working at transmission mode. It has been used as optical fiber sensors[54][55] and optical components such as optical modulators, optical filters etc.[56] A typical optical fiber Mach-Zehnder interferometric sensor system is shown in Figure 2.2. The light from the light source is launched into the fiber and split to two arms by the directional coupler. The phase of one arm is modulated by the environment parameter to be measured. Then the lights from the two arms are combined by another directional coupler and interfere with each other. The phase between the two arms is detected by measuring the interference signal from the Mach-Zehnder interferometer.

Multiple optical fiber Mach-Zehnder sensors can be multiplexed in a tapped sensor array, a ladder sensor network and other topologies.[54]–[58] However, when a fiber based Mach-Zehnder interferometer is used, the relative long fiber arms cause the stability problem due to the temperature change and the polarization-fading problem due to the birefringence of the optical fiber, which cause random change of the state of polarization and fluctuation of received light intensity. Furthermore, the multiplexing of Mach-Zehnder sensors needs a number of splitters and combiners, which increase the system complexity and the total costs.

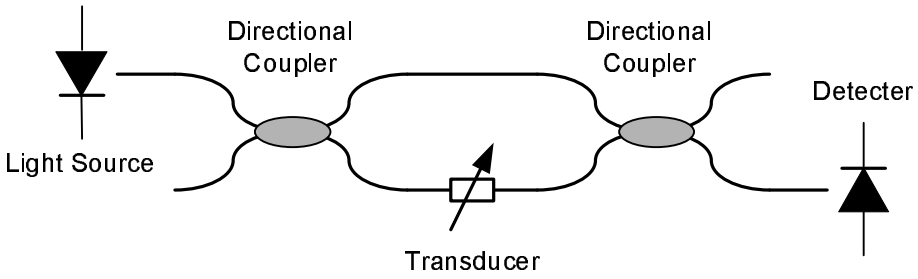

Figure 2.2: An optical fiber Mach-Zehnder interferometric sensor system.

Michelson

A typical optical fiber Michelson interferometric sensor system is shown in Fig. 2.3. The light from the light source is launched into the fiber and split to two arms by the directional coupler. These two light beams travel in different arms and are reflected by the end mirrors at the end of both arms while the phase of one light beam is modulated by the environment parameters to be measured. The two reflections are combined by the same directional coupler and interfere with each other. The phase difference between the two reflections is detected by measuring the interference signal.

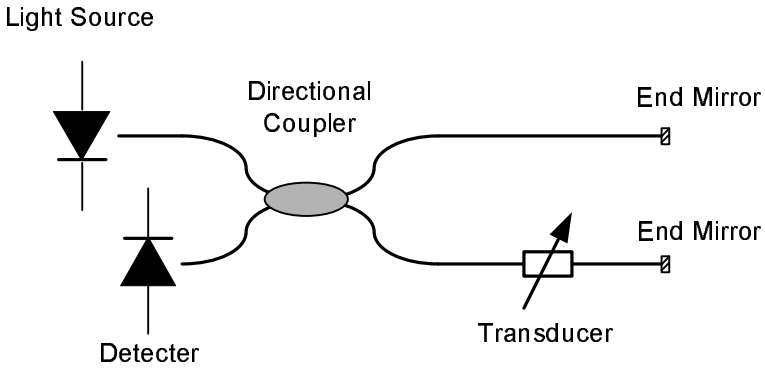

Figure 2.3: An optical fiber Michelson interferometric sensor system.

A Michelson interferometer is a two-beam interferometer working at reflection mode. Like an optical fiber Mach-Zehnder interferometer, an optical fiber Michelson interferometer also

suffers from the stability problem due to the phase change caused by the environment temperature variation and the polarization-fading problem caused by the birefringence of the fibers.[59] Some researchers reported a method to solve the polarization-fading problem by using Farady rotation mirrors as the end mirrors, which rotate the state of polarization for 90 degrees.[60][61] The multiplexing of Michelson interferometers has been reported in TDM, FDM and other schemes.[61]–[63]

Fabry-Perot

A Fabry-Perot (FP) interferometer contains a pair of partial mirrors. The multi-path reflected lights in the FP cavity interfere with one another. FP sensors can work at either transmissive mode or reflective mode, as shown in Figure 2.4. When the reflections at mirrors are high, a FP interferometer usually works in transmissive mode as shown in Figure 2.4(a), in which the FP cavity functions as an optical filter. When the reflections at mirrors are low, a FP interferometer usually works in reflection mode as shown in 2.4(b), in which the FP interferometer can be regarded as a two-beam interferometer with all the multi-path reflections neglected.

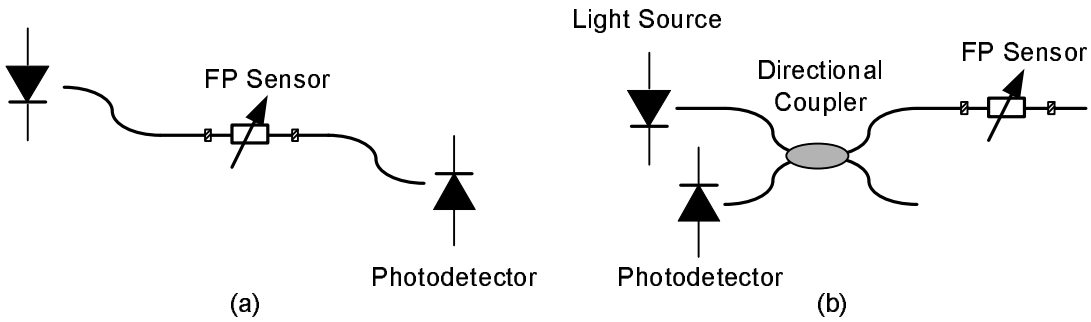

Figure 2.4: Fabry-Perot Sensors. (a) Transmissive mode. (b) Reflective Mode.

There are two main categories of fiber Fabry-Perot (FP) interferometric sensors, namely intrinsic FP interferometers (IFPI)[8]–[10],[14]–[17] and extrinsic FP interferometers (EFPI) [11]–[13] respectively. Basic structures of these two kinds of FP interferometers are shown in

Figure 2.5(a) and Figure 2.5(b), respectively.

An IFPI sensor contains two internal partial reflection mirrors. The fiber between the reflectors serves as both a sensing element and a light waveguide. A typical IFPI sensor is shown in Figure 2.5(a). An EFPI sensor contains a lead-in fiber with a partial mirror at the end-face, a cavity of air or other transparent medium and a reflector on the other end which may also be a piece of fiber. A typical EFPI sensor is shown is Figure 2.5(b). IFPI sensors usually have lower power loss than EFPI sensors and are more preferred in dense multiplexing applications.

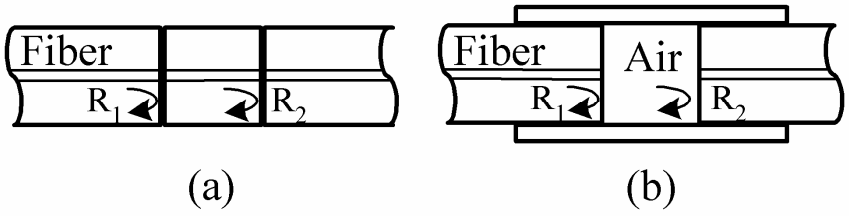

Figure 2.5: Fabry-Perot interferometric sensors. (a) IFPI sensor. (b) EFPI sensor.

FP sensors have some advantages over other fiber sensors for multiplexed sensor networks. One significant advantageous feature of FP sensor is that it can be configured as an in-line sensor and can be multiplexed along a single fiber for quasi-distributed temperature and strain sensing. Unlike the multiplexing of Mach-Zehnder and Michelson interferometers, which need many optical splitters and combiners, the multiplexing of FP sensors is relatively easer. One can arrange a large number of FP sensors along a single fiber without extra optical components if the power loss at each sensor can be controlled to a low level.

More details about FP sensors and their multiplexing will be discussed in Chapter 3 and Chapter 4 respectively.

Sagnac

A typical optical fiber Sagnac interferometer is shown in Figure 2.6. The light from the light source is split to two beams and injected into the fiber loop. The clockwise and counterclockwise propagated light beams combine at the coupler and form a two-beam interferometer. This configuration is used as a gyroscope for precise rotation measurement in which a rotation will cause an unbalance of propagation time and thus a phase difference between the two beams.

The loop structure of Sagnac interferometers has difficulty to be directly multiplexed. Some researchers use a Sagnac configuration to multiplex in-line FP fiber sensors in a loop topology and a coherence multiplexing scheme.[64]–[65]

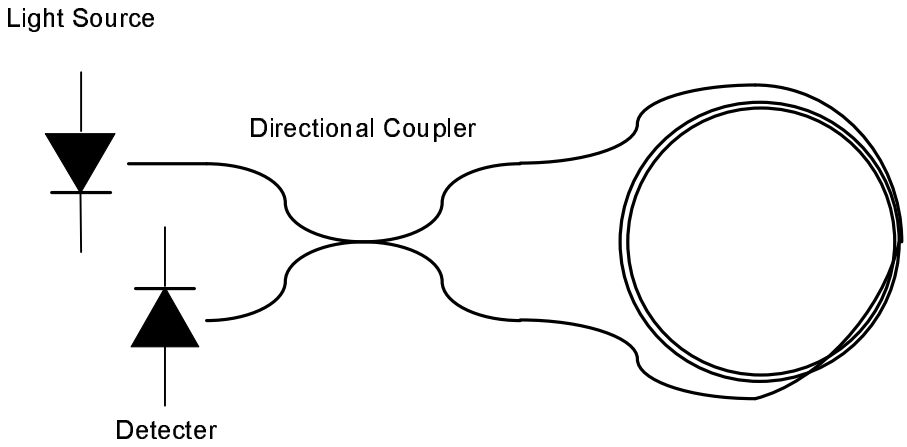

Figure 2.6: A typical Sagnac interferometer as a gyroscope

2.2.3 Wavelength-Modulated Sensors

Wavelength-modulated optical fiber sensors change the spectrum of the light being transmitted, reflected or emitted. Such sensors include blackbody radiation, fluorescence, phosphorescence and fiber Bragg grating (FBG) sensors.[1]

FBG sensors, whose reflection and transmission spectrum are dependent on temperature

and strain, are truly wavelength-modulated sensors. The diagram of a FBG is illustrated in Figure 2.7(a). A Bragg grating with periodic refractive index variation can be formed by UV irradiation. Different techniques, some of which include pointwise, interferometric, and phasemask-based writing methods, have been reported for the fabrication of FBGs.[18]–[20] A FBG is a narrow band reflector. The characteristic reflection spectrum of a FBG is shown in Figure 2.7(b).

The central wavelength in the reflection spectrum of a FBG, known as Bragg wavelength, is given by

$$\lambda_B = 2n_e\Lambda \tag{2.2}$$

where n_e is the effective refractive of the fiber and Λ is the period of the gratings. For a Bragg wavelength of $1.5\mu m$, Λ is selected to be $0.5\mu m$.

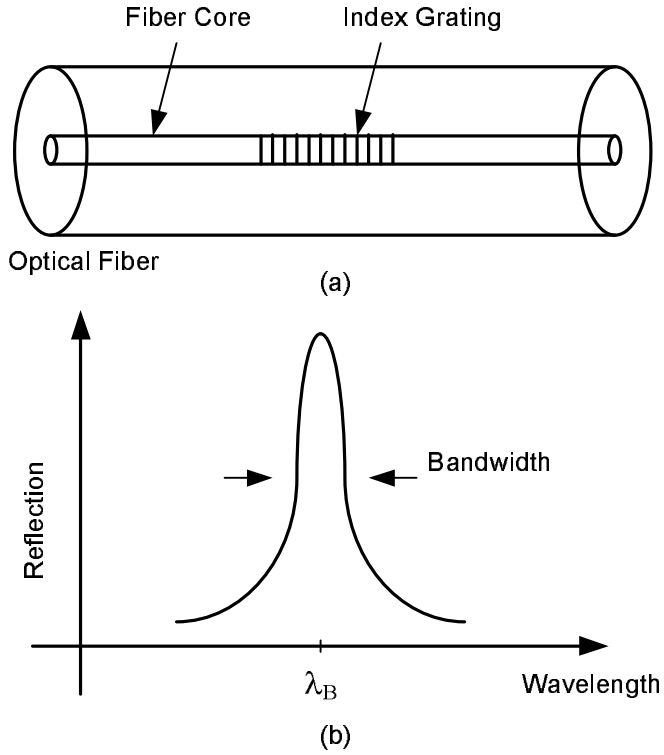

Figure 2.7: Fiber Bragg gratings. (a) Structure. (b) Reflection spectrum.

FBGs can be used for temperature and strain sensing. The central wavelength of an FBG is affected by the changes of the refractive index and the periodic spacing between gratings,

which are dependent on the environmental temperature and strain. Therefore, temperature and strain perturbations of a FBG sensor can be determined by monitoring the shift of the Bragg wavelength.

The shift of λ_B due to temperature change ΔT can be given as

$$\Delta\lambda_B = 2(\Lambda\frac{\partial n_e}{\partial T} + n_e\frac{\partial \Lambda}{\partial T})\Delta T = \lambda_B(\alpha + \sigma)\Delta T \tag{2.3}$$

where $\alpha = \frac{1}{\Lambda}\frac{\partial \Lambda}{\partial T}$ is the thermal expansion coefficient and $\sigma = \frac{1}{n_e}\frac{\partial n_e}{\partial T}$ is the thermo-optic coefficient of the fiber.

The shift of λ_B due to strain ε_z perturbation can be given by

$$\Delta\lambda_B = \lambda_B(1 - p_e)\varepsilon_z \tag{2.4}$$

where ε_z is the axial strain and p_e is the effective strain-optic constant. For a typical optical fiber, $p_e = 0.22$.

FBG sensors have several advantages including low power loss, high sensitivity, and large scale multiplexing capability. Quasi-distributed temperature and strain sensing with FBG sensors have been reported with different multiplexing schemes.[21],[66]–[71] Multiple FBG sensors are usually arranged in a serial array. The most common multiplexing schemes include TDM[66][67], WDM [68]–[70], FDM[21] and their combinations[71].

In a TDM scheme, the locations of FBG sensors are determined by the time delay of the reflected light pulse. The reflected light from each sensor is measured by a variety of wavelength-measurement technique including interferometric systems, scanning wavelength filters, and edge filters.[67] FBG sensors in a TDM scheme can either have different central wavelengths[66] or have nominally the same central wavelength with low reflectivity.[67] The interference and crosstalk between sensors have been a drawback for a TDM sensor array.

In a WDM scheme, FBG sensors are fabricated with different central wavelengths. When illuminated by a broadband light source, different FBGs will reflect the light at different wavelengths. One can either use a tunable optical filter to select the light from individual

sensor and a frequency discriminator to detect the wavelength change in time domain[68][69] or use an optical spectrometer to detect the wavelength shift in spectral domain[70]. Because each FBG has to occupy a certain bandwidth for wavelength shift, the multiplexing capacity of a WDM scheme is usually limited due to the available wavelength range. The fabrication of FBG sensors with different central wavelengths requires multiple phase masks or interferometric setups and is difficult for mass production.

Froggatt *et al.* demonstrated a FDM scheme for FBG sensors with nominally equal Bragg wavelength.[21] The system utilized a FMCW technique to modulate the frequency of a coherent light source. The locations of FBG sensors are determined by the beating frequencies between the reflections of FBG sensors and a reference air gap reflector. The spectrum of each FBG was obtained by inverse Fourier transforming the frequency band associated with each sensor. Hybrid multiplexing schemes, which may take advantages of different multiplexing schemes, can be used to increase the multiplexing capacity of FBG sensors. One example is a WDM/TDM combined multiplexing scheme given by Davis *et al.* [71]

2.2.4 Polarization-Modulated Sensors

Polarization-modulated optical fiber sensors are the sensors in which the polarization state of light is changed due to the external perturbation such as electric field, magnetic field etc. One of the polarization-modulated sensors is optical current sensor based on magneto-optic Faraday effect, which will rotate the polarization plane.[72][73] An optical fiber coil in a number of turns has been used as current or voltage sensing element.[72][73] Some other materials with larger magneto-optic constants, such as bulk-glass, yttrium iron garnet etc, have also been utilized in current sensors.[74] Another type of polarization-induced sensors is related to the anisotropic properties of crystal-like materials. Light traveling in crystals with orthogonal polarizations will have different propagation speeds and change its polarization states. Optical temperature and electric field sensors based on thermal-optic and Kerr effects have been reported, in which the environmental perturbation changed the refractive indices

of crystals and the polarization states of the light.

Polarization-modulated sensors usually use a polarimetric technique to detect the optical phase difference between orthogonal polarizations, which is similar to the interferometric technique for phase-modulated sensors. Some researchers regard polarization-modulated sensors as phase-modulated sensors because of their similarities in the phase-detection scheme.

The multiplexing of polarization-modulated sensors is rarely reported due to the complexity of the polarimetric detection, which may require polarizer, wave plate and other optical components. A FDM multiplexed current sensor array, which contains multiple polarization-modulated fiber lasers, was given by Yong *et al.*[75]

2.3 Multiplexing Schemes for Optical Fiber Sensors

Many multiplexing schemes for optical fiber sensors, some of which include time, frequency, wavelength, coherence, polarization, and spatial-division multiplexing schemes, have been reported. Together with the different multiplexing topologies discussed below, there are many different multiplexing configurations for different sensors. In this section, we will discuss common sensor topologies including serial, star, and ladder, and different multiplexing schemes including time-division-multiplexing (TDM), frequency-division-multiplexing (FDM), wavelength-division-multiplexing (WDM) and coherence-multiplexing (CM), especially for interferometric sensors.

2.3.1 Topology

Topology means the method how multiple sensors in a sensor network are arranged. Various topologies including serial, star, ladder, tree, matrix and their combinations have been reported. One can detect either the light transmitted by or reflected from the sensors. Correspondingly, sensor networks can work at either transmissive mode or reflective mode. A

good review of multiplexing topologies was given in Ref. [6].

- Serial Topology

  In a serial topology, multiple sensors are arranged in series as electrical components in a serial circuit. The biggest advantage of a serial topology is that one can arrange multiple in-line fiber sensors, such as Fabry-Perot sensors and FBG sensors, along a single fiber and thus simplify the deployment of quasi-distributed sensing. Figure 2.8 shows a typical sensor array with a serial topology. The sensors to be multiplexed are required to have low reflectivity and low power loss for dense multiplexing. The drawbacks of a serial topology include: the interference and crosstalk between sensors that may limit the performance of the sensor system and the reliability problem that one malfunctioned sensor may corrupt the signal of the whole sensor array. Various types of fiber sensors, including microbend[52], Mach-Zehnder[57], Fabry-Perot[76], FBG[67]–[71] etc, have been multiplexed in serial topologies.

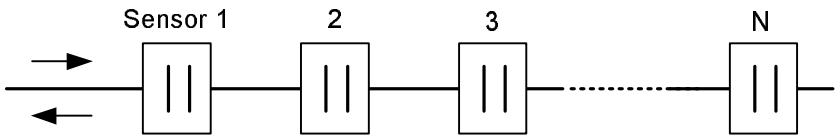

Figure 2.8: A sensor array with a serial topology.

- Star Topology

  In a star topology, multiple sensors are independently connected to a single central point. A typical sensor network with a star topology is given in Figure 2.9. A $1 \times N$ optical switch or optical splitter is used as the central unit. The biggest advantage of a star system is the independence between sensors that may lower the crosstalk and increase the reliability. However, the deployment for a large number of sensors may be difficult because of the splitting of optical power and embedding of multiple fibers into the structures.

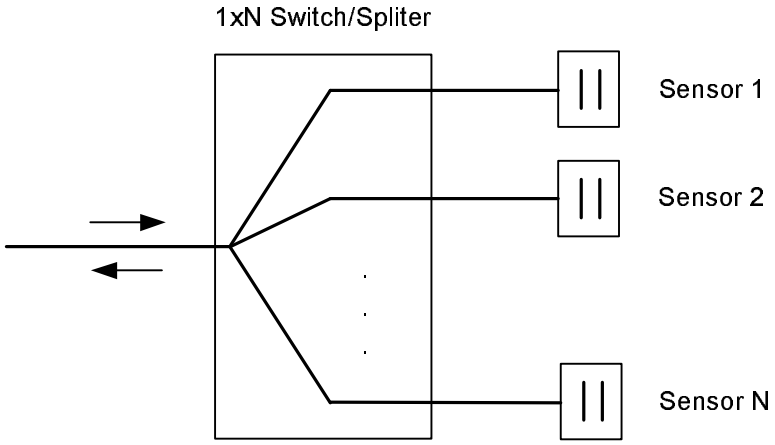

Figure 2.9: A sensor array with a star topology.

- Ladder Topology

  In a ladder topology, multiple sensors are arranged in parallel. Figure 2.10 shows a typical sensor network with a ladder topology. Multiple light beam splitters and combiner are use to guide light to different sensors. Although the ladder topology also has the advantage of independence between sensors, the usage of multiple splitters and combiners increase the system complexity.

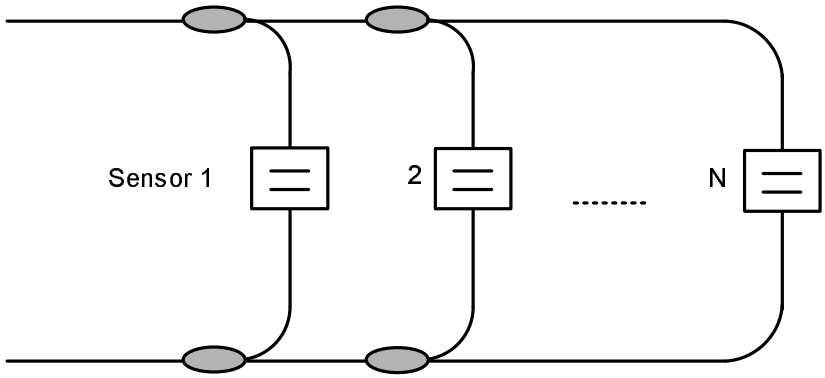

Figure 2.10: A sensor network with a ladder topology.

- Hybrid Topology

  One may use a hybrid topology that contains different fundamental topologies. Figure 2.11 shows a sensor network with a mixed star/serial topology. The basic structure is

a star topology. In each branch of the star network, multiple sensors are arranged in a serial topology. One can use this kind of hybrid topology to multiplex a large number of sensors and to balance the sensor performance and the reliability in a properly designed networks.

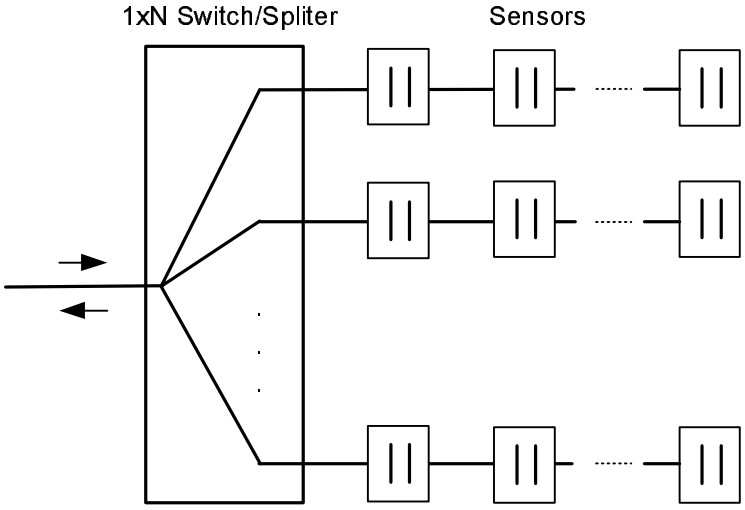

Figure 2.11: A hybrid star/serial topology.

The topologies of sensor network are not dependent on the multiplexing schemes of signals from the sensors. For example, a sensor array in a serial topology can be multiplexed in TDM, FDM, CM schemes, and so can a sensor array in a star topology. In following subsections, different multiplexing schemes for fiber sensors will be discussed.

2.3.2 Time Division Multiplexing

In a TDM scheme, the sensors are sequentially addressed by injecting a pulsed input signal into the sensor network. The light transmitted by or reflected from different sensors will have different delays of time flight and allow individual sensor to be distinguished.

TDM scheme has been used in sensor networks with different topologies, such as serial topology, ladder topology, star topology etc. The requirement of sensor arrangement in a

TDM system is that the signals from the different sensors have different delays. The most straightforward configuration for a TDM scheme is an OTDR based serial array working at reflective mode, as shown in Figure 2.12. An OTDR contains a laser diode, a light modulator to generate a light pulse, a photodetector as well as a delayed gater to detect the time delay of the reflected light from sensors. The intensity, frequency or the phase shift of the reflected light pulses are detected to determine the measurands of interests.

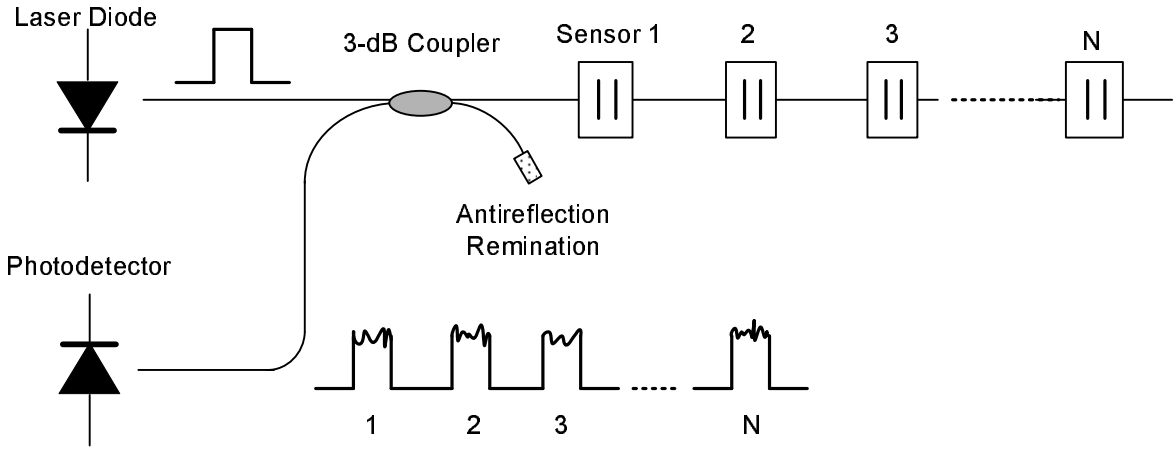

Figure 2.12: An OTDR based TDM sensor array.

TDM scheme has been used for the multiplexing of different sensors, such as microbend,[53] interferometric[16][54][57][77] and FBG[67][68] sensors, working at either transmissive mode or reflective mode.

2.3.3 Frequency Division Multiplexing

In a FDM scheme, signals from different sensors will have different frequencies. If the frequencies are optical frequencies, the multiplexing scheme is usually regarded as wavelength division multiplexed. Thus the frequency components in a FDM scheme are usually electrical signals with different frequencies.

FDM scheme usually use some modulation technique to modulate the light source periodically. Sinusoidal, sawtooth and triangle modulation are most common modulation

schemes.[78] Signals from different sensors have different frequencies due to the modulation of the light source. The different frequencies may stand for different physical meanings, which can be the carrier frequencies, positions of sensors, or optical path unbalance of sensors.

Dandrige *et al.* presented a FDM scheme based on phase carrier technique.[79][80] The sensor network had a $J \times K$ matrix topology. Multiple laser light sources were frequency-modulated with different sinusoidal carrier frequencies. The measured signal from sensors contained multiple frequency components corresponding to different modulation carrier frequencies.

The most attractive FDM scheme is the frequency modulated continuous wave (FMCW) based technique, which was originally developed for radar ranging,[28][29] and then applied to laser ranging and measurement of optical sensors.[81][82]

When FMCW technique is used in an optical fiber network, it is often called optical frequency domain reflectometry (OFDR).[83][85] An OFDR is essentially a FMCW technique working at reflective mode. Both coherent OFDR and incoherent OFDR have been developed based on different modulation method of the light source and have been reported for multiplexing of intensity-modulated,[86] interferometric,[63][81][82] and FBG sensors[21][87][88].

A coherent FMCW usually modulate the optical frequency directly in a wavelength range from picometers to tens of nanometers. The light beams propagating through different optical paths will have different optical frequencies and will beat with each other when combined. The beating frequency is equal to the difference of optical frequencies of the two light beams and can be used to determine the optical path difference between the two light beams.

An incoherent FMCW modulates the intensity of the light source instead of the optical carrier frequency, usually in a microwave frequency range of MHz - GHz. The intensity modulation is usually accomplished by modulating the driving current of a laser diode or the driving signal of an external optical modulator. The beating signal in an incoherent FMCW system comes from microwave frequencies instead of the optical frequencies in a coherent FMCW.

A typical FDM scheme of FMCW reflectometry based fiber sensor system is shown in Figure 2.13. A coherent light source is linearly frequency modulated. A reference reflection point is used. The reflections from sensors will beat with the reflection of reference point. The reflections from different sensors will generate electrical signals with different frequencies. A spectrum analyzer is used to analyze the frequency components of the beat signals. The positions of the sensors can be determined by measuring the frequencies of electrical signals. The environmental parameters of interests can be determined by detecting the intensity of the light reflected from the sensors, which is related to the amplitude of the beating frequencies. Froggatt *et al.* presented a similar configuration for interrogation of FBG sensors for strain sensing.[21] The reflection spectrum of each FBG sensor, instead of its intensity, was demodulated by inverse Fourier transforming the measured RF spectrum of each sensor and concatenating the recovered sequences in continuous sweeps. The strain information was determined according to the reflection spectrum shift of FBG sensors.

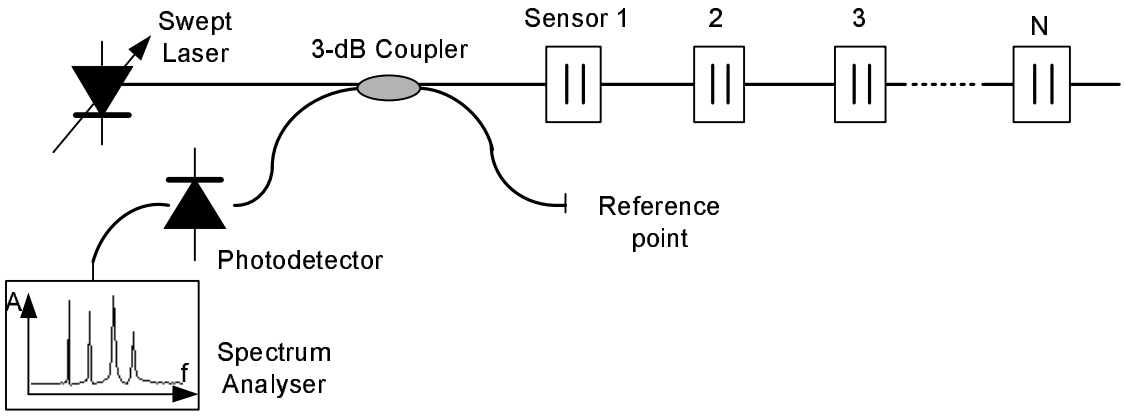

Figure 2.13: A FMCW based FDM sensor array.

If the beating signal in a FMCW configuration comes from the two different light beams of an interferometer, then the beating frequency is characteristic to the OPD between the two light beams. Sensors with different OPDs will have different beating frequencies and can be multiplexed in a subcarrier frequency domain. Sakai et al presented a FMCW based FDM sensor system for Mach-Zehnder interferometric sensors in a transmissive mode in which

the frequency-modulated light propagated through a series of unbalanced Mach-Zehnder interferometers and generated multiple frequency beating notes.[81] Collins *et al.* presented a FMCW based FDM scheme for Michelson interferometers in a star topologies.[63]

This research presents a subcarrier FDM scheme for UV-induced IFPI sensors in a serial topology. The measurement system and signal processing approach will be discussed in Chapter 4 and Chapter 5 respectively.

2.3.4 Wavelength Division Multiplexing

Wavelength division multiplexing has been proven to be a powerful technique to increase the capacity of optical communication systems and has been widely deployed in long-haul optical communication links and local optical networks.

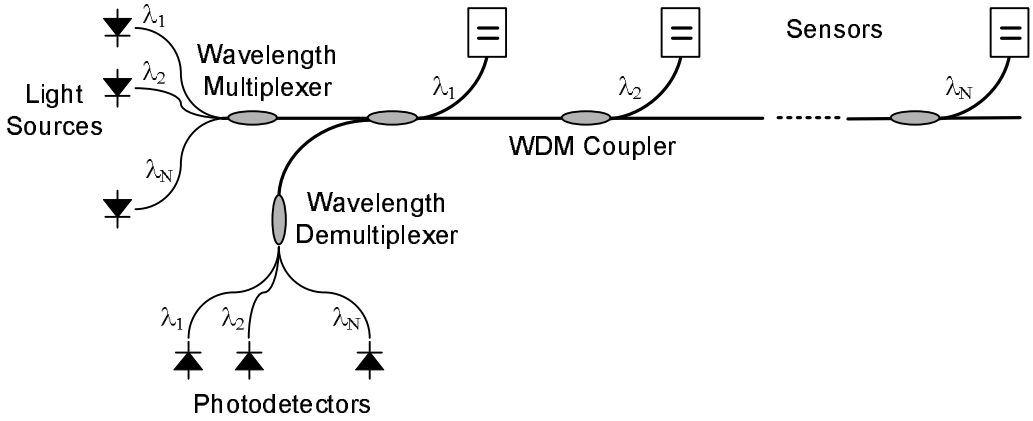

Figure 2.14: A wavelength division multiplexed sensor array.

The application of the WDM technique is straightforward in a sensor network, in which different sensors can be designed to work in different wavelengths. An arrangement of a sensor array using the WDM scheme is shown in Figure 2.14. The light from a particular source can be directed to a particular sensor and then received by a particular photodetector. Although sharing a common fiber link, the sensor elements are independent on each other in wavelength domain by using WDM splitters, couplers and combiners. The evolution

of the dense wavelength division multiplexing (DWDM) technique has made such optical components available in reasonable costs.

Another important WDM sensor interrogation scheme has been developed for FBG sensors, as shown in Figure 2.15. FBG sensors can be designed to reflect light at different wavelengths. When the sensor array is illuminated by a broadband light source, different FBG sensors will reflect different portions of lights with different wavelengths. An optical spectrometer can be used to monitor the central wavelength of each FBG sensor, and thus to determine the temperature and the strain. A tunable laser can also be used as the light source, while a photodetector is used as the detector instead of an optical spectrometer.

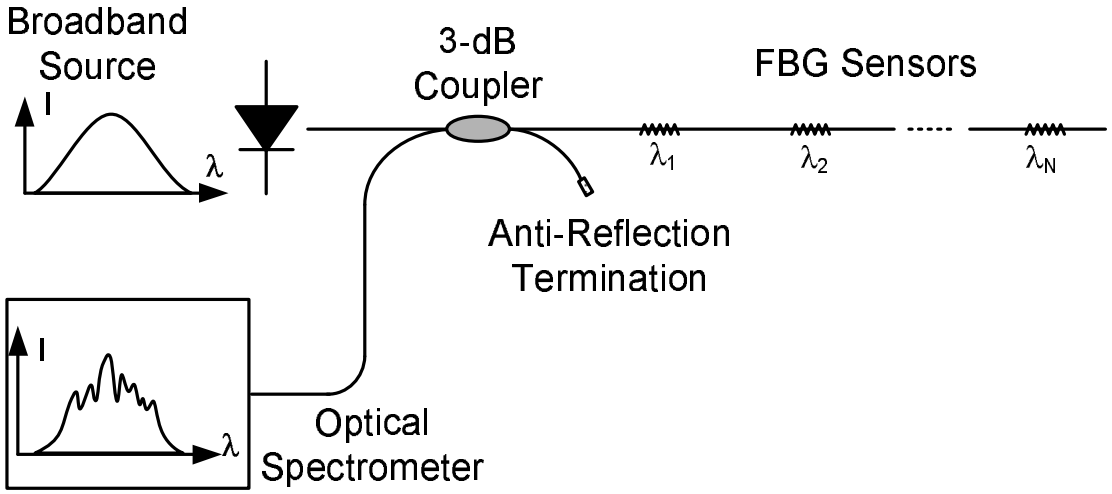

Figure 2.15: A WDM scheme for FBG sensors.

Sensors in a WDM scheme need to be designed to work at different wavelengths, which may increase the complexity of sensor design and fabrication. Due to the limited availability of light bandwidth, the multiplexing capacity of a WDM scheme is usually limited to a small number. For example, when FBG sensors are interrogated in a WDM scheme, each FBG needs to occupy a certain bandwidth that may be as large as several nanometers. The total available bandwidth of the light source is usually tens of nanometers. Thus the multiplexing number is limited by the ratio of the source spectral width over the spacing between two neighboring Bragg wavelengths.

2.3.5 Coherence Multiplexing

Coherence multiplexing is another important interrogation scheme for interferometric sensor arrays by using the coherence properties of the light from an optical source with a short coherence length. [89][90]

The core of the coherence-multiplexing scheme is the path-matched differential interferometric (PMDI) technique, which was first proposed by Al-Chalabi *et al.*[89] In a PMDI detection scheme, a broadband light emitting diode (LED) or a superluminescent light emitting diode (SLED), whose coherence length, L_c, is usually in order of micrometers to sub-millimeters, can be used as the light source, a receiving interferometer with an optical path imbalance of L_r is used to compensate the optical path imbalance, L_s, of a sensing interferometer. Both L_r and L_s are much larger than L_c. Thus either of the two interferometers alone will not give a significant interference fringe contrast. However, when L_r is arranged to be close to L_s, such that $|L_r - L_s| \ll L_c$, the tandem combination of the two interferometers will form a PMDI device and give a significant interference fringe contrast.

In a coherence multiplexed optical fiber sensor system, the path imbalance of each sensing interferometer is designed to be different from each other. One can use multiple receiving interferometers to path-match sensing interferometers simultaneously, as shown in Figure 2.16. One also can use a common receiving interferometer with tunable path imbalance to path-match sensing interferometers in series, as shown in Figure 2.17.

Coherence multiplexing is an elegant method for remotely interrogating a small numbers of interferometers including Mach-Zehnder, Michelson and Fabry-Perot sensors. However, as the number of multiplexed sensors increases, for the receiving interferometer, the light from unmatched sensing interferometers will give large intensity noise, thus signal to noise ratio for each sensor drops rapidly. Therefore, the multiplexing capacity of a coherence multiplexing system is usually limited to a small number.

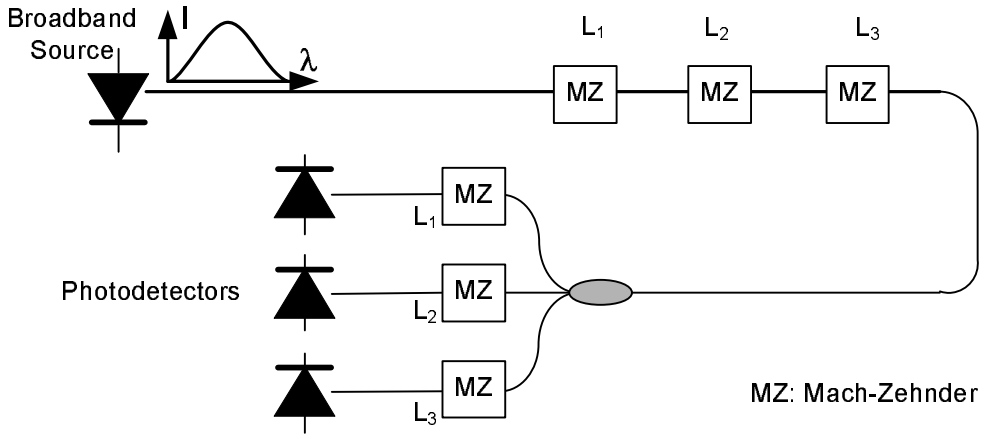

Figure 2.16: A CM scheme with multiple receiving interferometers.

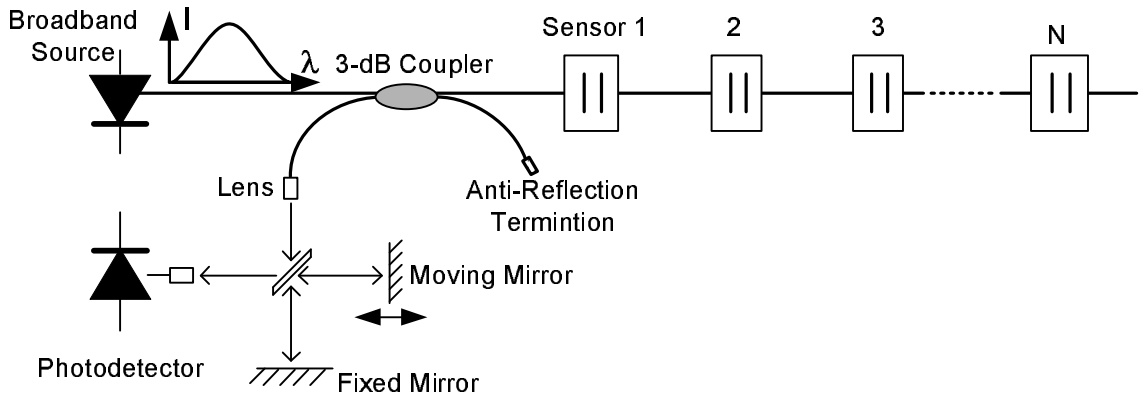

Figure 2.17: A CM scheme with a common receiving interferometer.

2.3.6 Other Multiplexing Schemes

There have been some other multiplexing schemes reported for optical fiber sensors, some of which include code-division-multiplexing (CDM) and spatial-division-multiplexing (SDM) schemes.

In a CDM scheme, the optical source is modulated using a pseudo-random bit sequence (PBRS) to generate a spread-spectrum signal. The locations of sensors are designed to be at delays that are multiple of the bit period. The received signals from the sensor array

are then encoded by delayed versions of the PBRS optical pulses. Synchronous correlation detection technique is used to extract individual signals from different sensors. CDM schemes for interferometric sensors have been reported.[91][92] CDM can be considered as a variant of conventional TDM. However, because a sequence of light pulses is used, stronger optical signals are produced at the output, thus the CDM method can provide better power budget than the TDM method.

In a SDM scheme, the light from a common source is split and directed to different locations for sensor interrogation. The sensors in a SDM scheme are addressed via different fiber links.[6] The most advantageous features of the SDM method include a balanced power budget for each fiber link and totally free of crosstalk between sensors.

2.3.7 Hybrid Multiplexing

Each of the multiplexing schemes discussed above has its advantages and disadvantages. For example, TDM scheme has a large multiplexing capacity but heavy crosstalk between sensors in a serial topology. WDM has low crosstalk between sensors but a poor multiplexing capacity. Thus one can use a combination to take advantages of both of them. TDM/WDM hybrid multiplexing has been applied to interferometric sensors[93][94] and FBG sensors[71]. Some other hybrid multiplexing schemes have also been developed. Dandridge *et al.* introduced a $J \times K$ scheme for the multiplexing of interferometric sensors.[79][80] It is actually a combination of the SDM and the FDM scheme. Farahi *et al.* demonstrated a combination of the TDM and the FDM.[95] Usually, the main purpose of a hybrid multiplexing scheme is to increase the number of sensors that can be multiplexed.

2.4 Summary

This chapter discusses the background of optical fiber sensors and their multiplexing schemes for distributed sensing. Two categories of distributed sensing systems, intrinsic distributed sensing and multiplexed point sensor networks, are introduced. Intrinsic distributed sensing systems usually use the Rayleigh, Raman, and Brillouin back scattered light to determine the perturbation along a fiber with a certain spatial resolution. Multiplexed point sensor networks measures the perturbation at certain locations of interest.

Section 2.2 introduces various kinds of optical fiber point sensors. The signal of a sensor in a sensor network can be modulated in intensity, wavelength, phase, or state of polarization. In-line fiber sensors, including FP interferometers and FBGs, are preferred in quasi-distributed temperature and sensing sensing.

The sensor arrangement topology, including serial, star, ladder, and the multiplexing schemes for optical fiber sensors, including FDM, FDM, WDM, CM, are discussed in Section 2.3

Chapter 3

UV-Induced Intrinsic Fabry-Perot Interferometric Sensors

In-line fiber Fabry-Perot interferometric (FFPI) sensors are good candidates for temperature and strain sensing and have attracted considerable interests in the past decade.[8]–[17] UV-induced FP sensors,[16]–[17] which feature low reflectance and low power loss, have the potential for large multiplexing capacity. However, the fabrication of UV-induced internal mirrors and the signal detection of low power reflection have been challenging tasks. In this chapter, after a brief review of FFPI sensors, the principle of operation and the fabrication system of UV-induced FP sensors are introduced. The performance of the sensor is analyzed with respect to the conditions of UV irradiation and the resultant refractive index profile along a fiber. The signal detection and demodulation method for UV-induced sensors are investigated.

3.1 Optical Fiber Fabry-Perot Interferometric Sensors

Fabry-Perot (FP) interferometric optic fiber sensors have been proven to be capable of temperature, strain, pressure and other physical parameter sensing with high sensitivity and resolution.[8]–[17] In order to multiplex a large number of sensors, in-line FP interferometers with low reflectance and low power loss are desirable.

Lee *et al.* demonstrated intrinsic FP interferometers (IFPI) by building dielectric mirrors into optical fiber.[8]–[10] Murphy *et al.* developed extrinsic FP interferometric (EFPI) sensors constructed by forming an air gap between end faces of two uncoated fibers inserted into an alignment tube. [11][12] Sirkis *et al.* introduced in-line fiber etalons by fusion splicing two fibers with a section of hollow core fiber of the same outside diameter.[13] Chen *et al.* introduced an IFPI sensor by constructing a pair of air-gap inside the fiber through HF-etching and fusion splicing.[14] These FP interferometers have been applied for various applications such as temperature, strain, and ultrasound sensing. But these interferometers usually have either relatively high reflectance or extensive insertion loss to the transmitted optical beam, thus the multiplexing capacity of these sensors are limited.

Greene *et al.* introduced UV-induced broadband Fresnel reflectors in hydrogen-loaded optical fiber and demonstrated optical time domain reflectometry (OTDR) based IFPI strain and temperature sensors.[15][16] These UV-induced IFPI sensors have the potential to be densely multiplexed because of their low reflectance and low power loss feature.

We developed a method to fabricate IFPI sensors by irradiating a masked UV beam onto the fiber side and proposed a spectrum based measurement system to measure the absolute optical path difference of an IFPI sensor by using a high-resolution swept laser interrogator.[17]

3.2 UV-induced Intrinsic Fabry-Perot Interferometric Sensors

The phenomenon of photosensitivity in a germanium doped silica fiber to UV irradiation has been widely used to make a variety of fiber components for communications and sensors.[18]–[20] In this research, this phenomenon is used directly to change the refractive index of a segment of a photosensitive fiber by exposing it to a UV laser. Local reflectors and IFPI sensors can be fabricated inside the fiber by this method.

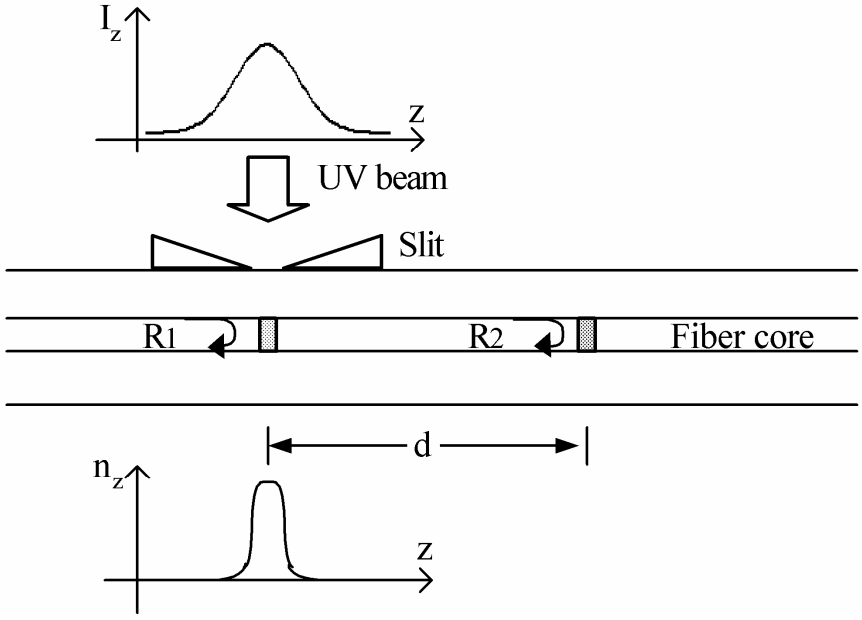

Figure 3.1: Structure of UV-induced IFPI sensor.

The basic structure and fabrication method of the UV-induced IFPI sensor are conceptually explained in Figure 3.1. A photosensitive single mode fiber is placed behind a masking slit and is illuminated on the side by a UV laser beam. Due to the photosensitivity of the fiber material, the refractive index of the exposed spot is permanently changed. This narrow segment of the fiber with the changed refractive index can then function as a broadband

Fresnel reflector. This Fresnel reflector will function as a partial mirror and reflect a portion of the incident light propagating in the fiber. A pair of such reflectors can therefore form an intrinsic Fabry-Perot interferometer.

The refractive index change caused by UV irradiation, Δn, is usually lower than 1%. The reflectivity at the UV-induced reflectors can be estimated as

$$R \approx (\frac{\Delta n}{2n})^2 \tag{3.1}$$

where n is the refractive index of the fiber core (for a typical single mode fiber, $n = 1.46$). The reflectivity, R, is usually lower than $-50dB$. An average reflectivity of -55dB can be obtained.

When a pair of reflectors is formed inside the fiber, they construct a low-finesse Fabry-Perot interferometer. Because of the low reflectance at each reflector, the FP interferometer can be approximated as a two-beam interferometer with all the multi-path interference neglected.

3.3 Sensor Fabrication

We developed an IFPI sensor fabrication system that consists of an excimer UV laser, optical components including a UV-grade mirror and a lens, a metal shadow mask, 3-D translation stages and a monitoring system. The diagram of the sensor fabrication system is shown in Figure 3.2.

A pulsed KrF excimer laser (MPB Communication Inc, MSX-250) with a 248nm wavelength is used as the UV source. A UV-grade mirror and a UV-grade lens are used to focus the laser beam onto the side of the photosensitive fiber. A pair of metallic blades are used to form a narrow slit that allows a small portion of the laser beam to pass through. The two blades are mounted onto 3-D stages. The slit width can be controlled by changing the positions of the two blades. The photosensitive fiber is placed behind the slit in contact with the metallic plates to reduce the influence of laser beam diffraction. The fiber is also mounted onto a

3-D translation stage so that the position of the laser writing point can be translated. The axial direction of the fiber is adjusted to be perpendicular to the metal slit. A microscope is used to observe the laser writing point so that the slit width can be monitored and the writing point can be visually inspected.

A high-resolution swept laser interrogator (HR-SLI) (Micron Optics, SI720), which functions as both a sweeping laser source and an optical spectrum analyzer, is used to monitor the sensor fabrication procedure. An optical circulator is used to couple the reflected light to the detector input port. The operating principle of the monitoring and measuring system will be explained in Section 4.2

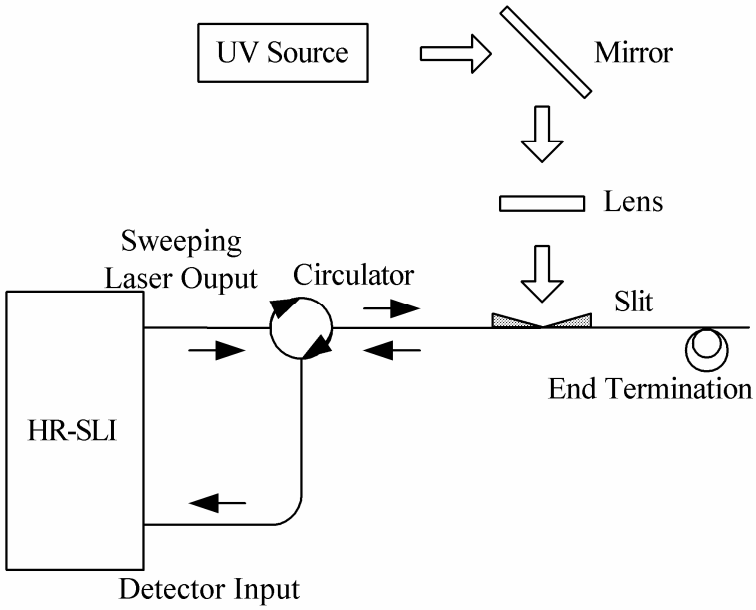

Figure 3.2: Diagram of IFPI sensor fabrication system.

The sensor fabrication procedure is described as follows. The photosensitive fiber, usually a piece of photosensitive fiber spliced between conventional Corning SMF-28 single mode fibers, is placed behind the slit that is close to the focus point of the lens. The end reflection of the fiber is eliminated by either curling the fiber end into a coil with a small diameter of several millimeters or immersing the fiber end into an index matching gel. At the beginning, the

signal detected by HR-SLI is the background reflection caused by the Raleigh backscattering in the fiber and the local reflection of the optical test system itself. The background reflection is lower than -60dB if the total fiber length is not very long. When the first reflector is written, the reflection at this writing point is in the range from -55dB to -50dB. When the second reflector is written, the interference fringes of the two reflections can be observed on the HR-SLI. Practically, an IFPI sensor with a cavity length from tens of micrometers to several centimeters can be fabricated.

The UV power density irradiated on the fiber is controlled to be $500mJ/cm^2$. The pulse duration is $20ns$. The repetition rate is set to $5Hz$. After hundreds of pulses, a significant refractive index change, which is 0.5% or higher, can be achieved.

Two kinds of commercially available photosensitive fibers, Thorlab GF1 and Newport S-FBG-15, as well as hydrogen loaded traditional SMF28 fiber, have been used to make IFPI sensors and all of them show satisfying photosensitivity.

A photograph of a fabricated IFPI sensor is shown in Figure 3.3. The laser writing points can clearly be seen due to the refractive index change of the fiber and the physical damage on the fiber side caused by the UV-irradiation. The distance between the two writing points is 1mm.

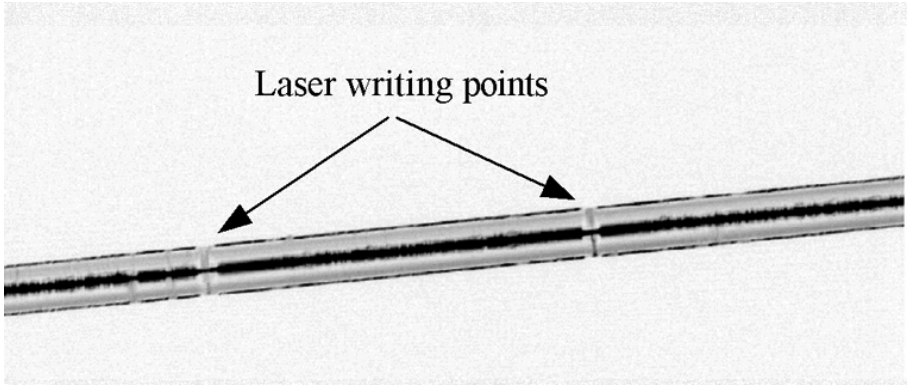

Figure 3.3: Photograph of a UV-induced IFPI sensor.

3.4 Photosensitivity of Fibers

Since the first observation of photosensitity in Germanium-doped fiber by Hill *et al.* in 1978,[96] the ability to inscribe Bragg gratings inside a fiber core has revolutionized the field of optical communications and fiber sensor technologies. Various kinds of optical components such as FBG based reflectors, Fabry-Perot FBG filters, chirped grating dispersion compensators and optical sensors such as FBG temperature and strain sensors and long period grating sensors have been reported.[18][20]

The photosensitivity of a Germanium-doped silica fiber is related to the concentration of the GeO bond defects in the fiber core. Although several models such as color-center, dipole, compaction, and stress-relief models have been established,[19] the mechanism of UV-induced refractive index change in a fiber is not fully understood. One classification of three types of photosensitivity was introduced based on the different UV irradiation conditions and different mechanisms. The three types of photosensitivity are Type-I, Type-IIA and type II, respectively.[97]

Type-I photosensitivity is a positive refractive change under low power density UV irradiation with continuous-wave (CW) laser or pulsed excimer laser. The refractive index of fiber core increases linearly to the irradiation time at first and then becomes saturated. The refractive index change of Type-I photosensitivity is low. A typical refractive index change of a standard fiber using a CW laser operating at $244nm$ is 2.5×10^{-4}.

Type IIA photosensitivity is a negative refractive change caused by long duration UV irradiation with relative low power density. In a Type-IIA regime, the initial first order grating of Type-I may be completely erased, a second order grating forms a demarcation between Type-I and type-IIA. The refractive index change of Type-IIA can be in the order of 1×10^{-3}.

Type-II photosensitivity is known as large positive refractive index change under high power density UV irradiation. Physical damages are caused in the core-cladding interface of the fiber on the side of laser writing beams. A pulsed excimer laser at 248 nm is usually used.

The energy density of a laser pulse may be as high as $1J/cm^2$. A threshold of $650mJ/cm^2$ has been reported. When the energy density is lower than this threshold, the refractive index change is small and is linear to the light power. However, when the energy density of the laser is above the threshold, the absorbed energy is high and triggers off a highly nonlinear mechanism, which initiates physical damage in a fiber and cause a dramatic refractive index change. Compared with Type-I and Type-IIA, Type-II photosensitivity can cause large refractive index change of 1% in fewer laser pulses, thus shortening the laser writing time. Type-II gratings have been fabricated by using a single laser pulse.

Different photosensitivity types have different thermal stabilities. Type-I gratings can withstand a temperature of 250^oC. In a higher temperature, the refractive index change in a Type-I grating will be reduced or even totally erased. Most FBG sensors are in Type-I regime and thus cannot work in a high temperature environment. Type-IIA gratings, which can withstand a temperature of 500^oC, have better thermal stability. Type-II gratings can withstand a temperature as high as 800^oC and thus can be used in a high temperature environment.

Table 3.1 compares the UV irradiation condition and the resulted refractive index change of the three kinds of photosensitivities. Their thermal stabilities are also compared.

Table 3.1: Photosensitivity of fibers.

Categories	UV laser	Power density	Typical Δn	Thermal stability
Type-I	CW or Pulsed	Low($100mJ/cm^2$)	2.5×10^{-4}	$< 250^oC$
Type-IIA	CW or Pulsed	Low($100mJ/cm^2$)	1×10^{-3}	$< 500^oC$
Type-II	Pulsed	High($1J/cm^2$)	up to 1×10^{-2}	$< 800^oC$

Unlike a Bragg grating, which contains thousands of periodical reflectors that are in-phase and may have a high reflectivity at certain wavelengths, the reflectors in a UV-induced FP interferometer cause a single-point reflection with the reflectivity depending on the change

of refractive index at the writing point. Type-I refractive index change is so small that the reflection from the laser writing point (-80dB) can hardly be detected. Although Type-IIA gives larger refractive index change, it needs a long UV irradiation time and the reflection from the laser writing point is still very low (-70dB). In practice, only the reflection of a Type-II refractive index change can be detected with a reasonable signal to noise ratio.

The physical damage in a Type-II sensitivity, which can be clearly seen under a microscope as Figure 3.3 shows, will reduce the mechanical strength of the fiber. High-energy laser pulses may also cause damages to the cladding of the fiber. Thus in the fabrication of UV-induced reflectors, the laser power has to be carefully controlled for both large refractive index change and good fiber mechanical strength. In this research, a moderate energy density around the damage threshold of Type-II photosensitivity is used. The UV irradiation is controlled by adjusting both the laser energy density and the number of laser pulses.

3.5 Refractive Index Profile Analysis

The performance of an IFPI sensor depends on the reflection at the laser writing point, which is determined by the UV-induced refractive index profile along the fiber axis. As shown in Figure 3.1, the refractive index profile n_z along the fiber depends on the intensity pattern of the UV beam, the position and size of the shadow mask and the photosensitivity of the fiber. For improved sensor performance, each laser writing point should behave as a broadband reflector with equal reflectance in a certain wavelength range, and the reflectivity of the reflectors should be as high as possible for a given UV-induced index change.

The reflectivity of a UV-induced reflector given in Eq. 3.1 is based on an ideal step change of refractive index. However, the refractive index profile along the fiber looks like a wall with rounded edges because of the UV beam diffraction and the photosensitivity of the fiber. The continuously varying refractive index changes at these edges make the reflection more complex than that of an ideal boundary between two media.

A multilayer sliced model, in which the refractive index profile is treated as a multilayer thin-film structure, is utilized to analyze the influence of the refractive index on the performance of the sensor. The model is illustrated in Figure 3.4.

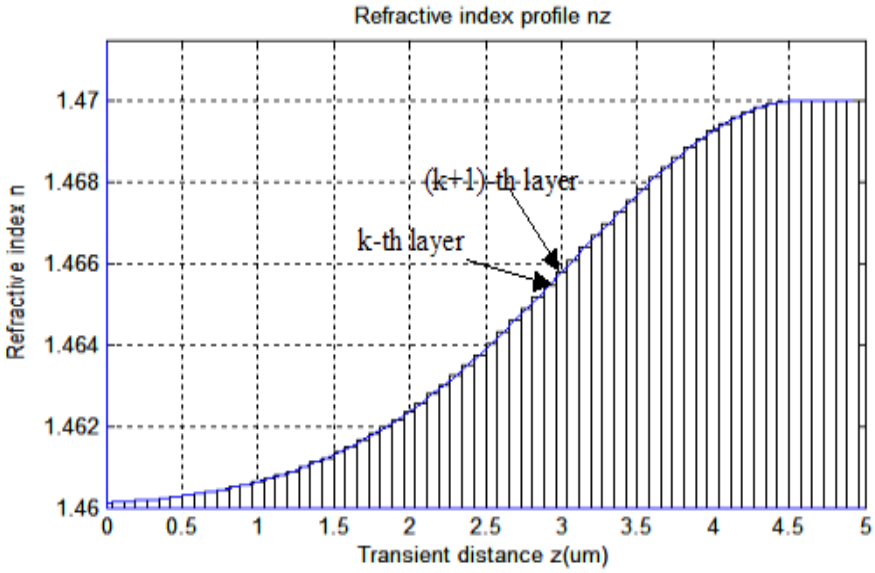

Figure 3.4: Multilayer model of the refractive index profile.

An impedance transformation method is used to calculate the input impedance and the reflection coefficient of the multilayer model.[98] The multilayer structure has a starting refractive index of n_s, an ending refractive index of n_r, and N layers between them. Assuming the impedance of the k-th layer is η_k, and the impedance of the starting and ending regions are η_s and η_r, respectively, the input impedance at the front surface of the k-th layer can be calculated iteratively by

$$\eta_{in,k} = \eta_k \frac{\eta_{in,k+1} + j\eta_k tan(\frac{2\pi}{\lambda} n_k d_k)}{\eta_k + j\eta_{in,k+1} tan(\frac{2\pi}{\lambda} n_k d_k)} \qquad (k = 1, 2, \cdots, N) \tag{3.2}$$

where n_k and d_k are the refractive index and the length of the k-th layer respectively, and λ is the wavelength of the light. The impedance of the k-th layer is

$$\eta_k = \frac{\eta_0}{n_k} \tag{3.3}$$

where $\eta_0 = 377\Omega$ is the impedance of the vacuum. The initial value of the iteration is the impedance of the ending region of the the multilayer structure

$$\eta_{in,N+1} = \eta_r = \frac{\eta_0}{n_r}. \tag{3.4}$$

The reflectivity of the multilayer structure can be calculated by

$$R = |\frac{\eta_{in,1} - \eta_s}{\eta_{in,1} - \eta_s}|^2 \tag{3.5}$$

The reflectivity of one edge for some typical index profiles at different wavelengths are calculated and are shown in Table 3.2. The refractive index of the fiber is assumed to change from 1.46 to 1.47 and the varying distance is assumed to be $5\mu m$. This model clearly demonstrates that the performance of a sensor is dependent on the refractive index profile along the fiber axis.

It can be seen that a sharp step refractive index change will give a relative high reflectivity while a continuously varying refractive index profile will greatly lower the reflectance of the writing point. Thus a refractive index profile with a sharp step change is desired. Although we used a pair of blades to form sharp edges, the edges of the light beam were blurred due to the diffraction of the UV beam. When a reflector is written, the fiber is in contact with the metal blades so that the distance between the fiber core and the blades is as short as possible and thus the influence of the UV beam diffraction is reduced to minimum.

For Type-I and Type-IIA photosensitivity, in which the refractive index changes are proportional to the light intensity or square of light intensity, it is hard to make a sharp edge reflector because of both the low refractive index change and the continuously varying refractive index profile. Type-II photosensitivity, which is based on highly non-linear physical damage inside a fiber and has a damage threshold, can generate a sharp edge of refractive index change and thus a broadband reflector with detectable reflectivity.

Table 3.2: Reflection at the edge for different refractive index profiles.

Profile	Edge	Reflection at the edge
Step	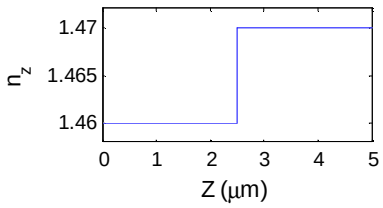	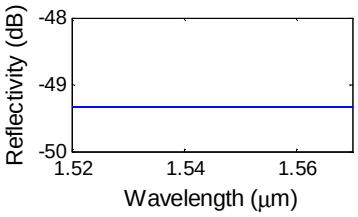
Gaussian	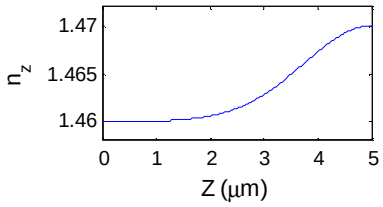	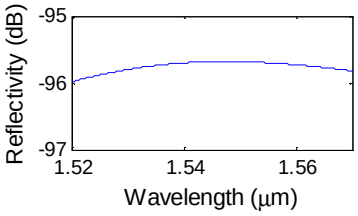
Linear	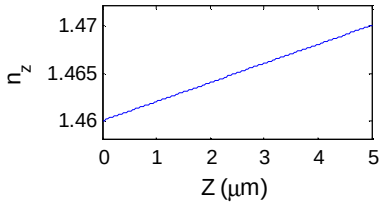	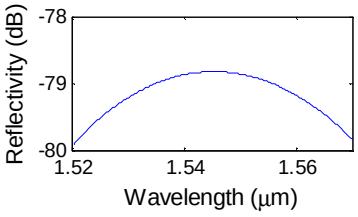

3.6 Sensor Signal

Single Edge Reflectors

In experiment, an asymmetric UV-irradiation condition is used to make a single edge reflector, which contains a sharp edge that gives significant reflection and a blurred edge on the other side with negligible reflection. An asymmetric condition can be obtained by controlling the shape of the mask slit and the power distribution of the UV laser beam. Some of the methods include

- Non-parallel slit edge

This method is to tilt the edge of one metallic plate such that a tilted refractive index edge can be inscribed inside the fiber. The reflection of the tilted edge will not be guided back.

- Back-positioned slit edge

  This method is to adjust the distance between the metallic plate and the photosensitive fiber. When the positions of the two metallic plates are not the same, the diffraction pattern of the UV beam at the two slit edges will be different and thus the refractive index profile might be controlled.

- UV power distribution control

  The intensity profile of the UV laser beam has a Gaussian-like shape. One can locate the mask slit onto the slope of the profile and thus obtain different power distributions at the two edges.

With properly tuned UV irradiation conditions, it is possible to obtain a broadband reflector with only one edge having significant reflectivity. This kind of single-edge reflector is optimal and the FP interferometer construed by a pair of such single-edge reflectors is simply a low-finesse FP interferometer.

The optical path difference (OPD) between the two reflectors in a FP interferometer is

$$L = 2n_e d \tag{3.6}$$

where d is the distance between the two reflectors and n_e is the effective refractive index of the fiber at the operating wavelength.

When the low-finesse FP interferometer is approximated to a two-beam interferometer, the interference between the reflected beams from the two partial mirrors at a wavelength λ is approximately given by

$$E = E_0[\sqrt{R_1} + \sqrt{R_2}exp(j(kL + \phi)] \tag{3.7}$$

$$I(k) = I_0(k)[R_1 + R_2 + 2\sqrt{R_1 R_2}cos(kL + \phi)] \tag{3.8}$$

$$k = \frac{2\pi}{\lambda} \tag{3.9}$$

where $I(k)$ is the reflected light power, $I_0(k)$ is the power of incident light, R_1 and R_2 are reflectivities of the two reflectors, ϕ is a constant phase term, k is the wave number, and λ is the wavelength of the light.

When the reflectivity

$$R(k) = \frac{I(k)}{I_0(k)} = R_1 + R_2 + 2\sqrt{R_1 R_2}cos(\frac{2\pi}{\lambda}kL + \phi) \quad = A + Bcos(kL + \phi) \tag{3.10}$$

is measured in a certain wave number range, it is a sinusoidal signal with a frequency of L, a phase of ϕ, a DC term of $A = R_1 + R_2$, and an amplitude of $B = 2\sqrt{R_1 R_2}$. The absolute OPD of the sensor, L, can be determined by estimating the frequency of the sinusoid.

Double Edge Reflectors

As shown in Figure 3.1, a UV-induced reflector contains two edges. If both edges give significant reflections, the reflector is then a local Fabry-Perot interferometer and its reflection is then wavelength dependent, which is not desired.

Although an asymmetric UV irradiation condition is used to make single-edge reflectors, the high non-linear feature of the physical damage based Type-II photosensivy makes it difficult to obtain complete control of the refractive index profile at the edges. A single-edge reflector may not be always obtained. Sometimes, even when a single-edge reflector is fabricated, a few more UV pulses will cause reflection from the other edge. Thus, it is preferable that the non-ideal signal caused by double edge reflections can be demodulated.

To simplify the signal analysis, the interference of a double edge reflector and a single edge reflector is investigated as Figure 3.5 shows.

Similar to Eq. 3.10, the normalized interference signal between the reflectors can be given

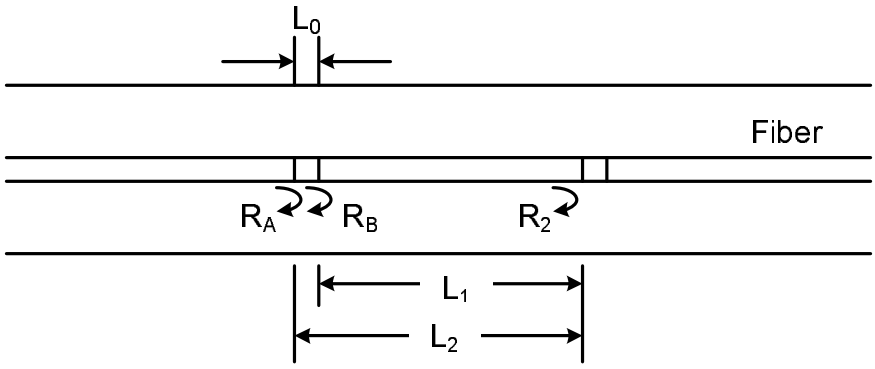

Figure 3.5: Interference between a double edge reflector and a single edge reflector.

by

$$\begin{aligned} R(k) = R_A + R_B + R_2 + 2\sqrt{R_A R_B}cos(kL_0 + \phi_0) \\ + 2\sqrt{R_B R_2}cos(kL_1 + \phi_1) + 2\sqrt{R_A R_2}cos(kL_2 + \phi_2) \end{aligned} \tag{3.11}$$

where L_0, L_1 and L_2 are the OPDs between the reflections at different edges. It is evident that there are three sinusoidal components with respect to wave number k.

The width of the laser writing point is much shorter than the distance between reflectors, thus $L_0 \ll L_1, L_2$, which means that the sinusoidal term with frequency L_0 is of low frequency and can be filtered out when the sensor signal is processed.

The sinusoids with frequencies L_1 and L_2 are so close that they can not be separated from each other, The measured signal is actually the beating of the two frequencies. If R_A and R_B are assumed to be equal, then the beating signal can be given by

$$cos(kL_1 + \phi_1) + cos(kL_2 + \phi_2) = cos(k\frac{L_2 - L_1}{2} + \frac{\phi_2 - \phi_1}{2})cos(k\frac{L_2 + L_1}{2} + \frac{\phi_2 + \phi_1}{2}). \tag{3.12}$$

The beating signal can be regarded as an amplitude modulated (AM) signal with an envelope of $cos(k\frac{L_2 - L_1}{2} + \frac{\phi_2 - \phi_1}{2})$ and a carrier frequency of $\frac{L_2 + L_1}{2}$. The carrier frequency $\frac{L_2 + L_1}{2}$ can be regarded as the effective OPD of the sensor and can be determined by using the frequency estimation method discussed in Chapter 5.

3.7 Signal Detection

For UV-induced IFPI sensors, there are two kinds of detection methods: intensity based detection and spectrum based detection. They will be discussed as follows.

3.7.1 Intensity-based Detection

One can use a narrow band laser to illuminate the sensor and monitor the intensity of the reflected light that is modulated by the perturbation. The measurand such as temperature and strain will affect the OPD of the sensor, thus change the output intensity of Eq. 3.8. The phase change caused by the measurand is restricted to be in the range of π, and the operation point of the sensor is located on a single slope of an interference fringe. To obtain the maximum sensitivity I to L, either λ or ϕ or initial L needs to be adjusted to enable the phase term in Eq. 3.8 to work at the operation point around $\pi/2$.

When an IFPI sensor is fabricated, it is hard to control L and ϕ accurately. Thus the operation point of the sensor for a given λ cannot be controlled exactly. If a tunable laser is used, one can tune λ to obtain an optimal operation point. However, for multiplexed IFPI sensors, it is difficult to obtain optimal operation points for all the sensors.

The output intensity of a sensor in Eq. 3.8 is also related to the reflectivities of R_1 and R_2, which are not the same for all sensors in a multiplexed sensor system. Thus one has to maintain a calibration curve for each sensor in the system, which is difficult for a multiplexed sensor system with a large number of sensors.

Intensity-based detection method also suffers from the instability of the light source, whose intensity and wavelength may vary. For example, the intensity and wavelength of a laser source are affected by variation of the laser driving current and the ambient temperature. The bending loss of the fiber and the power loss at connectors in the fiber link will also affect the performance of an intensity-based detection method. In a serially arranged sensor array,

the power loss of each sensor will affect the received signals of sensors behind. All these factors make it difficult to implement an intensity-based detection scheme with satisfactory performance for a multiplexed IFPI sensor array.

3.7.2 Spectrum-based Detection

A more attractive technique is the spectrum-based measurement method that measures the the sensor's response to different wavelengths and determines the sensor's absolute optical path imbalance. The measurand is determined by measuring the change of the OPDs of the sensors.

Usually, the spectrum of an interferometer can be measured by illuminating it with a broadband light source. A broadband light source such as a LED or a SLED can be used as the light source. A fringe pattern is produced by the light transmitted by or reflected from the sensor and recorded either spectrally by an optical spectrum analyzer (OSA) or temporally by a photodiode (PD) in a scanning interferometric system.[99][100] For UV-induced IFPI sensors, this method is difficult to be used. The light power of a broadband source, when coupled to a single mode fiber, is usually low. The total output power of a LED source and a SLED source are typically tens of microwatts and a few miliwatts. The light power at a single wavelength is low, usually a few microwatts per nanometer. The reflectivity of a UV-induced IFPI sensors is very low, typically $-55dB$. Thus the light power collected by the detector at a single wavelength is so low that it may be below the detection limit.

An alternative method to measure the spectral response of an interferometer is to use a tunable laser as the light source and to measure the spectrum at different wavelengths in series. A laser can have a high power output from the order of milliwatts to hundreds of watts and a narrow bandwidth of from the order of kilohertz to gigahertz. In Chapter 4, a swept laser based measurement system to measure the spectral response of UV-induced IFPI sensors will be discussed.

The spectrum-based detection method for interferometric sensors has several advantages. First, when the measurand is determined from the OPD of the sensor, L, it is independent on R_1, R_2 and ϕ in Eqs. 3.8. Thus once the relationship between the measurand and L is obtained, it can be applied to all of IFPI sensors interrogated. One does not need to maintain calibration curves for individual sensors as required in an intensity based detection scheme. Secondly, the intensity and wavelength variations of the light source, which have different frequencies from the sensor signal, can be compensated. In the measurement system that will be discussed in Chapter 4, intensity and wavelength references are accomplished. Furthermore, the intensity variation of the light source has low frequencies and can be separated from the sensor signal via the signal processing method that will be discussed in Chapter 5. Third, spectrum-based system is tolerant to the bending loss of the fiber and the power loss at the connectors because of their independence on wavelength.

A comparison of intensity-based measurement and spectrum-based measurement is listed in Table 3.3

Table 3.3: Comparison of intensity-based and spectrum-based measurement.

Items	Intensity Based	Spectrum Based
Absolute OPD measurement	No	Yes
Wavelength of light	Fixed single line	In a certain range
Operation point control	Needed	Not needed
Maximum phase change	$< \pi$	Not limited
Calibration	Sensor by sensor	Single calibration curve
Influence of power loss	Yes	No
Influence of source variation	Yes	No
High speed signal measurement	Yes	Limited

3.8 Summary

This chapter discusses the principle of operation of the UV-induced IFPI sensors. The sensor fabrication system and the fabrication procedure are introduced. The photosensitity of the fiber, the UV irradiation conditions, and the performance of the UV-induced reflectors are discussed. The signal of the sensor and the detection methods are investigated.

Chapter 4

Frequency Division Multiplexing Scheme

This chapter presents a spectrum based measurement system and a FDM scheme in which multiple IFPI sensors with different cavity lengths are multiplexed in a serial topology. The FDM scheme uses a FMCW technique to measure the mixed interference spectrum of multiple IFPI sensors, which has multiple frequency components corresponding to different sensors with different OPDs. The OPD of the IFPI sensors can be determined by estimating the frequency and phase information of these frequency components.

4.1 Multiplexing of Fabry-Perot Sensors

In-line fiber Fabry-Perot interferometric sensors can be arranged as a sensor array along a single fiber and thus can be configured for quasi-distributed sensing. Theoretically, FFPI sensors can be multiplexed in any of the multiplexing schemes discussed in Section 2.3 such as TDM, FDM, WDM, and CM. Multiplexed EFPI sensors in TDM, CDM, CM, and FDM schemes have been reported for temperature and strain sensing.[76][101][102][103][104]

However, the multiplexing of FFPI sensors has gained little success due to the relatively high power loss of the sensor. IFPI sensors with dielectric mirrors are difficult to fabricate and usually have high reflectivity. EFPI sensors formed by air-glass interfaces usually have high power loss at each sensor. Thus the multiplexing of FFPI sensors is limited to a small number usually less than ten. Wan *et al.* reported a multiplexing system of 3 dielectric mirror based IFPI sensors for temperature measurement.[104] Singh *et al.* reported a multiplexing system of 6 air gap based EFPI sensors for strain measurement.[76]

UV-induced FP sensors have low reflectivity and low insertion loss and thus have the potential to be densely multiplexed. However, due to the low reflectivity, the signal to noise ratio is low and thus the signal detection and signal processing have been challenging tasks. Greene *et al.* demonstrated an OTDR based method for 3 sensors to measure the reflectance of the IFPI sensors at a given wavelength or counting the fringe numbers due to the parameter changes.[16] Neither of these measurement methods is satisfying for practical applications. The intensity-based measurement has their drawbacks as discussed in Section 3.7. In the fringe counting method, the cavity lengths of IFPI sensors were designed to be as long as centimeters. When temperature or strain is changed, large phase change occurs, which may cover several interference fringes. The variation of temperature or strain is determined by counting the change of fringes. This method measures the variation of the measurand instead of the absolute value and its measurement accuracy is very poor.

This research uses a swept laser based spectrum measurement system to measure the normalized interference patterns of the sensors and uses a FDM scheme to multiplex UV-induced IFPI sensors along a single fiber.[22][23] The absolute OPD can be determined with a high accuracy.

4.2 Measurement System

The reflected light power from a UV-induced IFPI sensor is rather low (-55dB to -50dB). It is difficult to measure the interference spectrum by means of conventional methods that utilize a low-coherence light source and passive optical spectrum analyzers. In this research, a high resolution swept laser interrogator (HR-SLI, Micron Optics Si720), which contains a swept laser source, photodetectors, intensity and wavelength reference units, and supporting electronic circuits in a single standalone box, is used for the optical spectrum measurement. A diagram of the measurement system for UV-induced IFPI sensors is shown in Figure 4.1.

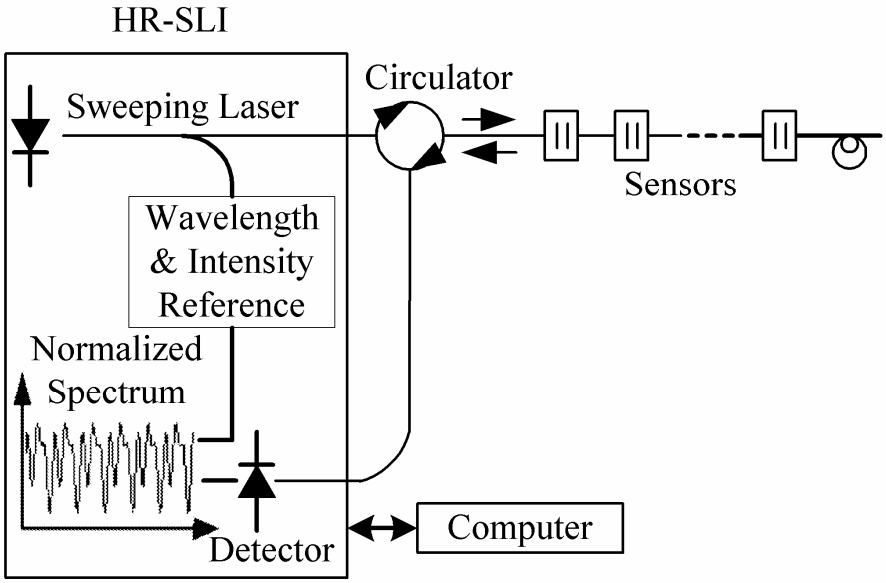

Figure 4.1: Diagram of the measurement system.

Continuous-wave coherent light from a swept laser is launched into an optical circulator, which transmits the light to the IFPI sensors. At each sensor, part of the light is reflected back to the circulator. The circulator then couples the reflected light to the photodetector. The wavelength of the laser output is swept in a range of 1520-1570 nm with a 2.5 pm wavelength step. 20,000 steps are sampled during one sweeping cycle of the laser source. The spectral responses of the IFPI sensors at these wavelength steps are measured. A portion

of the light is tapped from the light source inside the HR-SLI. The intensity and wavelength of the tapped light are then measured for intensity and wavelength calibrations. Thus the normalized interference fringes of the IFPI sensors can be measured in each sweeping period of the laser source. The laser is operated to finish a sweep in $200ms$. The average power injected to the fiber is $1mW$. The line width of the laser is $500MHz$.

The measured interference spectrum is transferred to a personal computer for signal processing via a GPIB or a TCP/IP interface. Both a Matlab program and a multi-threaded C/C++ win32 program running on the host computer were written to retrieve the spectrum from the HR-SLI and perform the signal processing tasks.

4.3 FDM Scheme

4.3.1 Sinusoidal Signal

From Eqs. 3.8 and 3.10, the measured normalized interference spectrum for a single IFPI sensor can be written as

$$R_n = A_n + B_n \cos(k_n L + \phi) + \upsilon_n \qquad n = [0, 1, \cdots, N-1] \tag{4.1}$$

where R_n is the reflectivity at wave number k_n, υ_n is the measurement noise, and N is the number of total samples.

Although the effective refractive index, n_e in Eq. 3.6, is not the same at all wavelengths for a dispersive silica fiber, it can be reasonably assumed to be constant in a small wavelength range. Thus the OPD L can be regarded as a constant in each sample of the interference spectrum. When the UV-induced partial mirrors are ideal broadband Fresnel reflectors, their reflections are wavelength independent, and thus A_n and B_n are constants for all wave numbers. Thus the normalized interference spectrum contains a pure sinusoid signal corrupted by measurement noise. When the partial mirrors are not ideal, A_n and B_n are

dependent on wave numbers. However, A_n and B_n are of low frequencies and can be separated from the signal frequencies (L).

Assuming that the laser source is swept linearly in wave numbers from a starting wave number of k_0 and a wave number step of k_s, then the interference spectrum can be written as

$$R_n = A_n + B_n \cos((k_0 + nk_s)L + \phi) + \upsilon_n = A_n + B_n cos(\omega_0 n + \phi_0) + \upsilon_n \tag{4.2}$$

$$\omega_0 = k_s L \tag{4.3}$$

$$\phi_0 = k_0 L + \phi \tag{4.4}$$

where ω_0 is the normalized radian frequency.

It is evident that L and ϕ can be derived by estimating the frequency and phase of the sinusoid described in Eqs. 4.1 and 4.2.

4.3.2 Multiplexing

As Figure 4.1 shows, multiple IFPI sensors can be arranged serially along a single fiber. If the sensors have different OPDs from one another, the measured interference spectrum will have multiple frequencies corresponding to sensors with different cavity lengths according to Eq. 4.1. By estimating frequency and phase information of each frequency component, we can determine the OPD of each IFPI sensor. It is evident that this kind of multiplexing scheme is derived from the traditional frequency division multiplexing technique in which signals occupy different frequency channels.

Figure 4.2 shows the multiplexing results of twenty IFPI sensors. The OPDs of these IFPI sensors were in the range of $3165\mu m$ to $7627\mu m$ with an approximately $235\mu m$ difference between adjacent OPDs.

The top graph shows the interference spectrum measured by the HR-SLI. The bottom graph shows the fast Fourier transformation (FFT) result of the interpolated interference spectrum.

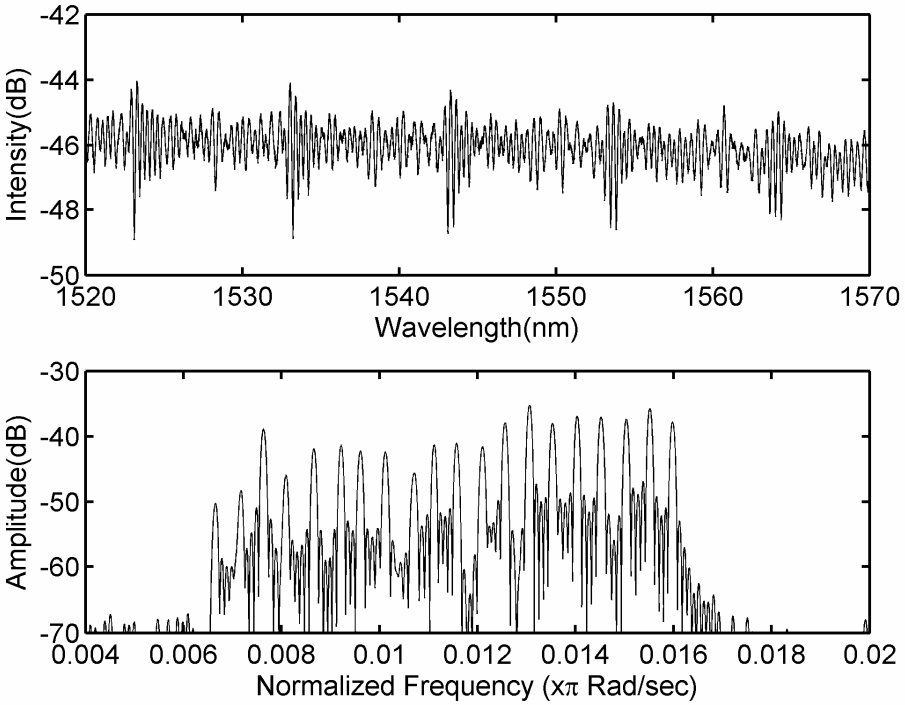

Figure 4.2: Experimental results of 20 IFPI sensors.

The horizontal axis of the bottom graph is the normalized frequency, which is the ratio of signal's frequency to Nyquist frequency. Different peaks show the frequency components from different sensors.

4.3.3 Signal of a sensor array

If the distance between any two sensors is larger than the coherence length of the light source, the photodetector in the HR-SLI will not see the interference between the reflections from different sensors. The interference spectrum measured can be expressed as

$$R_n = \sum_{j=1}^{J}[A_j + B_j cos(\omega_j n + \phi_j)] + \upsilon_n = \sum_{j=1}^{J} A_j + \sum_{j=1}^{J} B_j cos(\omega_j n + \phi_j) + \upsilon_n \qquad (4.5)$$

where J is the number of sensors, A_j, B_j, ω_j and ϕ_j are the dc part, amplitude, frequency and phase of the sinusoidal signal form the j-th sensor, respectively, and υ_n is the noise term of the measurement.

If the distance between two sensors is shorter than the coherence length of the light source, then the reflections from the first sensor will interfere with the reflections from the second sensor. There will be some unexpected frequency components corresponding to the reflection pairs from different sensors. The interference spectrum from multiplexed sensors can be given as

$$R_n = \sum_{j=1}^{J} A_j + \sum_{j=1}^{J} B_j cos(\omega_j n + \phi_j) + \sum C_{ij} cos(\omega_{ij} n + \phi_{ij}) + \upsilon_n \tag{4.6}$$

where A_j, B_j and J are the same as Eq. 4.5, C_{ij}, ω_{ij}, and ϕ_{ij} are the amplitude, frequency and phase of the frequency component caused by the interference between Fresnel reflections of i-th and j-th sensor.

The distances between sensors, which are usually in the range of tens of centimeters to meters, are much larger than the cavity lengths of the sensors. Therefore, ω_{ij} in Eq. 4.6 are usually much larger than ω_j. These additional frequency components are high frequency noise to the signal from the sensors and can be filtered out by using properly designed digital filters.

One can design a bandpass filter to select the j-th frequency components and filter other frequency components out. Then the frequency and phase of the j-th sensor can be estimated by the frequency estimation method discussed in Chapter 5.

4.3.4 Sensor array design

Sensor spacing

The line width of the laser source is $500MHz$, thus the coherence length of the light source is

$$L_c = \frac{c}{\Delta f} = \frac{3 \times 10^8}{500 \times 10^6} = 0.6m \tag{4.7}$$

The refractive index of the fiber is 1.46. From Eq. 3.6, if the distance between sensors exceeds $0.21m$, then the optical path difference between the reflectors of different sensors will be larger than L_c. Then the interference between different sensors cannot be observed. However, if the distance between sensors is comparable to the cavity length of IFPI sensors, then the interference between different sensors may cause unpredicted influence to the signal from sensor. Therefore, the cavity length of each sensor and distances between them must be carefully designed to avoid the influence of unexpected frequency components. One simple rule is that the minimum distance between sensors should be much larger than the maximum cavity length of sensors.

OPDs of sensors

The IFPI sensors are designed to have moderately long OPDs in the range of hundreds of micrometers to a few centimeters. An IFPI sensor with a very large OPD will show low interference fringe contrast due to the limited coherence length of the light source and the birefringence of the fiber. The signal of a sensor with a very short OPD will be influenced by the low frequency noise in the system.

In order to separate the frequency components corresponding to different sensors, the OPDs have to be designed to be of certain frequency spacing. For a non-parametric frequency estimation method such as Discrete Fourier Transform method demonstrated in Figure 4.2, the frequency resolution is restricted by the Rayleigh limit of $1/N$ where N is the total length

of the data samples. In this research, band pass filters are used to select individual frequency components. The filter itself has to occupy a certain bandwidth. In practice, the frequency spacing between adjacent frequencies can be designed to $(4-5)/N$. From Eq. 4.3, the OPD difference between adjacent frequency components can be designed to be about $200\mu m$

4.3.5 Further Discussion

The principle of this FDM scheme is derived from the FMCW technique discussed in Section 2.3.3. In a FMCW approach, the optical frequency of a continuous wave laser source is linearly swept. The frequency-chirped light reflected from the test point will beat with the light reflected from the local reference point. The beat frequency f_b can be expressed as

$$f_b = \frac{2n_e d}{c}\frac{f_s}{T} \tag{4.8}$$

where f_s is the frequency deviation of the light source, T is the chirp period, d is the distance between the test and reference points, and c/n_e is the light speed in the medium. The distance between the test point and the reference point can be estimated by measuring the beating frequency of the two reflections. For a certain measurement resolution of beat frequency, the measurement resolution of d is inversely proportional to the frequency sweeping rate of the light source, f_s/T. The larger the frequency sweeping speed of the light source, the higher the measurement resolution of d.

In the measurement system shown in Figure 4.1, no local reference point is used. The beat notes are actually sub-carriers generated by the chirped optical frequencies reflected from the two reflectors of an IFPI sensor. The beat frequency can be written as

$$\omega_b = \frac{2n_e d}{c}\frac{\omega_s}{T} = \frac{\omega_s}{Tc}2n_e d = k_s L \tag{4.9}$$

where $k_s = \dfrac{\omega_s}{Tc}$ is the wave number sweeping rate, and $L = 2n_e d$ is the OPD of the FP cavity. It is evident Eq. 4.9 is equivalent to Eq. 4.3.

Conventional FMCW systems usually change the optical wavelength by modulating the driving current of a laser diode. The wavelength variation is in the order of picometers.

The modulation of driving current also causes an intensity modulation, which is an envelope modulation to the carrier frequency, and will cause extra noise to the measurement. HR-SLI uses an optical tunable filter to change the wavelength of a fiber laser from 1520nm to 1570nm in a 200ms period. The frequency sweeping rate of HR-SLI is much higher than conventional FMCW systems and thus much higher measurement resolution of L and be obtained.

Usually, only the beat frequency is measured in conventional FMCW systems. The phase of the beat signal is ignored. This will restrict the resolution for the distance measurement. In the system shown in Figure 4.1, because a wavelength reference is provided, the absolute wave number at each sample point as well as the wave number sweeping rate can be obtained. Therefore, one may estimate both the frequency and the phase of the measured signal, and thus achieve higher measurement resolution. In this research, a relative measurement accuracy of L, which can be as high as 0.5×10^{-6}, is obtained. Experimental results will be demonstrated in Chapter 5.

4.4 Multiplexing Capacity

The sensor multiplexing capacity along a single fiber is determined by two factors: the system power budget and the bandwidth budget in frequency domain.

4.4.1 Power Budget

If the power loss of each sensor is controlled to be very low, then for a certain dynamic range, which is the allowable power loss from the original signal level to the detection limit of the system, more sensors can be multiplexed. The multiplexing capacity limited by power budget can be given by

$$J_P = \frac{P_s - P_l}{\eta} \tag{4.10}$$

where P_s is the signal in dBm, P_l is the detection limit in dBm, and η is the power loss in dB at each sensor.

The HR-SLI used in the measurement system has an average power output of 0 dBm and a dynamic range of 80dB. The average reflectivity of a UV-induced IFPI sensor is about $-55dB$, thus the power budget for the measurement system is about 25dB. Currently, the insertion loss of a sensor can be controlled to be as low as 0.1dB. Thus assuming the transmission loss between sensors is negligible, the multiplexing capacity is limited to about 250 by the power budget.

4.4.2 Bandwidth Budget

The multiplexing capacity of the FDM scheme is determined by the ratio of the available frequency bandwidth over the frequency spacing between sensors. The theoretically available bandwidth is 1 in the normalized frequency domain according to the Nyquist sampling theorem. If the frequency spacing is set to $(4-5)/N$, since N is a large number of 20,000, thus theoretically, thousands of sensors can be multiplexed.

4.4.3 Practical Consideration

The longest OPD of IFPI sensor should be less than the coherence length of the light source and its frequency should be less than the Nyquist frequency. A large OPD will cause large phase noise and lower the fringe contrast of the IFPI sensor, which will decrease the SNR of the sensor. Practically, the OPDs of the sensors can be located in the range from hundreds of micrometers to several centimeters with an OPD increment of $200\mu m$.

Based on the discussion of the system power and bandwidth budgets, about 200 sensors could be practically multiplexed along a single fiber. The multiplexing number can be increased if the insertion loss of each sensor can be lowered and the bandwidth requirement of each sensor can be reduced. However, more precise control is needed to lower the insertion loss of each

sensor and more efficient frequency estimation methods are desired to separate frequency components that are closely located. A swept laser with a narrower line width will also help to increase the SNR of the sensor and increase the multiplexing capacity.

4.5 Crosstalk Analysis

4.5.1 Serial Sensor Array

The multiplexed IFPI sensors in a serial topology will see some crosstalk between sensors. The signal of an IFPI sensor may affect other sensors in the array.

The reflectance and transmittance of the i-th sensor is assumed to be R_i and T_i respectively. T_i can be expressed as

$$T_i = \eta_i(1 - R_i) \tag{4.11}$$

where η_i is a term related to the power loss of the i-th sensor. When the power loss is low, η_i is close to 1.

The received power of i-th sensor can be given as

$$P_i = P_0 R_i \prod_{j=1}^{i-1} T_j^2 = P_0 R_i \prod_{j=1}^{i-1} \eta_j^2 (1 - R_j)^2 \tag{4.12}$$

where P_0 is the light power launched into the fiber, and T_j^2 denotes round-trip transmittance of j-th sensor. Because that R_j is a very small value due to the low reflectivity of the IFPI sensor, P_i can be simplified to

$$P_i \approx P_0 R_i \prod_{j=1}^{i-1} \eta_j^2 (1 - 2R_j) \approx P_0 R_i (1 - 2 \sum_{j=1}^{i-1} R_j) \prod_{j=1}^{i-1} \eta_j^2 \tag{4.13}$$

It is evident that the signal of the i-th sensor is affected by the power loss and the reflectance of the $i - 1$ sensors before it. For simplicity, we may assume that η_j is 1 for each sensor, which means the power loss of each sensor can be neglected. Then the normalized signal of

i-th sensor becomes

$$X_i = \frac{P_i}{P_0} \approx R_i(1 - 2\sum_{j=1}^{i-1} R_j) = R_i - 2R_i \sum_{j=1}^{i-1} R_j \tag{4.14}$$

The first term in the right side, R_i, is the uncorrupted signal of i-th sensor; The second term, $2R_i \sum_{j=1}^{i-1} R_j$, includes the crosstalk caused by the sensors in front of it. The ratio between them,

$$r_i = 2\sum_{j=1}^{i-1} R_j, \tag{4.15}$$

is a measure of the crosstalk.

It is evident that the crosstalk of the i-th sensor is proportional to the summation of the reflectance of all the $i-1$ sensors in front of it. Thus IFPI sensors with low reflectance may help to keep the crosstalk in a multiplexing sensor network at a low level even if a large number of sensors are multiplexed. The average reflectance of an IFPI sensor is less than -50dB (1×10^{-5}), thus when 100 sensors are multiplexed, the maximum crosstalk is less than 2×10^{-3} (-27dB), which is a very low value for most practical applications.

4.5.2 Frequency Spacing

The multiplexed IFPI sensors occupy different frequency channels. When non-parametric frequency estimation methods are used, the side lobes of one frequency will affect the estimation of adjacent frequencies. When the spacing between these frequencies is large enough that the side band of one sensor will not overlap with other frequencies, the crosstalk between different frequency components can be neglected. Practically, the difference between OPDs is about $200\mu m$, and is large enough. When Hamming windowed filter is used, a 40dB noise rejection level can be obtained.

4.5.3 Frequency Harmonics

The sinusoidal model of signal from IFPI sensors given in Eq. 4.1 is based on an assumption that the laser source is linearly swept in wave numbers. However, the sweeping of the laser may not be exactly linear. Thus the actual measured signal of an IFPI sensor may contain frequency harmonics that are multiple of its fundamental frequency. If the fundamental frequency of another sensor coincides with these harmonics, crosstalk occurs.

Compared with the fundamental frequency, the amplitude of harmonics is very low, usually about 25dB lower than the fundamental frequency. However, when a large number of sensors are multiplexed, the crosstalk may accumulate. Thus the OPDs of the sensors should be carefully designed to lower the crosstalk caused by the harmonics.

4.6 Summary

This chapter discusses a spectrum based measurement system and a FDM scheme for the multiplexing of IFPI sensors. A swept laser is used as the light source, the response of sensors at different wavelengths are measured and normalized by using intensity and wavelength references. The IFPI sensors in a sensor array have different OPDs and thus the measured signal has different frequency components. The multiplexing scheme uses a sub-carrier frequency division multiplexing technique derived from the traditional FMCW technique. The multiplexing capacity is determined by the power budget and the frequency bandwidth budget. A practical multiplexing number of 200 is estimated. The crosstalk between IFPI sensors is proportional to the reflections of other sensors. Because of the low reflectivity nature of IFPI sensors, a very low crosstalk is expected even when a large number of sensors are multiplexed.

Chapter 5

Signal Processing

This chapter presents frequency estimation based signal-processing algorithms to determine the OPD of sensors. These algorithms use bandpass finite impulse response (FIR) digital filters to select individual frequencies and use frequency estimation methods to estimate the frequencies and phases of the sensor signals. Two frequency estimation algorithms, namely the peak finding method and the phase linear regression method, are developed.

5.1 Overview

When multiple sensors are interrogated, the measured interference spectrum will have multiple sinusoidal components as given in Eqs. 4.5 and 4.6. When the OPDs of IFPI sensors are affected by environmental perturbation, the frequencies and phases of these sinusoids will be changed. The task of the signal processing is to estimate the frequency and phase of each frequency component and thus to determine the OPD of each sensor.

One straightforward approach is to use digital filters to separate an individual frequency component from others. Thus the multi-tone frequency estimation problem is converted to a single-tone estimation problem. This research presents a peak finding and a phase linear

regression method to estimate the frequency of the sinusoidal signal.

The procedure of the signal processing is described as follows. Steps 1-4 will be discussed in following Sections 5.2 - 5.6, respectively.

1. Retrieve the interference spectrum from the instrument and interpolate it to be equally spaced in wave numbers.
2. Use a bandpass FIR filter to select an individual frequency component and filter other frequency components and background noise out.
3. Obtain an estimation of the frequency and the phase for each sensor.
4. Determine the OPD of the sensor and the corresponding measurand.
5. For each frequency component, repeat steps 2-4.

5.2 Signal Interpolation

The optical spectral information retrieved from the HR-SLI is equally spaced in the $1520 - 1570nm$ range with a wavelength step of $2.5pm$. The spectrum expression in Eq. 4-3 requires the spectrum equally spaced in wave numbers. Thus the first step of the signal processing is to interpolate the measured optical spectrum of IFPI sensors to be equally spaced in wave numbers.

A linear interpolation method is utilized as

$$R(k_b) = R(k_0) + \frac{R(k_1) - R(k_0)}{k_1 - k_0}(k_b - k_0) \tag{5.1}$$

where $k_b \in [k_0, k_1]$ is the interpolated wave number, k_0 and k_1 are the wave numbers of measurement samples.

5.3 Filtering

The initial OPD of each sensor is known in advance during the sensor fabrication. Thus one can design digital band pass filters with different pass bands and store them into the computer for later use. FIR digital filters are used in this research. Different methods including windowing, least square, etc can be used for the design of the FIR filters.

For the sinusoid signal of the j-th sensor whose frequency is ω_j, a Hamming windowed or Hann windowed FIR band pass filter is designed as

$$f(n) = \frac{\omega_2}{\pi} sinc[\frac{\omega_2}{\pi}(n - \frac{M_f - 1}{2})] - \frac{\omega_1}{\pi} sinc[\frac{\omega_1}{\pi}(n - \frac{M_f - 1}{2})]w(n) \tag{5.2}$$

$$w(n) = \begin{cases} 0.54 - 0.46cos(2\pi \dfrac{n}{M_f - 1}), & \text{Hamming window} \\ 0.5 - 0.5cos(2\pi \dfrac{n}{M_f - 1}), & \text{Hann window} \end{cases} \tag{5.3}$$

$$sinc(x) = \frac{sin(\pi x)}{\pi x} \tag{5.4}$$

where $n = [0, 1, \cdots, M_f - 1]$, $f(n)$ are the coefficients of the filter, ω_1 and ω_2 are the cutoff frequencies of the bandpass filter ($\omega_1 < \omega_j < \omega_2$), and M_f is the order of the filter.

Because the interference spectrum has a large number of data samples ($N = 20000$), one can design a band pass filter with a high order to obtain a very narrow pass band. Figure 5.1 shows the magnitude responses of the Hamming and Hann windowed filters with an order of 1001 and a pass band of 0.005π rad/s at the central frequency of 0.2π rad/s. In practice, an order of $4000 - 5000$ or even higher can be used.

5.3.1 Linear Phase Filtering

It is well known that a symmetric FIR filter is a linear phase filter.[105] It introduces a pure delay into the signal without giving any other distortion to the signal in the pass band. The phase delay for the frequency ω_j is

$$\phi_d = -\frac{M_f - 1}{2}\omega_j = -n_d\omega_j = -n_d k_s L \tag{5.5}$$

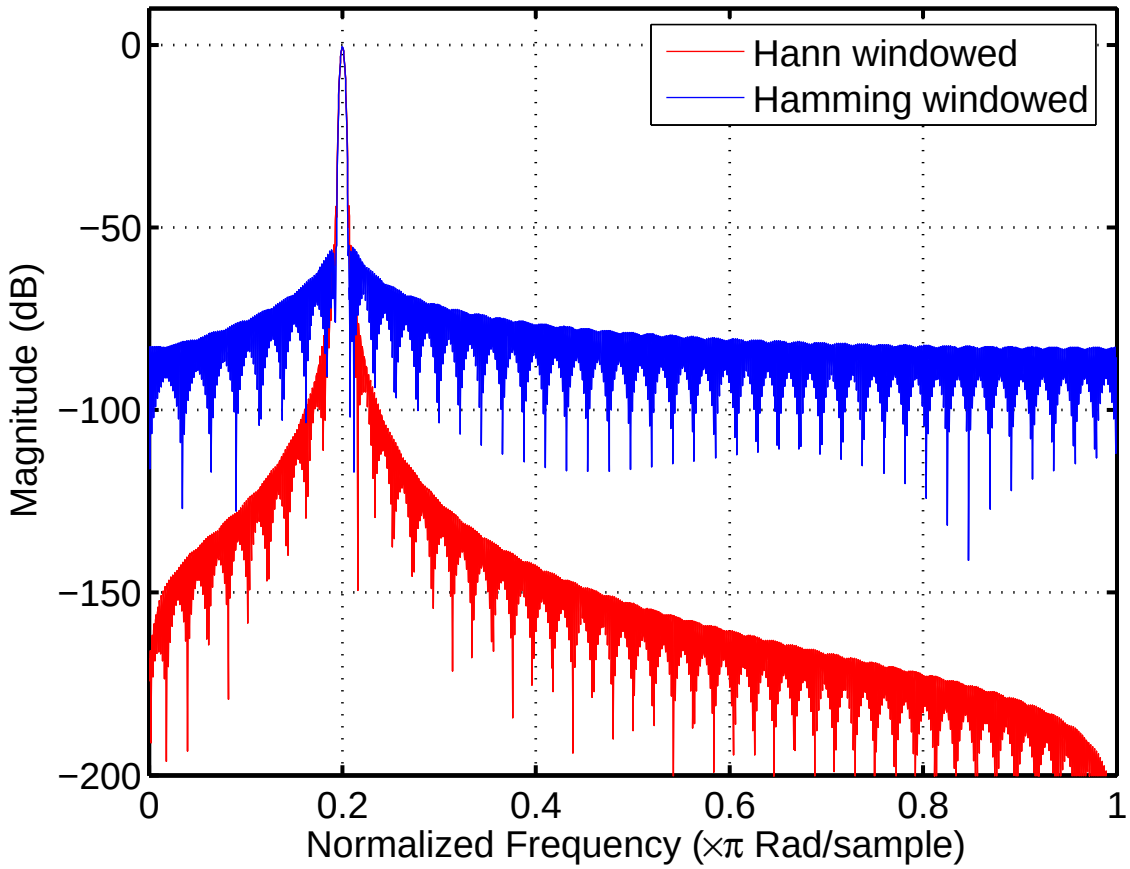

Figure 5.1: Magnitude response of Hamming/Hann windowed band pass filters.

where M_f is the order of the FIR filter and

$$n_d = \frac{M_f - 1}{2} \tag{5.6}$$

is the pure delay caused by the filter.

If M_f is selected to be an odd number, one can simply shift the filtered signal backward n_d samples to compensate the pure delay and the phase change caused by the FIR filter.

5.3.2 Zero Phase Filtering

One can perform zero-phase digital filtering by processing the input data in both the forward and reverse directions.[106] After filtering in the forward direction, one can reverse the filtered

sequence and run it back through the filter. The forward and reverse filtering has precisely zero-phase distortion and doubled magnitude response. Thus the filtering process will not introduce phase distortion to the frequencies in the pass band.

5.4 Frequency Estimation

After filtering and phase compensation, the signal in Eq. 4.1 can be written as

$$\overline{R}_n = \overline{B}_n cos(k_n L + \phi) + \overline{v}_n \tag{5.7}$$

where $\overline{R}_n$ is the filtered signal, $\overline{B}_n$ is the signal amplitude after the filtering and $\overline{v}_n$ is the residual noise after the filtering.

The task of the signal processing is to estimate the frequency and the phase of the sinusoid in Eq. 5.7. In this research, a peak finding method and a phase linear regression method were developed to estimate the frequency, L, and phase, ϕ, from the filtered signal given by Eq. 5.7. They will be discussed respectively as follows.

5.4.1 Peak Finding Method

This is a simple method in which the peak and valley positions of a sinusoid are detected and used to estimate the frequency and the phase of the sinusoid. Similar approaches have been reported for white light interferometry [107] and profilometry[108].

The peak positions of the sinusoids in Eq. 5.7 in wave number domain, k_m, are detected by using a centroid method. Assuming that the peak position falls in a certain wave number range, $k_m \in [k_p, k_q]$, it can be calculated by

$$k_m = \sum_{j=p}^{q} (\overline{R}_j k_j) / \sum_{j=p}^{q} \overline{R}_j \tag{5.8}$$

where $\overline{R}_j$ is the filtered signal.

At peak positions, the phases of the sinusoid are multiples of 2π, which is

$$k_m L + \phi = 2\pi(m_0 + m) \tag{5.9}$$

for $m = [0, 1, ..., M-1]$ where m_0 is an integer indicating the starting fringe order and M is the number of peaks.

Assuming the constant phase

$$\phi = 2\pi l \tag{5.10}$$

Eq. 5.9 can be written as

$$a_m L + K = m \tag{5.11}$$

where $a_m = k_m/2\pi$ and $K = l - m_0$.

A least square method is applied to solve Eq. 5.11 with two variables L and K by minimizing the variance

$$S = \sum_{m=0}^{M-1} [m - (a_m L + K)]^2. \tag{5.12}$$

The estimates of L and K can be solved as

$$[\hat{L}\ \hat{K}]^T = (A^T A)^{-1} A^T B \tag{5.13}$$

$$A^T = \begin{bmatrix} a_0 & a_1 & \cdots & a_{M-1} \\ 1 & 1 & \cdots & 1 \end{bmatrix} \tag{5.14}$$

$$B^T = [0\ 1\ \cdots\ M-1] \tag{5.15}$$

where $\hat{L}$ and $\hat{K}$ denote the estimate of L and K, respectively, and ^{T} denotes matrix transverse.

It should be noted that only the peak positions are used in the equations discussed above. Actually, all extreme positions, including both the peaks and valleys, can be used with minor modifications in Eq. 5.11. Thus more data points can be used to get better frequency estimation.

5.4.2 Phase Linear Regression Method

The peak finding method discussed above uses only the samples around the extreme positions. The detection of the peak and valley positions requires a relatively high signal to noise ratio to obtain accurate extreme positions, which may not be always available.

It is possible to use the information from all the sample points to get better estimation. This research derived a frequency estimation algorithm based on the linear regression of the instantaneous phase of sinusoidal signal.[24]

A single band filter, which can be implemented by a double band filter followed by a Hilbert transform, is used to obtain an analytical signal of a sinusoid. The filtering and Hilbert transformation can be calculated effectively by fast Fourier transform (FFT).

The analytical signal of a sinusoidal signal can be expressed as

$$\overline{R}_n = \overline{B}_n exp(j(k_n L + \phi)) + \overline{\upsilon}_n = \overline{B}_n exp(j(\omega_0 n + \phi_0)) + \overline{\upsilon}_n \tag{5.16}$$

whose carrier frequency L or normalized carrier frequency ω_0 can be estimated by the method of phase linear regression given in Refs. [109] - [111]. The unwrapped phase of the sinusoid in Eq. 5.16 can be given as

$$\phi_n = [\angle \overline{x}_n]_{2\phi} = k_n L + \phi + \xi_n \tag{5.17}$$

where

$$[\angle \overline{x}_n]_{2\phi} = \tan^{-1}[Im(\overline{x}_n)/Re(\overline{x}_n)] + 2m\pi \tag{5.18}$$

is the unwrapped phase of $\overline{x}_n$, and ξ_n is the equivalent phase noise of the additive noise υ_n.

The parameters L and ϕ can be estimated by the method of least square estimation or linear regression to minimize the square error

$$S = \sum_{n=1}^{N} [\phi_n - k_n L - \phi]^2. \tag{5.19}$$

The solution is

$$[\hat{L}\ \hat{\phi}]^T = (A^T A)^{-1} A^T \Phi \tag{5.20}$$

$$A^T = \begin{bmatrix} k_1 & k_2 & \cdots & k_N \\ 1 & 1 & \cdots & 1 \end{bmatrix} \tag{5.21}$$

$$\Phi^T = [\phi_1 \ \phi_2 \ \cdots \ \phi_N] \tag{5.22}$$

The frequency estimation based on the phase linear regression in Eq. 5.20 is the optimal maximum likelihood estimation for a pure sinusoid when ξ_n is Gaussian white noise.[110][111] When the SNR is moderately high, the estimator can attain the Cramer-Rao bound for a sinusoidal signal with a constant amplitude.[110][111] In Section 5.7, simulation results for different SNRs are given to evaluate the performance of the estimator given by Eq. 5.20

5.5 Amplitude Modulated Signal

As discussed in Section 3.6, when an IFPI sensor is not formed by ideal broadband reflectors, the reflections of the reflectors are wavelength dependent and thus the sinusoidal interference signal is amplitude-modulated. It is desired that the signal processing algorithms can estimate the frequencies of the amplitude modulated (AM) signal.

The frequency estimation for an AM signal can benefit from the analytical signal model given by Eq. 5.16. For an AM signal, the amplitude B_n is not constant. One can use the analytical signal to derive a pure sinusoid with a normalized amplitude as

$$x_n = \frac{real(\overline{R}_n)}{|\overline{R}_n|} = cos(k_n L + \phi) + \upsilon_n. \tag{5.23}$$

Then one can use the peak finding method to estimate the frequency and phase of the signal.

In the phase regression method discussed above, although $\overline{B}_n$ is not constant for an AM signal, the unwrapped phase of the AM signal, which is independent on the amplitude, is of the same form as in Eq. 5.17. Thus the phase regression method, which is initially developed for sinusoidal signal with a constant amplitude, can be extended to the carrier frequency estimation of AM signals. Simulation results for the phase regression method for both pure sinusoidal and AM signal will be compared in Section 5.7.

5.6 Frequency Estimation for Known Phase

The phase term Φ of the sinusoidal signal is assumed to be unknown and is estimated in Eqs. 5.13 and 5.20. The estimation of $\hat{L}$ for unknown phase ϕ usually does not have high accuracy especially when the SNR is not high. In practice, the phase term, which is a constant, can be known via accurate modeling or empirical calibration in advance. One can use it to get a higher frequency estimation accuracy than that of unknown phase.

5.6.1 Peak Finding for Known Phase

As described in Refs. [107] and [108], the estimation of $\hat{L}$ in Eq. 5.13 has no fringe order ambiguity problem. However, it does not have a high resolution compared with the peak finding method discussed in Ref. [107]. The reason is that the phase term l in Eq. 5.10 is assumed to be a unknown number and is estimated for each frame of data sequence. This is equivalent to the single-tone frequency estimation for unknown phase.

The initial phase l in Eq. 5.10 can be calibrated in advance. One can obtain average values of $\hat{L}$ and $\hat{K}$ from multiple estimations and store them as calibrated values of $\overline{L}$ and $\overline{K}$. Thus a calibrated l

$$l = \overline{K} - round(\overline{K}) \tag{5.24}$$

can be obtained as the fractional part of $\overline{K}$ and stored for peak order determination discussed below. Thus the determination of L becomes a single-tone frequency estimation problem for known phase.

By using the calibrated value of l, the fringe order of each peak can be determined by determining m_0 as the closest integer number to $l - K$

$$m_0 = round(l - K) \tag{5.25}$$

Unlike the method in Ref. [107] that tracks an individual peak in the interference spectrum,

we substitute m_0 into Eq. 5.11 and get another set of equations with only one variable

$$a_m L = m + m_0 - l \tag{5.26}$$

An estimation of L, $\hat{L}$, can be solved by minimizing the variance

$$S = \sum_{m=0}^{M-1} [m + m_0 - l - a_m]^2. \tag{5.27}$$

The solution is

$$\hat{L} = (C^T C)^{-1} C^T D \tag{5.28}$$

$$C^T = \begin{bmatrix} a_0 & a_1 & \cdots & a_{M-1} \end{bmatrix} \tag{5.29}$$

$$D^T = \begin{bmatrix} m_0 - l & m_0 - l + 1 & \cdots & m_0 - l + M - 1 \end{bmatrix} \tag{5.30}$$

The estimation $\hat{L}$ in Eq. 5.28 will have a higher resolution than that of the individual peak tracking because it uses more peak positions to estimate L. Actually, it can be regarded as a multiple peak tracking approach in which all the peak positions are used.

5.6.2 Linear Regression for Known Phase

In the phase linear regression method, one can obtain average values of multiple estimations $\hat{L}$ and $\hat{\phi}$ from Eq. 5.20 and store them as calibrated values of $\overline{L}$ and $\overline{\Phi}$. The modulus of $\overline{\Phi}$ with 2π, $[\overline{\Phi}]_{2\pi}$, whose value falls in $[-\pi, \pi]$, can be used as a good calibrated approximation of ϕ .

If the estimation error $\Delta L = \hat{L} - L$ is less than $\lambda/2$, where λ is the wavelength of the light, the phase error caused by ΔL,

$$\Delta\phi_n = k_n \Delta L \tag{5.31}$$

will be in the range of $[-\pi, \pi]$. Therefore, for the estimation of $\hat{L}$ and $\hat{\phi}$ from Eq. 5.20, one can select

$$\Delta\phi = [\hat{\phi} - \phi]_{2\pi} \tag{5.32}$$

whose value falls in $[-\pi, \pi]$, as an estimation of phase error caused by ΔL. Then ΔL can be estimated by minimizing the variance

$$S = \sum_{n=1}^{N} [\Delta\phi - k_n \Delta L]^2. \tag{5.33}$$

with the solutions of

$$\Delta\hat{L} = (C^T C)^{-1} C^T D \tag{5.34}$$

$$C = [k_1 \ k_2 \ \cdots \ k_n]^T \tag{5.35}$$

$$D = [\Delta\Phi \ \Delta\Phi \ \cdots \ \Delta\Phi]^T \tag{5.36}$$

One can use the estimation of $\Delta\hat{L}$ in Eq. 5.34 as a compensation of the frequency estimation of $\hat{L}$ in Eq. 5.20. The compensated frequency estimation for known ϕ is

$$L = \hat{L} + \Delta\hat{L} \tag{5.37}$$

which will have a higher accuracy than that for the unknown phase case.

5.7 Simulation Results

The performance of the estimator Eq. 5.20 for a unknown phase was investigated for pure sinusoidal and AM signals at different SNR levels. The simulation results with and without pre-filtering were compared. The simulation was based on a sequence of 1000 samples of a sinusoid whose normalized frequency is 0.024 rad/s. The AM signal has an envelope of Gaussian shape. Figure 5.2 shows the relationship between the mean square errors (MSE) of the frequency estimation and SNR levels. The horizontal axis shows the SNR in dB, the vertical axis shows the inversion of the MSE of the frequency estimation in dB. The curves marked with plus (+) and circle (o) symbols show the simulation results of frequency estimation for a pure sinusoid, and the curve marked with left triangle ($\triangleleft$) and up triangle ($\triangle$) symbols show the simulation results for an AM signal, with and without pre-filtering,

respectively. The Cramer-Rao bound of the frequency estimation for Eq. 5.16 with unknown phase, which is given by

$$B = \frac{6}{N(N^2-1)S} \tag{5.38}$$

where S is the SNR and N is the length of the data sequence, is plotted for comparison.

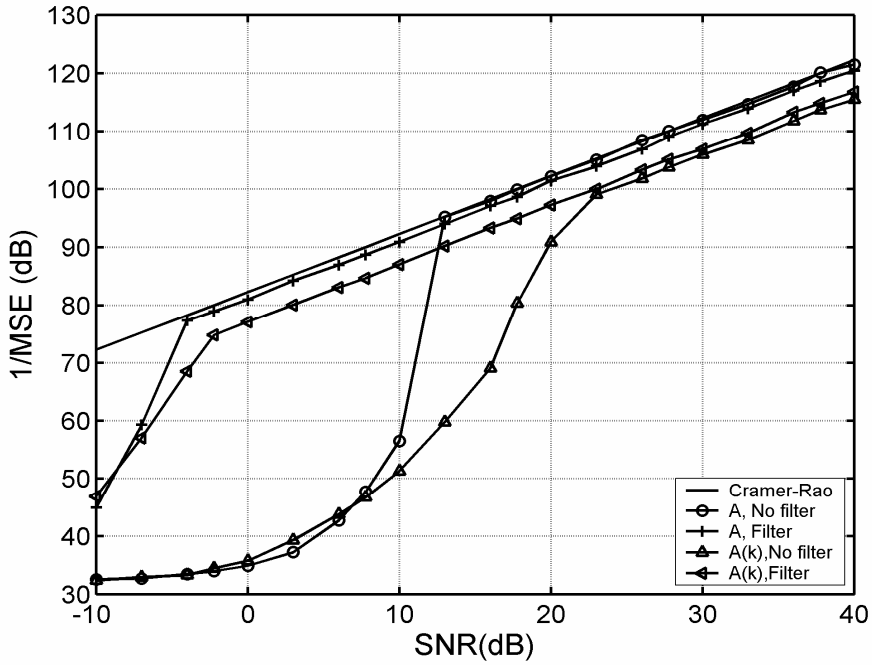

Figure 5.2: Simulation result of frequency estimation for unknown phase.

It can be seen that the estimator Eq. 5.20 can obtain a good estimation for a high SNR but has poor performance for a low SNR. It can also be expected that the pre-filtering with a band pass filter will reject the noise outside the pass band and increase the SNR greatly. Therefore, the pre-filtering will greatly improve the performance of the estimator especially for a low SNR case. Compared with a pure sinusoid signal with a constant amplitude, an AM signal has a lower signal power because of the amplitude modulation and thus a lower SNR. From Figure 5.2, it can also be seen that when the signal is amplitude modulated, the performance of the estimator decreases to some degree because of the decrease of the average SNR.

The comparison of frequency estimation for unknown phase and known phase, as described in Eq. 5.20 and Eq. 5.37, is shown in Figure 5.3. The simulation data was based on an amplitude-modulated signal of a FP interferometer with a Gaussian shape envelope. It can be seen that the frequency estimation error for known phase can be much smaller than that for unknown phase, which means that the frequency estimation for known phase can have much higher accuracy than that for unknown phase.

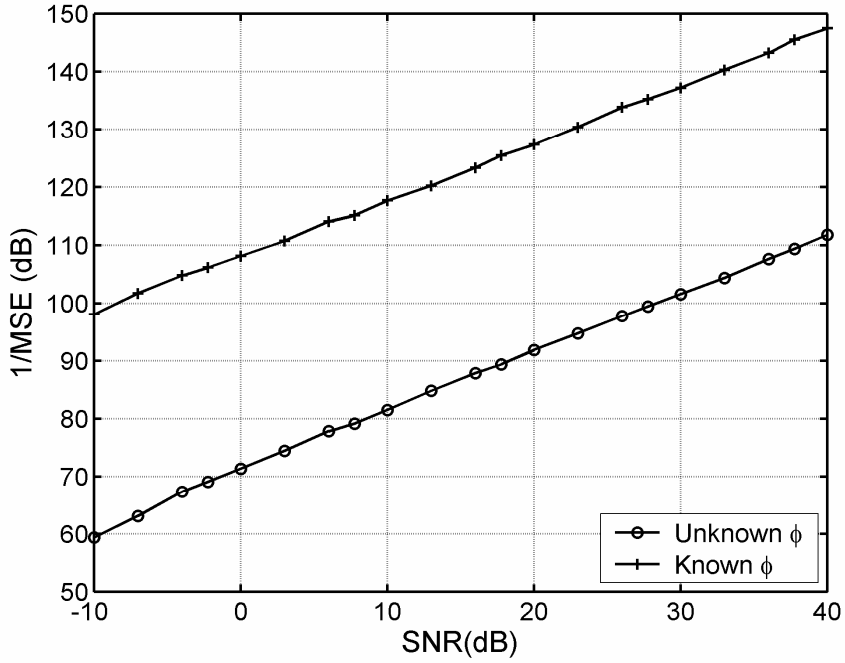

Figure 5.3: Comparison of frequency estimation error for unknown and known phase.

5.8 Noise Source

5.8.1 Intensity Measurement Noise

The noises of optical detection mainly come from the quantum shot noise related to input light power and the thermal noise related to the electrical system. One may assume that the

thermal noise is of a constant level which is independent of the input light power. The noise analysis of a sensor below is mainly focused on the shot noise caused by the input power of other sensors.

From Eq. 4.5, one can know that the signal power of the j-th sensor is determined by the amplitude of the j-th sinusoidal signal, B_j, which in turn is determined by the fringe contrast of the interference between the two reflectors in the j-th sensor. To increase the signal power, one should make the reflection at each reflector as high as possible and make the contrast as large as possible. However, due to the limited refractive index change, the reflectivity of the reflector is limited. A high reflectivity will also increase the crosstalk between sensors and decrease the multiplexing capacity, which are not desirable.

The signal in Eq. 4.5 has a DC portion of $\sum_{j=1}^{J} A_j$ where J is the number of sensors and A_j is the DC part of the j-th signal. It is evident that the DC level increase linearly with the number of sensors. Thus, the sinusoidal signal, an AC signal, has a large DC bias.

The Rayleigh backscattering, which can be regarded as wavelength independent in the 1520-1570nm range, gives another significant contribution to the DC part of the measured spectrum. The reflectivity of each sensor is as low as -55dB, which is equivalent to the Rayleigh backscattering of the fiber with a length of tens of meters. Therefore, if the length of the fiber is very long, the Rayleigh backscattering may be much stronger than the sensor signal.

Another DC noise source is the optical components in the measurement system. For example, a low quality connector may have a reflectivity of -45dB, which might be 10 times stronger than the sensor signal.

The measurement instrument HR-SLI uses a DC-coupled pre-amplifier to amplify the input signal. It not only amplifies the signal, but also the DC bias. This is the main problem of the signal detection in this system. When the DC portion is high, a low gain has to be used to avoid the signal saturation. Therefore, unless an AC-coupled pre-amplifier is used, the signal is not significantly amplified, and thus the SNR of the system is limited.

The increase of the DC part also causes linear increase of shot noise to the detection of the optical signals. Even when an AC-coupled detection method is used, the linear increase of the shot noise is inevitable because of the random nature of the quantum process.

In conclusion, the most efficient way to improve the SNR level is to reduce the unnecessary reflection in the system and use an AC-coupled signal amplification approach.

5.8.2 Phase Noise

Another noise source of the system is the phase noise related to the wavelength uncertainty of the spectrum measurement. The HR-SLI has a wavelength length accuracy of 1 pm. The corresponding wave number uncertainty is about $2 \times 10^{-6} rad/\mu m$.

It needs to be noted that the phase noise caused by the wavelength uncertainty for an IFPI interferometer is proportional to its OPD. Therefore, for the frequency estimator based on the phase linear regression of Eq. 5.17, one can expect a higher noise level and thus a poorer estimation accuracy for a larger OPD. However, the relative measurement accuracy, which is defined as the ratio of the OPD estimation error over the original OPD, $\Delta L/L$, may keep at a constant level as discussed below.

5.9 Measurement Accuracy

The measurement accuracy of the OPD of an IFPI sensor depends on the SNR of the sensor signal. Assume that the FIR filter used is ideal and rejects all the noise outside the pass band, the SNR is mainly limited by the low reflection of the optical signal.

Figure 5.4 shows the measurement accuracy test results of an IFPI sensor in a sensor array with 4 sensors multiplexed. The sensor was kept at $25 \pm 0.1^o C$ for about 4 hours. The top graph shows the calculated OPD of the sensor, the bottom graph shows the distribution of the measurement error. The standard deviation of OPD change is less than $0.5 ppm$ of the

original OPD. The corresponding temperature resolution is better than 0.1^oC.

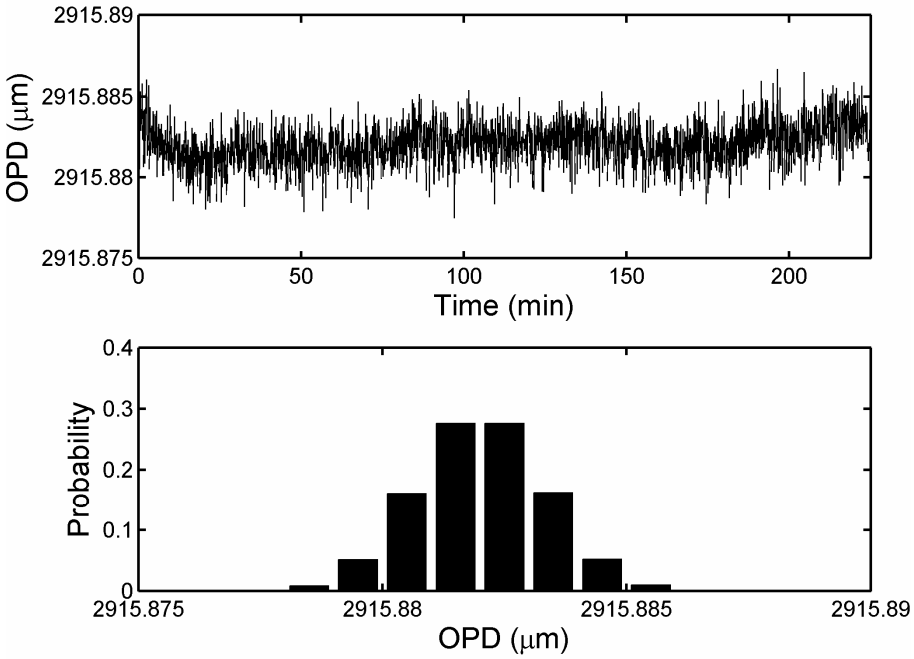

Figure 5.4: Measurement accuracy test of IFPI sensor.

Similar OPD measurement accuracy was also obtained for strain sensing. The standard deviation of the OPD measurement is with the same value of $0.5ppm$, and the corresponding strain measurement resolution is $0.5\mu\epsilon$.

5.10 Summary

This chapter discusses the signal processing procedures including signal interpolation, filtering, and frequency estimation. Two frequency estimation methods, peak finding and phase linear regression methods, are discussed for both unknown and known phases, and for both pure sinusoidal and amplitude modulated signals. The performance of the frequency estimation methods are investigated. An accuracy of OPD measurement of 0.5×10^{-6} is obtained.

Chapter 6

Applications

UV-induced IFPI sensors can be used to measure any quantity that can change either the refractive index or the fiber dimension or both. From Eq. 3.6, it can be derived that

$$\Delta L = 2(\Delta n_e d + n_e \Delta d) = L(\frac{\Delta n_e}{n_e} + \frac{\Delta d}{d}). \tag{6.1}$$

It is evident that the OPD of an IFPI sensor will change due to the refractive index change Δn_e and the fiber dimension change Δd caused by environment parameters such as temperature and strain.

The environmental parameters can be measured at multiple points by multiplexing IFPI sensors and estimating the OPD change of each sensor. Potentially, a large number of sensors can be multiplexed into a single optical fiber. This chapter demonstrates experimental results for temperature and strain sensing, and discusses the discrimination of temperature and strain measurement. The sensor packaging and the software implementation are also discussed.

6.1 Temperature Sensing

When an IFPI sensor is put into a temperature-varying environment, the OPD of the sensor will change due to the thermo-optic effect and the thermal expansion of the silica fiber. The dimensional change of the fiber due to a temperature change is

$$\frac{\Delta d}{d} = \alpha_T \Delta T \tag{6.2}$$

where α_T is the coefficient of thermal expansion (CTE). For silica, $\alpha_T = 0.5 \times 10^{-6}(1/^oC)$. The refractive index change due to the temperature change is

$$\Delta n_e = \frac{\partial n_e}{\partial T}\Delta T. \tag{6.3}$$

Thus the total OPD change can be written as

$$\frac{\Delta L}{L} = (\alpha_T + \frac{\partial n_e}{\partial T}/n_e)\Delta T = (\alpha_T + \sigma_T)\Delta T \tag{6.4}$$

where $\sigma_T = \frac{\partial n_e}{\partial T}/n_e$ is the thermo-optic coefficient. For silica fiber, $\sigma_T = 0.65 \times 10^{-5}(1/^oC)$ at room temperature, which is much larger than α_T. For temperature dependence, the thermo-optic effect is thus dominant.

Figure 6.1 shows the temperature response of an IFPI sensor in a sensor array of 4 IFPI sensors with OPDs of $2200\mu m$, $2916\mu m$, $3744\mu m$, and $4375\mu m$ respectively. The sensor with OPD of $2916\mu m$ was put into a miniature furnace. The measuring range was from room temperature to 650^oC. The temperature and OPD of the sensor during a thermal cycle were recorded. The varying rate of temperature was 2^oC per minute. As shown in Figure 6.1, the sensor responses to increasing and decreasing temperature were nearly the same. A measurement resolution of 0.1^oC was obtained. In our experiments, the IFPI sensors, which are in the Type-II regime, were proven to be capable of operation at 600^oC or even higher without significant signal degradation.

As shown in Eq. 6.4, the relative OPD change is proportional to the temperature change. If IFPI sensors are fabricated with the same photosensitive fiber, then the temperature response

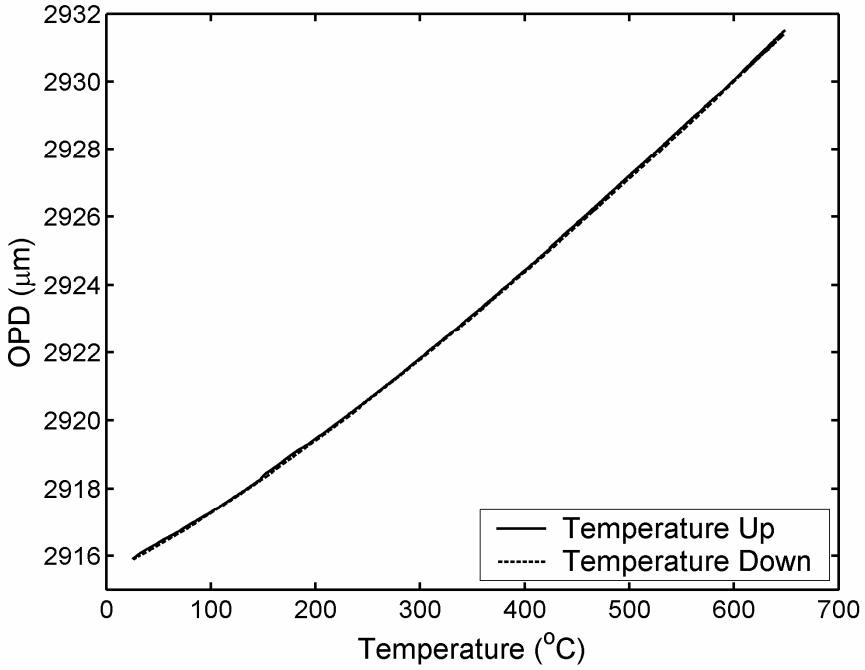

Figure 6.1: Response of IFPI sensor for temperature.

of relative OPD change will be the same, which means that one can use a single calibration curve for all the sensors.

6.2 Strain Sensing

The UV-induced IFPI sensor can also be used for strain sensing. The OPD change is due to the dimensional change and the stress-optic effect in the silica fiber. The refractive index change caused by the strain is

$$\Delta n_e = -\frac{n_e^3}{2}[p_{12} - \upsilon(p_{11} + p_{12})]\epsilon \tag{6.5}$$

where p_{11} and p_{12} are components of the strain-optic tensors, υ is the Poisson's ratio and ϵ is the axial strain. Therefore, from Eq. 6.1, the total OPD change can be written as

$$\Delta L = L(1 - P_e)\epsilon \tag{6.6}$$

where

$$p_e = \frac{n_e^2}{2}[p_{12} - \upsilon(p_{11} + p_{12})]\epsilon \tag{6.7}$$

is known as the effective strain-optic constant. For a typical optical fiber, $p_{11} = 0.113$, $p_{12} = 0.252$, $\upsilon = 0.16$, $n_e = 1.468$, and $p_e = 0.21$.

The experimental setup shown in Figure 6.2 is used to measure the strain response of an IFPI sensor. One end of the fiber is fixed. The other end of the fiber is stretched by a dead weight to apply tensile stress to the sensor located between the fixing point and the dead weight.

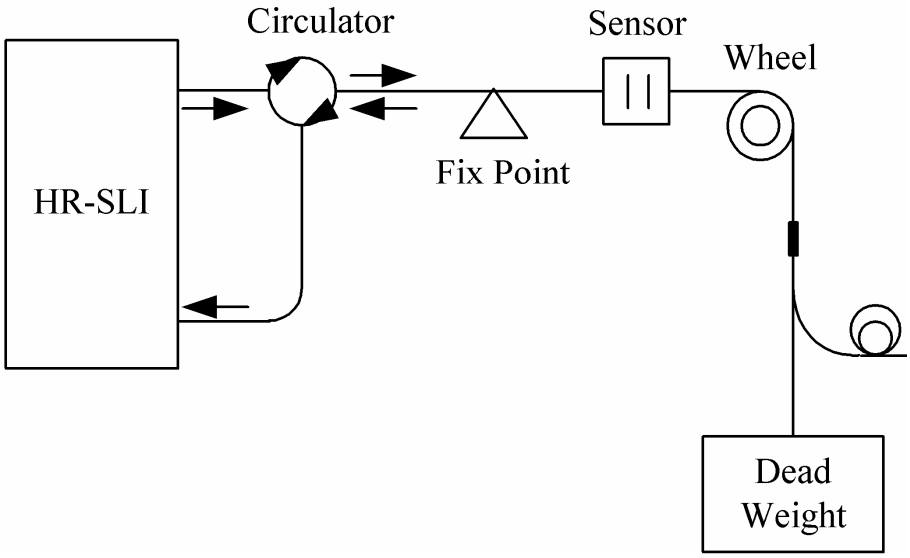

Figure 6.2: Experimental setup for IFPI strain sensing.

The strain caused by the dead weight can be written as

$$\epsilon = \frac{P}{G} \tag{6.8}$$

where G is the Young's modulus of the silica fiber ($73.4GPa$) and P is the tensile stress, which is given by

$$P = \frac{mg}{\pi r^2} \tag{6.9}$$

where m is the mass of the dead weight, g is the acceleration of gravity and r is the radius of the fiber.

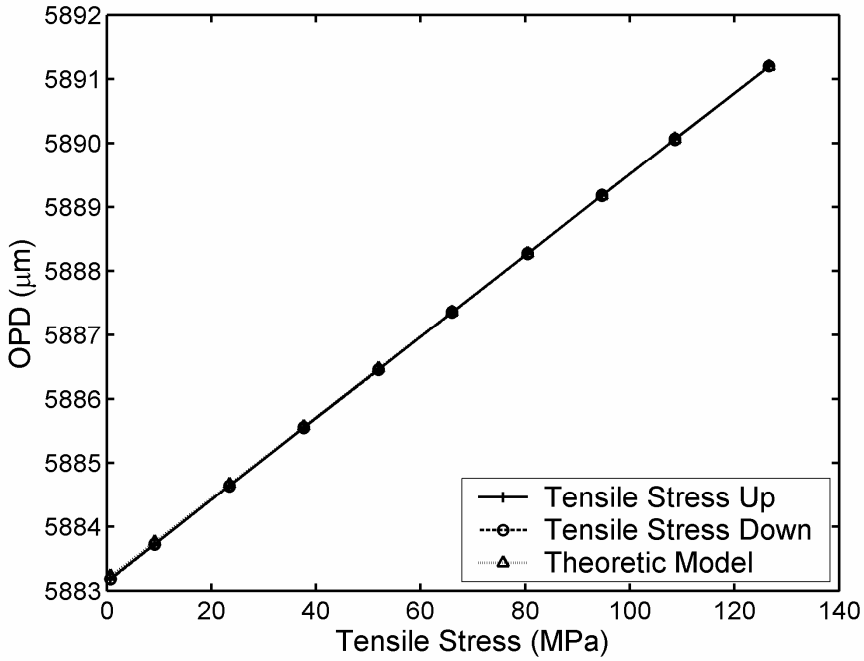

Figure 6.3: Response of IFPI sensor for strain measurement.

The test result of the IFPI strain sensor is shown in Figure 6.3. A tensile stress increasing and decreasing cycle as well as the theoretic model curve are plotted in the same figure. It can be seen that the test results match the model as given in Eqs 6.6, 6.8 and 6.9. A measurement resolution of $0.5\mu\epsilon$ was obtained.

6.3 Discrimination of Temperature and Strain

The UV-induced IFPI sensor uses silica fiber between the two reflectors as the sensing element. As discussed in the preceding sections, the fiber is sensitive to both temperature and strain. Therefore, unless the strain measurement is performed in a temperature-controlled environment or temperature measurement is performed without any external strain, the

perturbations of strain and temperature have to be separated, which is required for some applications such as health monitoring of civil structures. Some researchers have reported a matrix method to separate them using two sensors with different sensitivities to temperature and strain.[19]

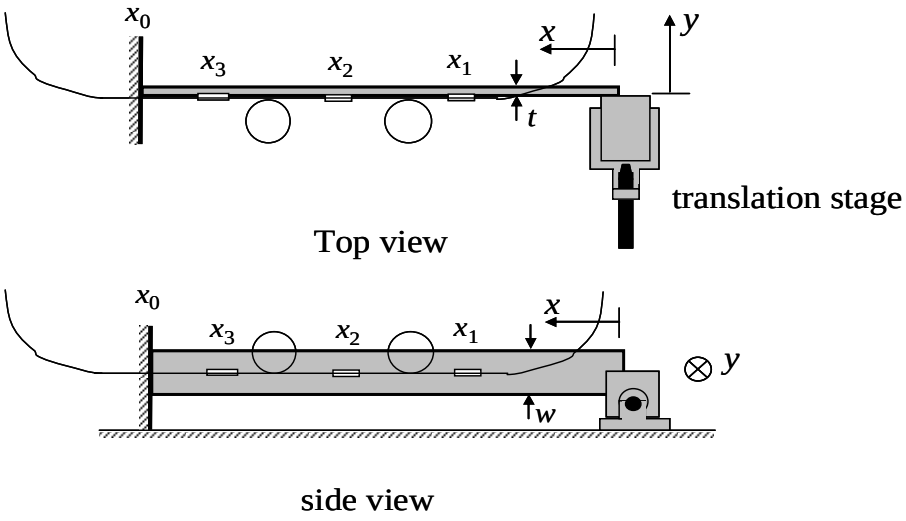

Figure 6.4: Cantilever beam setup for strain measurement.

This research focuses on a temperature-compensation approach for strain measurement. An experimental setup shown in Figure 6.4 was used. At each of the three positions of a cantilever beam, x_i, a pair of IFPI sensors was mounted. One IFPI sensor is firmly bonded onto the surface of the iron beam and acts as a strain sensor. The other IFPI sensor is loosely attached next to the strain sensor and acts as a temperature sensor that will not see the beam strain. Three pairs of sensors were arranged along a single fiber. One end of the iron beam was fixed while the other end can be moved in the y-direction by adjusting the translation stage. The strain distribution along the beam can be given as

$$\epsilon_i = \frac{3x_i t}{2x_0^3} y \tag{6.10}$$

where ϵ_i is the strain induced at the position x_i, y is the beam tip displacement, x_0 is the length and t is the thickness of the beam.

The response of the strain sensor for the induced strain at x_i is given by Eq. 6.6, while the temperature response of the strain sensor can be expressed as

$$\frac{\Delta L}{L} = (\alpha_T + \sigma_T)\Delta T + (1 - p_e)(\alpha_I - \alpha_T)\Delta T \tag{6.11}$$

where α_T and σ_T are the thermal expansion and thermal-optic coefficients of the silica fiber, respectively, and α_I is the thermal thermal expansion coefficient of the iron beam. The second term on the right side in Eq. 6.10 is the OPD change caused by the CTE mismatch between the iron beam and the fiber. Thus the total relative OPD change subject to both strain and temperature is

$$\frac{\Delta L}{L} = (1 - p_e)\epsilon_i + (\alpha_T + \sigma_T)\Delta T + (1 - p_e)(\alpha_I - \alpha_T)\Delta T \tag{6.12}$$

For strain measurement, the OPD change caused by the temperature variation, as given in Eq. 6.11, needs to be compensated.

The response of the temperature sensor is given by Eq. 6.4. Once ΔT is measured, it can be substituted into Eq. 6.11 to obtain the temperature induced OPD change of the strain sensor. Then the temperature induced OPD change could be subtracted from Eq. 6.12 and thus the information of strain, ϵ_u, can be determined.

In experiment, a constant displacement was applied to the cantilever beam so that there was a constant strain distribution along the beam surface. The displacement of the translation stage was $17.0mm$, which resulted strains at x_1, x_2 and x_3 to be $-265.2\mu\epsilon$, $-472.3\mu\epsilon$ and $-648.6\mu\epsilon$ respectively. The temperature of the beam was varied under the illumination of an incandescent bulb. The OPDs of the six sensors were calculated during a period of 25 hours, in which the temperature fluctuation range was from 23^oC to 33^oC. The experimental results of one pair of sensors are shown in Figure 6.5. The top graph shows the temperature curve and bottom graph shows the results of strain measurement as well as the compensation of the temperature variation.

In Eq. 6.4, the sensitivity of the OPD to temperature is about $6.5ppm/^oC$ and the OPD change caused by the CTE mismatch in Eq. 6.11 is about $10.6ppm/^oC$. The total tempera-

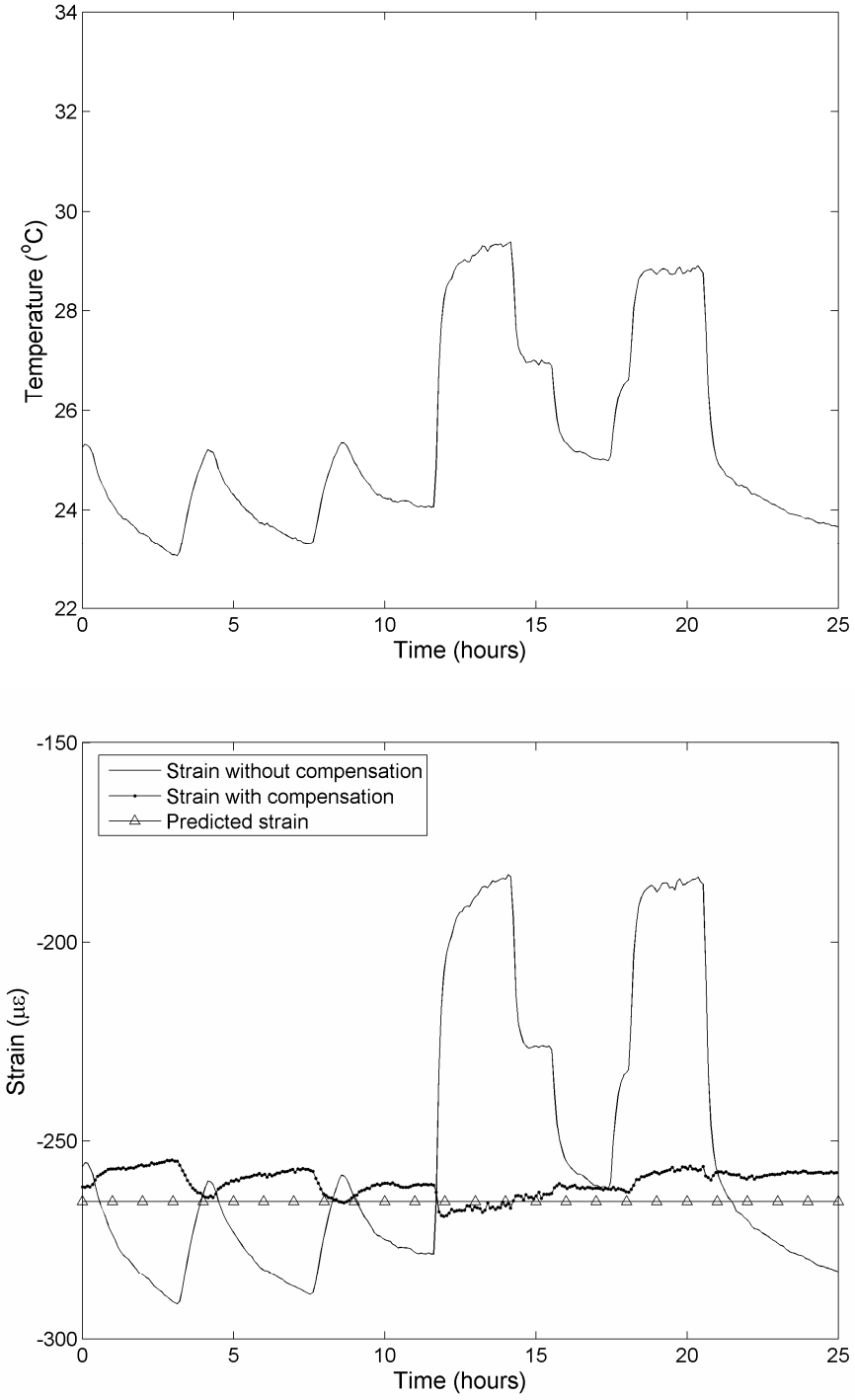

Figure 6.5: Temperature compensated strain measurement. (a) Temperature Curve. (b) Strain curve and temperature compensation.

ture induced OPD change is $17.1 ppm/^oC$, which is equivalent to the OPD change caused by about $21\mu\epsilon$ strain. Thus, for the measurement of strain, the compensation of temperature variation is important.

From Figure 6.5, it can be seen that the temperature compensated strains show much less fluctuations. The temperature effect was reduced by more than 85%. The compensation performance depends on the accuracy of measured temperature and the temperature difference between the temperature and the strain sensors. Thus the temperature sensor should be mounted as close to the strain sensor as possible to ensure that they see the same temperature.

6.4 Sensor Packaging

Due to the physical damage caused to the fiber core and claddings by the high power UV irradiation, the mechanical strength of the fiber is reduced. While an original fiber can withstanding a tensile stress of 100K pounds per square inch (psi), the UV-induced sensor can withstand a tensile stress of only 20K psi. The mechanical strength drops to 1/5 of the original level. It is thus important to protect the sensor with properly designed sensor packaging.

Two kinds of protection methods are investigated to protect the sensors. The first method is to recoat the bare fiber with polymer material by using an optical fiber recoater. After recoating, the sensor part is protected by the polymer jacket that is made of the same material as the ordinary fiber jacket. The polymer jacket can not withstand a temperature beyond 250^oC and thus can not be used in a high temperature environment. The other method is to protect the sensor with a capillary silica tube. The structure of the sensor packaging with a capillary tube is illustrated in Figure 6.6.

The capillary silica tube based sensor packing is targeted for the distributed high temperature sensing application in a field test at Kinston Fossil Plant, Harriman, TN. The structure to be

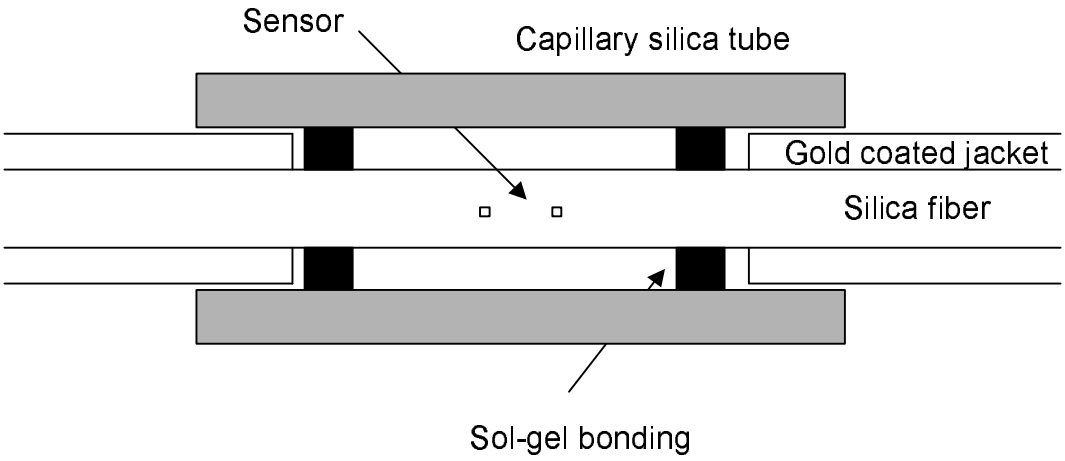

Figure 6.6: Sensor packaging with a capillary silica tube.

monitored is a selective catalyst reduction (SCR) unit whose temperature in operation may be as high as 400^oC. Gold coated fiber, which can withstand a temperature up to 700^oC, is used. The outer diameter of the fiber with the gold jacket is $170\mu m$. A capillary silica tube with an inner diameter of $178\mu m$ is used for sensor protection. A special kind of sol-gel material is used as the glue to bond the silica fiber and the capillary tube. When the sol-gel is heated, the silica tube and the silica fiber can be bonded together. Because both the tube and the fiber are made of fused silica, they have the same thermal expansion coefficient, thus the influence of the packaging to the sensor response is minimum.

In experiment, 20 sensors were connected along the gold coated fiber. Then the sensor array was packaged into a stainless steel tube with an outside diameter of 1 mm. Angle polished FC connectors were made ready for each sensor set. Two packaged sensor sets were installed into the SCR unit. The diagram of the sensor set and the sensor installation is shown in Figure 6.7.

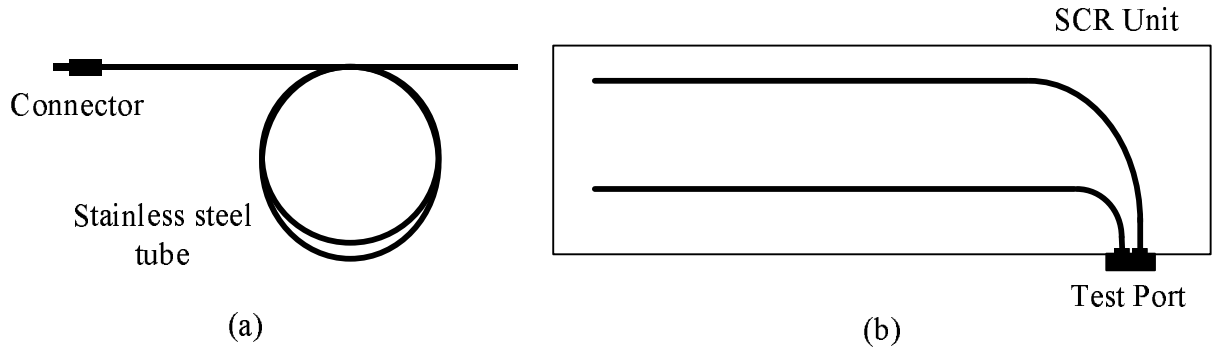

Figure 6.7: Sensor set in stainless steel tube and the installation at test site.

6.5 Software Implementation

In this research, both a Matlab program and a multi-threaded C/C++ Win32 program running on the host computer were written to retrieve the spectrum from the HR-SLI and perform the signal processing tasks.

The main purpose of the Matlab program is to rapidly prototype and investigate the signal processing algorithms. The vector and matrix computing ability, built-in functions such as FFT and Hilbert transformation, and the modules to control the GPIB and TCP/IP interface make Matlab a powerful platform to develop and deploy the software applications effectively.

The main objective of the Win32 C/C++ program is to implement a high speed measurement system that can perform the signal processing tasks rapidly for multiplexed sensor arrays. The application was developed for a distributed temperature measurement field test application performed at Kingston Fossil Plant, Harriman, TN. The structure of the software program is illustrated in Figure 6.8.

The software program is a multithreaded application running on a Win32 platform such as a Windows 2000/XP. The program contains 3 threads: the main thread, the data acquisition thread, and the signal processing thread. The functions of the main thread include the initialization and the parameter configuration of the system, the thread creation and

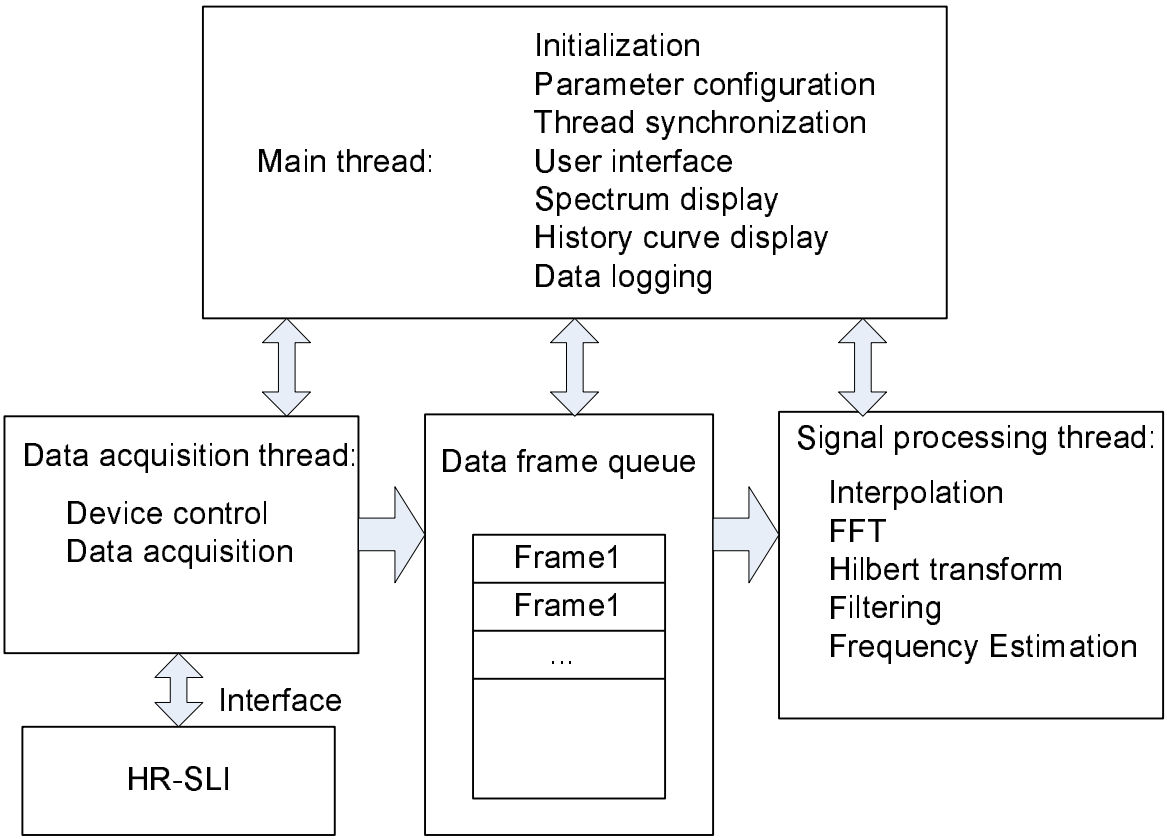

Figure 6.8: Structure of the multithreaded software program for multiplexed sensor system.

termination, the data synchronization between threads, the user interface, the display of the raw spectrum, the real time temperature monitoring, the history cure display, and the data logging. The main functions of the data acquisition thread include the control of the instrument, the data acquisition of the spectrum, etc. The signal processing thread interpolates the measured spectrum, uses filters to select individual frequency components, and estimate the frequency and phase of each signal. All these 3 threads run simultaneously and are synchronized to do the data acquisition, signal processing, and real time monitoring at the same time.

A global first-in-first-out (FIFO) queue of raw spectrum is used to store the measured spectra. The data acquisition captures the raw spectrum and adds it to the tail of the queue. The signal processing thread gets the raw spectrum from the head, and sends the signal processing

results to the main thread.

The software can capture a raw spectrum with 20,000 samples in a period of 1 second and process the signal demodulation of 20 IFPI sensors in 200 ms.

6.6 Summary

This chapter discusses the application of multiplexed IFPI sensors for temperature and strain sensing. The experimental setups are described and the measurement results are demonstrated. The temperature compensation technique is investigated for the discrimination of temperature and strain cross-sensitivities. The protection packaging of the sensor and the software implementation are discussed.

Chapter 7

Conclusions and Future Work

7.1 Conclusions

This research presents a frequency division multiplexed sensor array of UV-induced Fabry-Perot optical fiber sensors for quasi-distributed temperature and strain sensing. The objective of this research is to develop optical fiber sensors and optical measurement systems that can multiplex a large number of sensors and have high measurement accuracy.

The principle of operation of the UV-induced IFPI sensors and the sensor fabrication system are discussed. A sensor fabrication system and a point-by-point fabrication procedure are developed to make IFPI sensors by UV-irradiation. UV-induced partial reflectors can be written inside the fiber core by irradiating a photosensitive fiber to UV laser beam. A pair of such reflectors will form a FP interferometer that can be used for temperature and strain sensing. The relationship between the sensor performance and the UV-induced refractive index profile along the fiber is analyzed.

This research proposes a spectrum based measurement system for multiplexed IFPI sensors. The measurement system uses a swept laser source as well as intensity and wavelength references to measure the normalized spectrum of IFPI sensors. This research also presents

a FDM scheme based on FMCW technique for the multiplexing of IFPI sensors. IFPI sensors with different OPDs will have different frequencies with respect to wave numbers. The absolute OPD of each sensor is determined by estimating the frequency and the phase of each frequency component.

We developed frequency-estimation based signal processing algorithms for the OPD determination of IFPI sensors. FIR filters are designed to select each frequency component and filter the noise out. Two frequency estimation methods, namely the peak finding and the phase linear regression methods, are developed. The performance of these algorithms are investigated by both simulation and laboratory experiment.

The performance of the multiplexing system, including the system noise, the measurement accuracy, the multiplexing capacity, and the crosstalk between sensors are investigated. A relative accuracy of 0.5×10^{-6} for OPD measurement is obtained. A multiplexing capacity of hundreds of sensors is predicted.

The experimental results of IFPI sensors for temperature and strain sensing are demonstrated. Experimental results show a measurement resolution of 0.1^oC for temperature sensing and $0.5\mu\epsilon$ for strain sensing. The discrimination of temperature and strain measurement is discussed. Up to 85% of tempareture influence can be compensated for strain sensing.

We developed software programs for the measurement system. Matlab codes are developed for rapid prototype and laboratory experiment. A Win32 multithreaded software is programmed for real time measurement of temperature and strain with a high speed. The signal of tens of sensors can be demodulated in 200ms.

In conclusion, this research presents a promising technology for the quasi-distributed temperature and strain sensing applications by integrating a large number of optical fiber sensors into a sensor network in a large area. One can use the FMCW based FDM scheme to multiplex a large number of sensors with different OPDs and use the frequency-estimation based signal processing algorithms to determine the OPD of each sensor with high accuracy, and thus to obtain a high precision measurement for temperature and strain sensing.

7.2 Contributions and Publications

The major contributions of this dissertation include

- Developed a sensor fabrication system and a shadow-masked point by point laser writing technique for the fabrication of UV-induced IFPI sensors.
- Analyzed, for the first time, the relationship between the performance of the sensor and the refractive index profile of the writing point.
- Utilized, for the first time, a spectrum based measurement approach to determine the absolute OPD of a UV-induced IFPI sensors.
- Developed a FMCW-based FDM scheme that can multiplex a larger number of UV-induced sensors along a single fiber.
- Developed frequency-estimation based signal processing algorithms for the determination of OPDs of multiple sensors. The sensor signal can be both pure sinusoidal and amplitude modulated.
- Investigated the performance of the multiplexed sensor array, including the multiplexing capacity and the crosstalk.
- Programmed Win32 multithreaded software to demodulate the sensor signal with a high speed.
- Demonstrated the experimental result of temperature and strain sensing and the discrimination of cross-sensitivity between them.

Major publications by the author during the research of dissertation.

- **Fabin Shen** and Anbo Wang, "FFT-based numerical integration method for Rayleigh-Sommerfeld diffraction formula," Applied Optics, Vol. 45, Issue 6, pp. 1102-1110, Feb. 2006.

- Daewoong Kim, **Fabin Shen**, Xiaopei Chen, and Anbo Wang, "Simultaneous measurement of refractive index and temperature based on a reflection mode LPG and an IFPI sensor," Optics Letters, Vol. 30, Issue 22, pp. 3000-3002, Nov. 2005.

- **Fabin Shen** and Anbo Wang, "Frequency estimation-based signal processing algorithm for whitelight optical fiber Fabry-Perot interferometers," Applied Optics, Vol. 44, No. 25, pp 5206-14, Sep. 2005.

- **Fabin Shen**, Juncheng Xu and Anbo Wang, "Frequency response measurement of diaphragm-based pressure sensors by using the radiation pressure of an excimer laser pulse," Optic Letters, vol. 30, no. 15, 1935-37, Aug. 2005.

- Yizheng Zhu, Zhengyu Huang, **Fabin Shen**, Anbo Wang, "Sapphire-fiber-based white-light interferometric sensor for high-temperature measurements," Optics Letters, Vol. 30, Issue 7, 711-713, Apr. 2005.

- Wei Peng, Gary Pickrell, **Fabin Shen**, and Anbo Wang, "Experimental investigation of optical waveguide-based multigas sensing," Photonics Technology Letters, IEEE, Volume: 16, Issue: 10, Pages: 2317-2319. Oct. 2004.

- Ming Han, Yan Zhang, **Fabin Shen**, Gary R. Pickrell, Anbo Wang, "Signal-processing algorithm for white-light optical fiber extrinsic Fabry-Perot interferometric sensors", Optics Letters, Vol. 29, Issue 15, Page 1736, Aug. 2004.

- **Fabin Shen**, Zhuang Wang, Wei Peng, Kristie Cooper, Gary Pickrell, and Anbo Wang, "UV-induced intrinsic Fabry-Perot interferometric sensors and their multiplexing for temperature and strain sensing," Proc. SPIE Vol. 6174, p. 111-120, Smart Structures and Materials 2006: Sensors and Smart Structures Technologies for Civil, Mechanical, and Aerospace Systems; M. Tomizuka, C. Yun, V. Giurgiutiu; Eds., Mar. 2006.

- **Fabin Shen**, Zhengyu Huang, Yizheng Zhu, Mike Coffey, Robert Frank, Gary Pickrell, and Anbo Wang, "Frequency-Division-Multiplexed Fabry-Perot Interferometric Fiber

Sensors for Temperature Monitoring in a Selective Catalytic Reduction Unit," Proc. SPIE Vol. 5998, p. 136-143, Sensors for Harsh Environments II; A. Wang; Ed. Nov. 2005 (Invited paper).

- **Fabin Shen**, Wei Peng, Kristie L. Cooper, Gary Pickrell, Anbo Wang, "UV-induced intrinsic Fabry-Perot interferometric fiber sensors," Proc. SPIE Vol. 5590, p. 47-56, Sensors for Harsh Environments; A. Wang; Ed. Dec. 2004.

- Yizheng Zhu, Zhengyu Huang, Ming Han, **Fabin Shen**, Gary Pickrell, Anbo Wang, "Fiber optic high-temperature thermometer using sapphire fiber," Proc. SPIE Vol. 5590, p. 19-26, Sensors for Harsh Environments; A. Wang; Ed. Dec. 2004.

- Xiaopei Chen, **Fabin Shen**, Anbo Wang, Zhuang Wang, Yan Zhang and Anbo Wang, "Novel Fabry-Perot fiber optic sensor with multiple applications," Proc. SPIE Vol. 5590, p. 111-121, Sensors for Harsh Environments; A. Wang; Ed. Dec. 2004.

- Wei Peng, Gary R. Pickrell, **Fabin Shen**, Anbo Wang, "Hollow fiber optic waveguide gas sensor for simultaneous monitoring of multiple gas species," Proc. SPIE Vol. 5589, p. 1-7, Fiber Optic Sensor Technology and Applications III; M. A. Marcus, B. Culshaw, J. P. Dakin; Eds. Dec. 2004.

7.3 Recommendation of Future Work

7.3.1 Optimization of UV Irradiation Conditions

The performance of the UV-induced FP sensors depends on the refractive index profile at the laser writing point, which is determined mainly by the UV-irradiation conditions. Thus to improve the performance of the sensors, the UV-irradiation condition need to be optimized. The goal of the optimization is to generate a reflector with relative high reflectivity in a wide wavelength range.

Future work on the refractive index profile optimization may include:

- Investigate the relationship between the sensor signal and the refractive index profile and develop a mathematical or computational model.
- Design an optimized index profile that can produce optimal sensor performance including high reflectance for allowable maximum refractive index change and equal reflectance in a certain wavelength window.
- Develop a sensor fabrication system that can produce IFPI sensors with optimal performance and high throughput fabrication capability.

7.3.2 Sensor Improvement and Packaging

In order to multiplex a large number of sensors, the power loss of each sensor has to be controlled to be as low as possible. Hydrogen-loaded fiber can be used to reduce the power loss because no splicing is needed anymore. Another advantage is that Hydrogen-loaded fiber may give higher photosensitivity, which can increase the reflectivity of UV-induced reflector and the performance of the sensor.

The Type-II photosensitivity is based on the physical damage at the core/cladding interface of the fiber. However, the physical damage will cause the degradation of mechanical strength. Thus the physical damage has to be controlled to minimum and protection packaging needs to be developed.

This research has inspired another project that uses a short section of FBG that in tens of micrometers as partial reflectors. The performance of an FP interferometer with twin short-FBG reflectors is being investigated.

7.3.3 Improvement of Signal Processing Algorithms

The measurement accuracy of temperature and strain sensing is determined by the accuracy of the frequency and phase estimation for the signal from IFPI sensors. The multiplexing capacity is determined by the ratio of available frequency over the frequency spacing. Thus effective signal processing algorithms, which can accurately recover closely located frequency components, are essential for IFPI sensors multiplexed in a FDM scheme. More effective signal-processing algorithms with both high estimation accuracy and high frequency resolution need to be developed.

FFT-based non-parametric frequency estimation techniques are commonly used to estimate frequency component. The frequency resolution is limited to about 1/N because of the Rayleigh limit of the FFT method. Further, because of the energy leakage of each frequency component in FFT result, the separation between two adjacent frequency components must be large enough to obtain good measurement accuracy.

There have been some model-based frequency estimation methods reported with improved estimation accuracy and frequency resolution. Such methods include auto-regression (AR) model estimator and some eigen-decomposition based estimators. Their performance needed be investigated for IFPI sensors.

7.3.4 Hybrid Multiplexing Scheme

Another goal of the future work is to develop a sensor network with maximum multiplexing capability by utilizing hybrid-multiplexing schemes. A hybrid FDM/SDM with a structre similar to Figure 2.11 can be used to multiplex a large number of sensors in a sensor network. In each sensor array, a FDM scheme caan be used. A SDM schem can be used for the multiplexing of sensor arrays. The singal processing unit interrogates multiple sensor arrays in a serial manner. One may also use a TDM/FDM hybrid multiplexing as shown in Figure 7.1. The sensors are arranged to different groups. Sensors in the same group have different

OPDs while sensors in different groups may have the same OPDs. The sensor group is addressed by laser pulse as in a traditional TDM scheme. For each group, the fringe patterns of sensors are measured and the OPD of each sensor is determined. Thus, we may reuse these frequency bands for different sensors groups and thus increase the multiplexing capacity of the whole system.

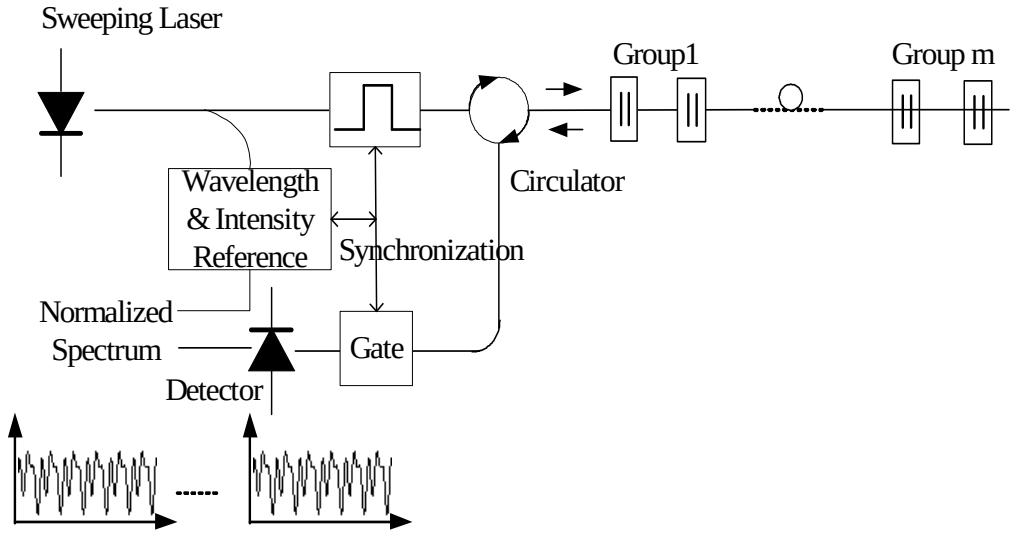

Figure 7.1: A TDM/FDM hybrid multiplexing scheme for IFPI sensors.

7.3.5 Demonstration of Dense Multiplexing System

The demonstration of a densely multiplexed sensor network for practical applications of temperature and strain sensing is essential. The features of IFPI sensor systems, including the sensor performance, sensor packaging, interrogation system, signal-processing technique and multiplexing capacity, can be verified during the demonstration.

Bibliography

[1] D. A. Krohn, Fiber Optical Sensors, Fundamentals and Applications, 3rd Ed., Research Triangle Park, NC, Instrument Society of America, 2000.

[2] J. M. Lopez-Higuera Ed., Handbook of Optical Fiber Sensing Technology, Chichester, U.K., John Wiley & Sons Ltd., 2001.

[3] J. P. Dakin, "Distributed optical fiber systems", in Optical Fiber Sensors: Systems and Applications, B. Culshaw, J. Dakin, Eds. Norwood, MA, Artech House, 1988, vol. 2, ch. 15, p. 575-598.

[4] J. P. Dakin, "Distributed optical fiber sensors", in Fiber Optic Smart Structures, E. Udd Eds. New York, NY, John Wiley & Sons, Inc, 1995, Ch. 14, p.373-408.

[5] A. Rogers, "Distributed optical-fiber sensing", in Handbook of Optical Fiber Sensing Technology, J. M. Lopez-Higuera Ed. Chichester, U.K., John Wiley & Sons Ltd., 2001, ch. 14, p.271-312.

[6] R. Kist, "Point sensor multiplexing principles," in Optical Fiber Sensors: Systems and Applications, B. Culshaw, J. P. Dakin Eds., Norwood, MA, Artech House, 1988, vol. 2, ch. 14, pp. 511-574.

[7] A. D. Kersey, "Fiber optic sensor multiplexing technique", in Fiber Optic Smart Structures, E. Udd eds. New York, NY, John Wiley & Sons, Inc, 1995, Ch. 15, pp. 409-444.

[8] C. E. Lee and H. F. Taylor, "Interferometric optical fiber sensors using internal mirrors", Electron. Lett. 24, pp. 193, 1988.

[9] C. E. Lee, H. F. Taylor, A. M. Markus and E. Udd, "Optical Fiber Fabry-Perot Embedded Sensor," Opt. Lett. 14, 1225-1227, 1989.

[10] C. E. Lee and H. F. Taylor, "In-line Fiber Fabry Perot Interferometer With High Reflectance Internal Mirrors", J. Lightwave Technol. 10, 1992.

[11] K. A. Murphy, "Extrinsic Fabry Perot Optical Fiber Sensor", Proc. IEEE Optical Fiber Sensors, 8th, Monterey, CA, pp. 193, 1992.

[12] Vivik Arya, Marten De Vries, Kent A. Murphy, Anbo Wang, and Richard O. Claus, "Exact Analysis of the Extrinsic Fabry-perot Interometric Optical Fiber Sensor Using Kirchhoff's Diffraction Formalism", Optical Fiber Technology 1, 380-384, 1995.

[13] J. Sirkis, T. A. Berkoff, R. T. Jones, H. Singh, A. D. Kersey, E. J. Friebele and M. A. Putnam, "In-line fiber etalon (ILFE) fiber-optic strain sensors", J. Lightwave Technol. 13, 1256-1268, 1995.

[14] X. Chen, F. Shen, A. Wang, Z. Wang, Y. Zhang, "Novel Fabry-Perot fiber optic sensor with multiple applications," Proc. SPIE Vol. 5590, p. 111-121, 2004.

[15] J. A. Greene, K. A. Murphy, A. J. Plante, V. Bhatia and M. Sen, "Broadband photoinduced Fresnel reflectors", Lasers and Electro-Optics Society Annual Meeting, LEOS '94, vol. 2, pp. 157, 1994.

[16] J. A. Greene, T. A. Tran, K. A. Murphy, A. J. Plante, V. Bhatia, M. Sen and R. O. Claus, "Photoinduced Fresnel Reflectors for Point-wise and Distributed Sensing Applications," Proc. SPIE, vol. 2444, pp. 64, 1995.

[17] F. Shen, W. Peng, A. Wang, K. L. Cooper, G. R. Pickrell, "UV-Induced Intrinsic Fabry-Perot Interferometric Fiber Sensors," Proc. SPIE, Vol. 5590, pp. 47-56, 2004.

[18] R. Kashyap, Fiber Bragg Gratings, Academic Press, San Diego, 1999.

[19] Andreas Othonos, "Fiber Bragg gratings", Review of Scientific Instruments, 68(12), pp. 4309-4341, 1997.

[20] Kenneth O. Hill and Gerald Meltz, "Fiber Bragg grating technology fundamentals and overview." J. Lightwave Technol. 15(8), pp. 1263-1276, 1997.

[21] M. Froggatt and J. Moore, "Distributed measurement of static strain in an optical fiber with multiple Bragg gratings at nominally equal wavelengths," Appl. Opt., Vol. 37, No. 10, pp1741-46 , 1998.

[22] F. Shen, Z. Wang, W. Peng, K. Cooper, G. Pickrell, and A. Wang, "UV-induced intrinsic Fabry-Perot interferometric sensors and their multiplexing for temperature and strain sensing," Proc. SPIE Vol. 6174, p. 111-120, Smart Structures and Materials 2006: Sensors and Smart Structures Technologies for Civil, Mechanical, and Aerospace Systems; M. Tomizuka, C. Yun, V. Giurgiutiu; Eds., Mar. 2006.

[23] F. Shen, Z. Huang, Y. Zhu, M. Coffey, R, Frank, G. Pickrell, and A. Wang, "Frequency-Division-Multiplexed Fabry-Perot Interferometric Fiber Sensors for Temperature Monitoring in a Selective Catalytic Reduction Unit," Proc. SPIE Vol. 5998, p. 136-143, Sensors for Harsh Environments II; A. Wang; Ed. Nov. 2005 (Invited paper).

[24] F. Shen and A. Wang, "Frequency estimation-based signal processing algorithm for whitelight optical fiber Fabry-Perot interferometers," Applied Optics, Vol. 44, No. 25, pp 5206-14, Sep. 2005.

[25] A. H. Hartog, "A distributed temperature sensor based on liquid-core optical fibers", J. Lightwave Technol. 1(3), pp. 498 - 509, 1983.

[26] P. Healey, "Instrumentation principles for optical time domain reflectometry," J. Phys. E: Sci. Instrum. 19, 334-341, 1986.

[27] S. V. Shatalin, V. N. Treschikov, A. J. Rogers, "Interferometric Optical Time-Domain Reflectometry for Distributed Optical-Fiber Sensing", Applied Optics, 37(24), 5600-5604, 1998.

[28] A. J. Hymans and J. Lait, "Analysis of a frequency-modulated continuous-wave ranging system," Proc. Inst. Elect. Eng., vol. 107B, pp.365-372, 1960.

[29] M. I. Skolnik, Introduction to Radar Systems, New York, McGraw-Hill, 1967. Chap. 3.

[30] R. L. Jungerman, and D. W. Dolfi, "Frequency Domain Optical Network Analysis Using Integrated Optics", IEEE J. of Quantum Electronics, 27(3), p580-587, 1991.

[31] R. Juskaitis, A. M. Mamedov, V. T. Potapov, S. V. Shatalin, "Distributed interferometric fiber sensor system", Optics Letters, 17(22), 1623-1625, 1992.

[32] H. Ghafoori-Shiraz and T. Okoshi, "Optical-fiber diagnosis using optical-frequency-domain reflectometry," Optics Letters, 10(3), 160-163, 1985.

[33] T. Horiguchi, A. Rogers, W. C. Michie, G. Stewart, B. Culshaw, "Distributed sensors: recent developments," in Optical Fiber Sensors: Applications, analysis, and future trends, J. Dakin, B. Culshaw, Eds., London, Artech House, 1988, vol. 4, ch. 14, p. 309-369.

[34] T. Horiguchi, T. Kurashima, M. Tateda, "A technique to measure distributed strain in optical fibers", Photonics Technology Letters, 2(5), 352-354, 1990.

[35] D. Garcus, T. Gogolla, K. Krebber, F. Schliep, "Brillouin optical-fiber frequency-domain analysis for distributed temperature and strain measurements", J. Lightwave Technol., 15(4), pp. 654 - 662, 1997.

[36] M. Froggatt, J. Moore, "High-Spatial-Resolution Distributed Strain Measurement in Optical Fiber with Rayleigh Scatter", Appl. Opt. , 37(10), 1735-40, 1998.

[37] A. Rogers, "Polarisation Optical Time Domain Reflectometry", Electron. Lett. 16, 489-490, 1980.

[38] J. P. Dakin, D. J. Pratt, G. W. Bibby and J. N. Ross, "Distributed Optical Fibre Raman Temperature Sensor Using a Semiconductor Light Source and Detector," Electron. Lett. 21, 569-570, 1985.

[39] A. H. Hartog, A. P. Leach, and M. P. Gold, "Distributed Temperature Sensing in Solid-Core Fibres," Electron. Lett. 21, 1061-1062, 1985.

[40] M. A. Farahani and T. Gogolla, "Spontaneous Raman Scattering in Optical Fibers with Modulated Probe Light for Distributed Temperature Raman Remote Sensing", J. Lightwave Technol. 17(8), 1379-1391, 1999.

[41] T. Horiguchi, T. Kurashima, and M. Tateda, "Tensile strain dependence of Brillouin frequency shift in silica optical fibers," IEEE Photon. Technol. Lett., 1(5), 107-108, 1989.

[42] J. Smith, A. Brown, M. DeMechant, and X. Bao, "Simutaneous distributed strain and temperature measurement," Appl. Opt. 38(25), 5372-5377, 1999.

[43] T. R. Parker, M. Farhadiroushan, V. A. Handerek, and A. J. Rogers, "A Fully Distributed Simultaneous Strain and Temperature Sensor using Spontaneous Brillouin Backscatter." IEEE Photon. Technol. Lett. 9(7), 979-981, 1997.

[44] H. H. Kee, G. P. Lees, and T. P. Newton, "All-fiber system for simultaneous interrogation of distributed strain and temperature sensing by spontaneous Brillouin scattering," Opt. Lett. 25, 695-697, 2000.

[45] S. M. Maughan, H. H. Kee, and T. P. Newson, "Simultaneous distributed fibre temperature and strain sensor using microwave coherent detection of spontaneous Brillouin backscatter," Meas. Sci. and Technol. 12, 834-842, 2001.

[46] S. M. Maughan, H. H. Kee, and T. P. Newson, "57-km single-ended spontaneous Brillouin-based distributed fiber temperature sensing using microwave coherent detection," Opt. Lett. 26, 331-333, 2001.

[47] T. Horiguchi, M. Tateda, "BOTDA-nondestructive measurement of single-mode optical fiber attenuation characteristics using Brillouin interaction: theory" J. Lightwave Technol. 7, 1170-1176, 1989.

[48] T. Kurashima, T. Horiguchi, M. Tateda, "Distributed-temperature sensing using stimulated Brillouin scattering in optical silica fibers," Opt. Lett. 15(18), 1038-1041, 1990.

[49] D. Garus, T. Gololla, K. Krebber, F. Schliep,"Brillouin Optical-Fiber Frequency-Domain Analysis for Distributed Temperature and Strain Measurements," J. Lightwave Technol. 15(4), 654-662, 1997.

[50] J. W. Berthold, "Histrical review of microbend fiber-optic sensors," J. Lighwave Technol., vol. 13, No. 7, pp. 1193-1199, 1995.

[51] N. Lagakos, J. H. Cole, and J. A. Bucaro, "Microbend sensors," Appl. Opt., vol. 26, pp. 2171-2180, 1987.

[52] A. J. Rogers, "Distributed optical fiber sensing," Proc. SPIE, vol. 1508, pp. 2-24, 1991.

[53] Denis Donlagic, Brian Culshaw, "Microbend Sensor Structure for Use in Distributed and Quasi-Distributed Sensor Systems Based on Selective Launching and Filtering of the Modes in Graded Index Multimode Fiber," J. Lightwave Technol. 17(10), 1856-1868, 1999.

[54] J. L. Brooks, R. H.Wentworth, R. C. Youngquist, M. Tur, B. Y. Kim, and H. J. Shaw, "Coherence multiplexing of fiber-optic interferometric sensors," J. Lightwave Technology, vol. LT-3, pp. 1062-1072, May 1985.

[55] A. D. Kersey, A. Dandridge, "Multiplexed Mach-Zehnder ladder array with ten sensor elements", Electron. Lett. 25(19), pp. 1298 - 1299, 1989.

[56] G. P. Agrawal, Lightwave Technology Components and Devices, John Wiley & Sons, Hoboken, NJ, 2004. Ch. 2,6,8.

[57] A. D. Kersey, K. L. Dorsey, A. Dandridge, "Demonstration of an eight-element time-division multiplexed interferometric fibre sensor array", Electron. Lett. 24(11), pp. 689 - 691, 1988.

[58] K. Blotekjaer, R. Wentworth, H. Shaw, "Choosing relative optical path delays in series-topology interferometric sensor arrays," J. Lightwave Technol. 5(2), pp. 229 - 235, 1987.

[59] A. D. Kersey, M. J. Marrone, A. Dandridge, "Experimental investigation of polarisation induced fading in interferometric fibre sensor arrays," Electron. Lett., 27(7), pp.562 - 563, 1991.

[60] A. D. Kersey, M. J. Marrone, and M. A. Davis, "Polarization-insensitive fiber optic Michelson interferometer," Electron. Lett., vol. 27, pp. 518-520, Mar. 1991.

[61] M. J. Marrone, A. D. Kersey, and A. Dandridge, "Fiber optic Michelson array with passive elimination of polarization fading and source feed-back isolation," in Proc. IEEE Optic Fiber Sensors, 8th, Monterey, CA, pp. 69-72, 1992.

[62] S. Huang; W. Lin; M. Chen; S. Hung; H. Chao, "Crosstalk analysis and system design of time-division multiplexing of polarization-insensitive fiber optic Michelson interferometric sensors," J. Lightwave Technol., 14(6), pp. 1488 - 1500, 1996.

[63] S. F. Collins, B. T. Meggit, A. W. Palmer and K. T. V. Grattan, "A multiplexing scheme for optical fiber interferometetric sensors using an FMCW generated carrier", in Proc. IEEE Optical Fiber Sensor, 8th, Monterey, CA, pp. 209, 1992.

[64] L. Yuan, W. Jin, .L, Zhou, Y. L. Hoo, M. S. Demokan, "Enhanced multiplexing capacity of low-coherence reflectometric sensors with a loop topology," IEEE Photonics Technol. Lett. 14(8), pp.1157 - 1159, 2002.

[65] L. Yuan, W. Jin, .L, Zhou, Y. L. Hoo, M. S. Demokan, "Enhancement of multiplexing capability of low-coherence interferometric fiber sensor array by use of a loop topology", J. Lightwave Technol. 21(5), pp.1313-1319, 2003.

[66] R. S. Weis, A. D. Kersey, and T. A. Berkoff, "A four element fiber grating sensor array with phase sensitive detection," IEEE Photon. Technol. Lett., vol. 6, no. 12, pp. 1469-1472, 1994.

[67] D. J. F. Cooper, T. Coroy, and P. W. E. Smith, "Time-division Multiplexing of large serial fiber-optic Bragg grating sensor arrays," Appl. Opt. 40(16), pp. 2643-2654, 2001.

[68] A. D. Kersey, T. A. Berkoff, and W. W. Morey, "Multiplexed fiber Bragg grating strain-sensor system with a fiber Fabry-Perot wavelength filter," Opt. Lett., vol. 18, no. 16, pp. 1370-1372, 1993.

[69] T. A. Berkoff, and A. D. Kersey, "Fiber Bragg Grating Array Sensor System Using a Bandpass Wavelength Division Multiplexer and Interferometric Detection," IEEE Photonoics Technol. Lett. 8(11). pp. 1522-1524, 1996.

[70] A. Ezbiri, A. Munoz, S. E. Kanellopoulos and V. A. Handerek, "High resolution fibre Bragg grating sensor demodulation using a diffraction grating spectrometer and CCD detection," in IEE Colloquium on Optical Techniques for Smart Structures and Structural Monitoring, Feb. 1997, pp.5/1 - 5/6.

[71] T. A. Berkoff, M. A. Davis, D. G. Bellemore, A. D. Kersey, G. M. Williams, M. A. Putnam, "Hybrid time- and wavelength-division multiplexed fiber Bragg grating sensor array," Proc. SPIE, Vol. 2444, p.288-294, 1995.

[72] Y. N. Ning, Z. P. Wang, A. W. Palmer, K. T. V. Grattan, and D. A. Jackson, "Recent progress in optical current sensing techniques," Rev. Sci. Instrum., vol. 66, no. 5, pp. 3097-3111, 1995.

[73] K. Bohnert, P. Gabus, J. Nehring, and H. Brandle, "Temperature and Vibration Insensitive Fiber-Optic Current Sensor," J. Lightwave Technol., 20(2), pp.267-276, 2002.

[74] M. N. Deeter, "High sensitivity fiber-optic magnetic field sensors based on iron garnets," IEEE Trans. Instrum. and Meas. 44(2), pp. 464 - 467, 1995.

[75] J. C. Yong, S. H. Yun, M. L. Lee, B. Y. Kim, "Frequency-division-multiplexed polarimetric fiber laser current-sensor array", Opt. Lett. 24(16), pp. 1097-1099, 1999.

[76] M. Singh, C. J. Tuck and G. F. Fernando, "Multiplexed optical fibre Fabry-Perot sensors for strain metrology," Smart Mater. Struct. 8, pp. 549-553, 1999.

[77] A. D. Kersey, A. Dandridge and A. B. Tveten, "Time-division multiplexing of interferometric fiber sensors using passive phase generated carrier interrogation", Opt. Lett. 12 (10), 775, 1987.

[78] J. Zheng, "Analysis of Optical Frequency-Modulated Continuous-Wave Interference," Applied Optics, 43(21), pp. 4189-4198, 2004.

[79] A. Dandridge, A. Tveten, A. Kersey, A. Yurek, "Multiplexing of interferometric sensors using phase-generated carrier techniques", Electron. Lett. 23(13), pp. 665-666, 1987.

[80] A. Dandridge, A. Tveten, A. Kersey, A. Yurek, "Multiplexing of interferometric sensors using phase carrier techniques" J. Lightwave Technol. 5, pp. 947, 1987.

[81] I. Sakai, "Frequency division multiplexing of fibre sensors using a frequency modulated source," Opt. & Quantum Electron. 18, p. 279, 1986.

[82] K. R. Mallalieu, R. Youngquist, D. E. N. Davis, "FMCW of Optical Source Envelope Modulation for Passive Multiplexing of Frequency-Based Fibre-Optic Sensors," Electron. Lett. 17, pp. 809-810, 1986.

[83] K. Y. Huang, G. M. Carter, "Coherent optical frequency domain reflectometry (OFDR) using a fiber grating external cavity laser", IEEE Photonics Technol. Lett., 6(12), pp. 1466 - 1468, 1994.

[84] J. P. Von der Weid, R. Passy, N. Gisin, "Mid-range coherent optical frequency domain reflectometry with a DFB laser diode coupled to an external cavity", J. Lightwave Technol. 13(5), pp. 954 - 960, 1995.

[85] U. Glombitza, E. Brinkmeyer, "Coherent frequency-domain reflectometry for characterization of single-mode integrated-optical waveguides", J. Lightwave Technol., 11(8), pp.1377-1384, 1993.

[86] H. L. Ho, W. Jin, H. B. Yu, K. C. Chan, C. C. Chan, and M. S. Demokan, "Experimental Demonstration of a Fiber-Optic Gas Sensor Network Addressed by FMCW", IEEE Photon. Technol. Lett., vol. 12, No. 11, pp. 1546-1548, 2000.

[87] P. K. C. Chan, W. Jin, J. M. Gong, and M. S. Demokan, "Multiplexing of fiber bragg grating sensors using an FMCW technique," IEEE Photon. Technol. Lett., vol. 11, pp. 1470-1472, Nov. 1999.

[88] P. K. C. Chan, W. Jin; M. S. Demokan, "FMCW multiplexing of fiber Bragg grating sensors", J. of Selected Topics in Quantum Electronics, 6(5), p756 - 763, 2000.

[89] S. A. Al-chalabi, B. Culshaw, D. E. N. Davis, "Partially coherenct sources ininterferometric sensors," Proc. 1st Intern. Conf. On Optical Fiber Sensors, London, pp. 132-135, 1983.

[90] J. Brooks, R. Wentworth, R. Youngquist, M. Tur, B. Kim and H. Shaw, "Coherence multiplexing of fiber-optic interferometric sensors", J. Lightwave Technol. Vol. 3, pp. 1062-1072, 1985.

[91] A. D. Kersey and A. Dandridge, "Low Crosstalk Code Division Multiplexed Interferometric Array," Electron. Lett. 28, pp. 351, 1992.

[92] F. Kullander, "Code division multiplexing in interferometric optical fiber sensor networks," Optical Fiber Sensors Conference Technical Digest, vol. 1, pp. 523, 2002.

[93] A. D. Kersey, "Demonstration of a Hybrid Time/Wavelength Division Multiplexed Interferometric Fibre Sensor Array," Electron. Lett. 27(7), pp.554-555, 1991.

[94] G. A. Cranch and P. J. Nash, "Large-Scale Multiplexing of Interferometric Fiber-Optic Sensors Using TDM and DWDM," J. Lightwave Technol. 19(5), pp. 687-698, 2001

[95] F. Farahi, J. D. C. Jones and D. A. Jacken, "Multiplexed Fibre-Optic Interfero-metric sensing system: Combined Frequency and Time Division," Electron. Lett. 24(7), pp. 409-410, 1998.

[96] K. O. Hill, Y. Fujii, D. C. Johnson and B. S. Kawasaki, "Photosensitivity in optical waveguides: application to reflection filter fabrication", Appl. Phys. Lett. 32 (10), 647-649, 1978.

[97] A. Othonos and K. Kalli, Fiber Bragg Gratings: Fundamentals and Applications in Telecommunications and Sensing, Artech House, 1999. Chap. 1.

[98] W. H. Hayt, Jr. and J. A. Buck, Engineering Electromagnrtics, 7th ed., McGraw-Hill, 2006, Section 13.3.

[99] B. T. Meggit, "Fiber Optic White Light Interferometric Sensors," Optical Fiber Sensor Technology, K.T.V. Grattan and B.T. Meggitt (eds.), Vol. 4, Kluwer Acadamic, pp. 193-238, 2000.

[100] S. Chen, A. W. Palmer, K. T. V. Grattan, B. T. Meggitt, "Digital signal-processing techniques for electronically scanned optical-fiber white-light interferometry," Applied Optics, Vol. 31(28), pp. 6003-, 1992.

[101] S. H. Poland, J. P. Bengtsson, M. Bhatnagar, K. C. Ravikumar, M. J. de Vries and R. O. Claus, "Multi-measured multiplexed extrinsic Fabry-Perot interferometric sensors," Proc. Conf. on Smart Structures and Materials, SPIE '94, Orlando, FL, pp 58-66,1994.

[102] M. E. Jones, J. L. Grace, V. Bhatia, K. A. Murphy, R. O. Claus, J. A. Greene and T. A. Tran, "Multiplexed absolute strain measurements using extrinsic Fabry-Perot

interferometers," Proc. Conf on Smart Structures and Materials, SPIE 95 paper 2444-28, 1995.

[103] Y. Chen and H. F. Taylor, "Multiplexed fiber Fabry-Perot temperature sensors system using white light interferometry", Opt. Lett. 27, 903-905 (2002).

[104] X. Wan and H. F. Taylor, "Monitoring and Multiplexing Technique for Interferometric Fiber Optic Sensors with a Linearly Chirped Er Fiber Laser", Appl. Opt. 41, 7607-7611 (2002).

[105] T. J. Cavicchi, Digital Signal Processing, John Wiley & Sons, New York, 2000. Chap. 9.

[106] S. K. Mitra, Digital Signal Processing, 2nd ed., McGraw-Hill, 2001, Sections 4.4.2 and 8.2.5.

[107] B. Qi, G. R. Pickrell, J. Xu, P. Zhang, Y. Duan, W. Peng, Z. Huang, W. Huo, H. Xiao, R. G. May, and A. Wang, "Novel data processing techniques for dispersive white light interferometer," Opt. Eng., Vol. 42, pp. 3165-3171, 2003.

[108] J. Schwider and L. Zhou, "Dispersive interferometric profilometer," Opt. Lett., Vol. 19(13), pp. 995-997, 1994.

[109] S. A. Tretter, "Estimating the frequency of a noisy sinusoid by linear regression," IEEE Trans. Inform. Theory, vol. IT-31, pp. 832-835, Nov. 1985.

[110] S. M. Kay, "A fast and accurate single frequency estimator," IEEE Trans. Acoust., Speech, Signal Processing, vol. 37, pp. 1987-1990, 1989.

[111] D. C. Rife and R. R. Boorstyn, "Single-tone parameter estimation from discrete-time observations," IEEE Trans. Inform. Theory, vol. IT-20, pp. 591-598, 1974.